Effect of dolerite intrusions on coal quality in the Secunda Coal Fields of South Africa

By

John Paul Bussio

Submitted in partial fulfilment of the requirements for the degree of
MSc Geology

In the Faculty of Natural & Agricultural Sciences

University of Pretoria

Pretoria

MARCH 2012

ABSTRACT

The coalfields of South Africa contain numerous dolerite intrusions, which are believed to have affected the quality of the surrounding coal by a thermal process, controlled by the size of the magmatic body. Data gathered from a working coalfield in Secunda, South Africa, suggest that the relationship between intrusive sills and coal is complex and factors other than intrusion width must be considered in relation to the contact metamorphic effect. The study area contains multiple dolerite intrusions of Karoo age, separated according to their geometric relationship to the local coal seams. Three intrusions were selected for detailed study. The three dolerite bodies, namely the DO4, DO8 and DO10 dolerites, occur as sills intruded close to the main coal seam of the area. The dolerite sills have identical mineralogy and can only be distinguished through textural variations in thin section.

Coal quality data was obtained from Sasol Mining Secunda and used to investigate the presence or absence of a change in coal quality relative to dolerite proximity. Reduction in coal quality was defined using three main proximate analysis values, termed Ash, Volatile content (Vols) and Dry Ash Free Volatile (DAFV) in the coal industry. These parameters were used to determine the extent of any effect deleterious to coal quality induced by the intrusion of the dolerite sills. The resultant investigation showed no correlation between the position and thickness of the dolerites, and a change in coal quality (as measured by proximate analysis).

In the absence of a linear relationship between coal quality and dolerite proximity, two processes are proposed to explain the absence of the contact metamorphic effects expected from previous studies:

-Dolerite emplacement dynamics may influence the size of the metamorphic aureole produced by an intrusion, and invalidating intrusion size as a measure of thermal output,

- Hydrothermal fluids mobilised by the dolerite intrusions, either from the country rock or the intrusion itself may percolate through the coal and act as the metamorphic agent responsible for changing coal quality, by dissolving the volatile components of the coal and transporting them to other locations

These two processes are sufficient to explain the lack of a clear “metamorphic effect” related to the dolerite intrusions.

REPORT DECLARATION

I, John Paul Bussio declare that the thesis/dissertation, which I hereby submit for the degree MSc Geology at the University of Pretoria, is my own work and has not previously been submitted by me for a degree at this or any other tertiary institution

SIGNATURE: .....

DATE: .....

ACKNOWLEDGEMENTS

I would like to thank the following people for their assistance and input to the success of this project: my supervisor Dr R.J. Roberts whom enlightened me to new ideas and concepts which greatly enhanced the project; Sasol Mining and the Sasol exploration team of Fabian Francis, Sam Ndigna, Patrick Ndlovu and Karen van der Merwe for all the help with obtaining samples and allowing me such fantastic access to a wealth of data; Prof J.S. Marsh who allowed the use of his data within this project; the University of Pretoria MSc discussion group for feedback and problem solving; and Coaltech and Mr Johann Beukes for funding the project and supporting the research.

TABLE OF CONTENTS

Contents

LIST OF FIGURES

LIST OF TABLES

CHAPTER 1: INTRODUCTION AND PROJECT AIM

1.1 Introduction

The coal fields on the Highveld of South Africa are intersected by many dolerite dyke and sill complexes which form the plumbing network of the Karoo large igneous province (van Niekerk 1995; Riley *et al.,* 2006). The thermal contact metamorphic effects of this pervasive network of intrusions have been held responsible for strongly influencing the coal quality in the Highveld region, and creating dangerous mining conditions. In the terms used by the coal industry, "poor quality" coal is characterised by increased ash content, reduced volatile content and increased friability.

In simple terms, the contact metamorphic effect of an igneous intrusion (at a specific temperature and composition) is thought to be directly related to the volume of the intrusive material which passes through the conduit at the time of emplacement and the nature of the surrounding material (Mussett and Khan, 2000). Thus the greater the volume of magma passing through the dolerite conduit, the larger the metamorphic aureole that should be produced. It is the purpose of this thesis to investigate the thermal metamorphic effects of these Karoo dolerites in an attempt to understand the extent and mechanics of the metamorphism occurring.

1.2. Geological setting of the study area

1.2.1 Karoo Basin stratigraphy

The area under investigation is located in the Mpumalanga Province of South Africa, as seen in Figure 1. The region lies within the Karoo sedimentary basin, and the dolerites under investigation and contained within the Ecca group of the Karoo Supergroup (SACS, 1980). The Karoo Supergroup is found in a retro-arc foreland basin covering a large portion of South Africa (approximately 550 000 km^2; see Figure 2). This basin contains volcanic deposits and a variety of sedimentary sequences formed within an array of sedimentary environments ranging from glacial to peat bogs (du Toit, 1954; de Olivera and Cawthorn, 1999). The Supergroup is separated on stratigraphic principles into five main groups, namely the Dwyka, Ecca, Beaufort, Stormberg and Drakensberg groups. (du Toit, 1954;).

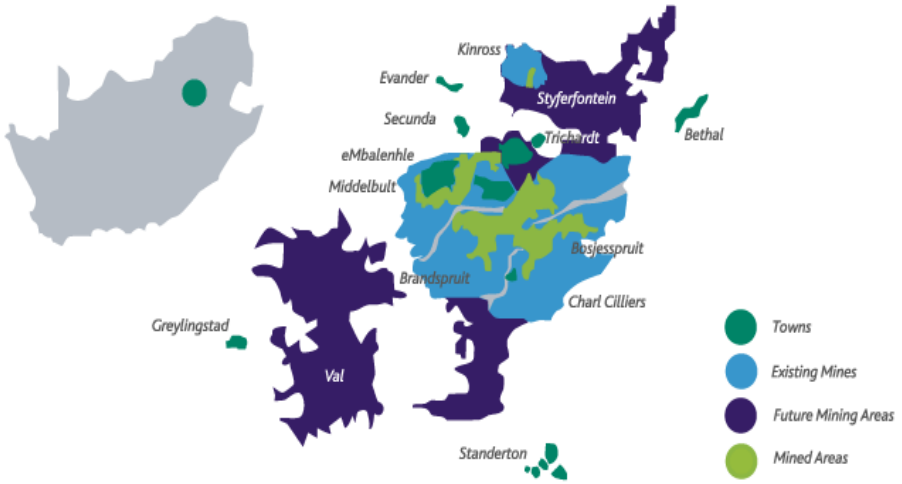

Figure 1: Geographic position of the Sasol mining operations in the Highveld coal fields within South Africa (Sasol Mining).

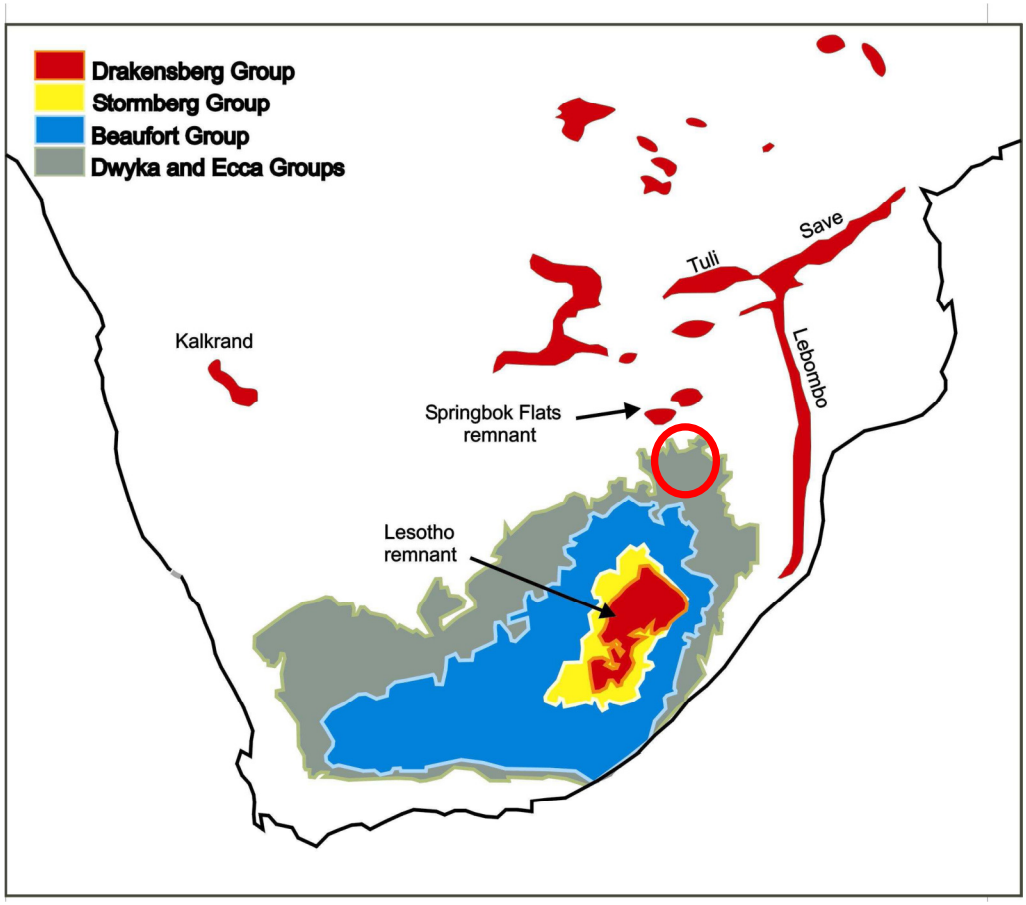

Figure 2: Map of Southern Africa showing the extent of the main Karoo basin and the distribution of volcanic units (Hancox *et al.,* 2001). Highlighted in red is the sampled area.

Dwyka Group

The Dwyka Group of the Karoo sequence is primarily formed within a glacial environment with the onset of sedimentation occurring during the Late Carboniferous and continued to the Early Permian. The sedimentary material deposited in this group unconformably overlies the pre-Karoo formations of the Cape Supergroup which shows large striated glacial pavements showing evidence for the glacially related sedimentation of the Dwyka Group (see Figure 5) (SACS, 1980 and Johnson et al.,1996). The sediments hosted in the Dwyka Group consist of diamictite, varved shale, mudstones with dropped pebbles and fluvioglacial conglomerate (SACS, 1980).

Ecca Group

The Ecca Group lies conformably on the Dwyka tillites and is comprised of four sedimentary facies dispersed over the Karoo basin. The facies are identified as the Southern or Green Ecca, the Central or Blue Ecca, the Coal Measure Ecca and the Red Ecca, with each of these being predominantly fluvial deltaic sedimentary environments (du Toit, 1954; van Niekerk, 1995).

The Green, Blue and Red Ecca statigraphic intervals contain sandstones, mudstones and minor organic materials while the Coal Measure Ecca consist of high levels of organic materials such as coal shales and coal beds. It is from within this stratigraphic interval that most of the coal data in the project has been obtained (du Toit, 1954; van Niekerk, 1995).

Beaufort Group

The Beaufort Group lies above the Ecca Group, marked by a gradual contact between the two sequences. Thus the separation of the two groups relies on sedimentological differences (SACS, 1980). Noted changes from the Ecca Group to the Beaufort Group:

1. Argillaceous rocks of the Ecca Group are layered and micaceous whereas those in the Beaufort Group are massive.
2. Carbonaceous grey shales of the Ecca Group change to the green, blue or red shales of the Beaufort Group.
3. The Beaufort Group shows an increase in cross bedding structures relative to the Ecca sediments.

4. The Beaufort Group contains upward fining sedimentary sequences.
5. Reptilian fossils occur in the Beaufort Group.

These differences show a change in environment with regard to climate and depositional mechanisms, shifting from a fluvial system of high-sinuosity rivers, deltas and braided rivers in the Ecca Group, to a more arid environment of alluvial fans and dune fields in the Beaufort Group (Johnson et al.,1996).

Stormberg Group

The Stormberg Group lies above the Beaufort Group conformably. The group is subdivided into three formations, namely the Molteno, Elliot and Clarens Formations (SACS, 1980). These formations are comprised of shale, sandstones and minor coal beds (Du Toit, 1954). The Stormberg Group appears similar to the Beaufort Group but has been distinguished due to the distinct colour variations of the shales (SACS, 1980).

Drakensberg Group

The final group at the top of the Karoo sequence is dominated by the volcanic products of the Karoo flood basalt event. These extrusive outpourings are mixed in with minor pyroclastic and sedimentary layers in a thick sequence of basaltic rock (Jourdan *et al.*, 2004). The volcanic and intrusive portions of this group are covered in detail elsewhere in this thesis.

1.2.2 Karoo magmatism

The voluminous magmatism that erupted in the Karoo basin at 183 Ma consists not only of extrusive Drakensberg flood basalts, but also an extensive network of intrusive plumbing found throughout the lower Karoo sediments. This magmatic event has been referred to as a "Large Igneous Province" (LIP) by some authors (Jourdan *et al.*, 2004) and has been associated in the literature with continental breakup and the presence of a mantle plume in the Weddell Sea at this stage in Gondwana evolution (Jourdan *et al.*, 2004). The magmatism in the central Karoo basin is commonly correlated with the Lebombo lavas on the eastern side of the Kaapvaal craton, as well as with the Ferrar dolerites found on the Antarctic Plate.

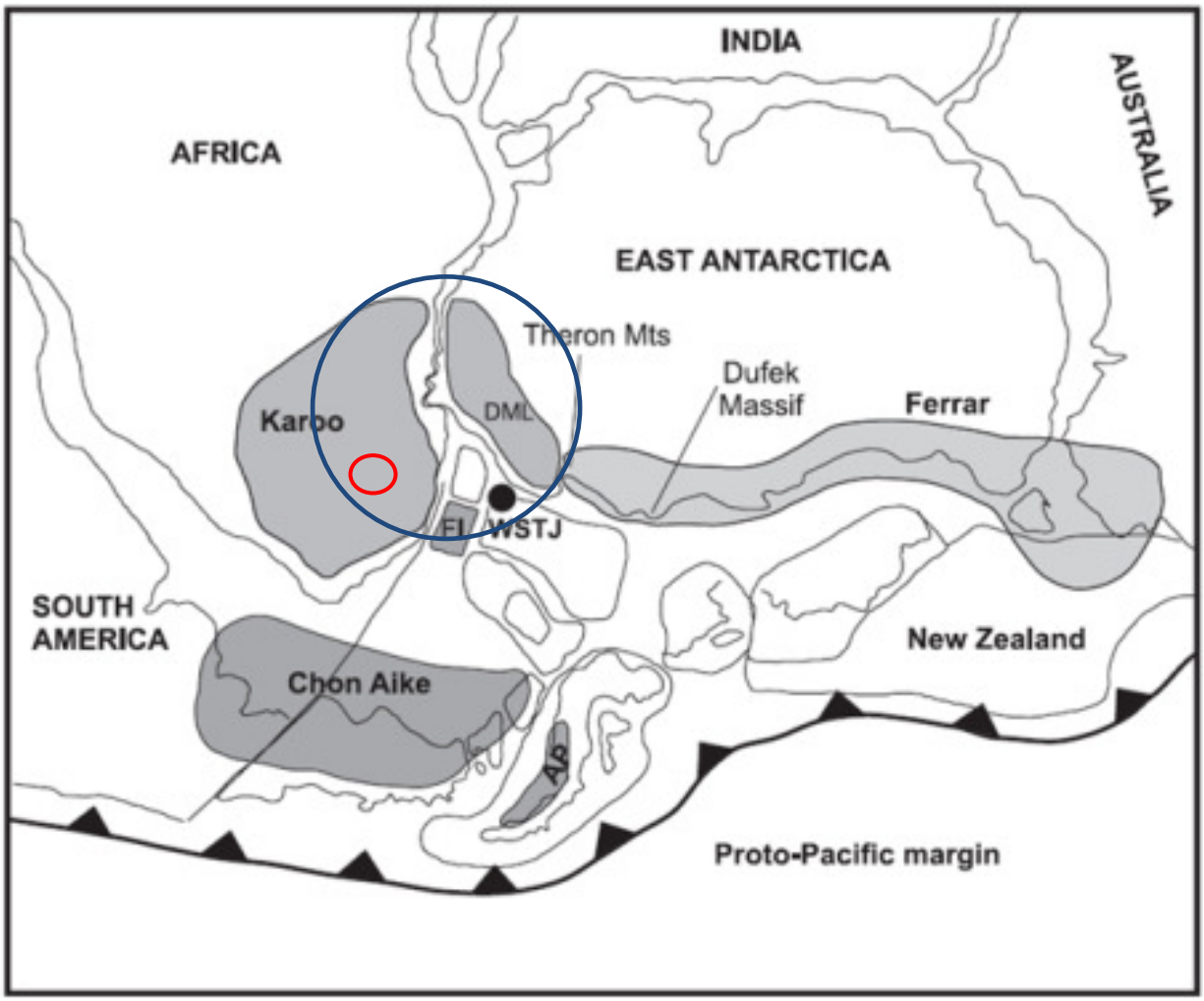

Figure 3: Paleomap of Gondwanaland at ~178-184Ma (adapted from Riley *et al.,* 2006). Highlighted in red is the study area. Highlighted in blue is an approximation of the plume head size and dimensions suggested by White and McKenzie, (1989). FL Falkland Islands, DML Dronning Maud Land, AP Antarctic Peninsula and WSTJ Weddell Sea Triple Junction

Numerous age determinations have been performed on the Karoo, Lebombo and Ferrar volcanics, with most showing the age of peak volcanism to be between 178 Ma-184 Ma. The eruptive sequence of the Karoo, Lebombo and Ferrar lavas is a point which has been highly contested (Encarnacion *et al.,* 1996; Le Gall *et al.,* 2002; Jourdan *et al.*, 2004). Authors such as Jourdan *et al., (*2004) have suggested that there are much earlier dates for some of the Lebombo region dykes, thus implying separate source regions for the magmatic provinces, but most workers believe the two sequences are related to a singular magmatic source, which may possibly be the mantle plume suggested by McKenzie and White (1989)

The dolerite complexes of the Secunda region are most often referred to as Karoo dolerites and as such all dolerites in this area are assumed to have similar intrusive age, source materials and thermogenic properties (van Niekerk 1995). It has thus been assumed that the dolerites produced from this magmatism all have similar metamorphic properties.

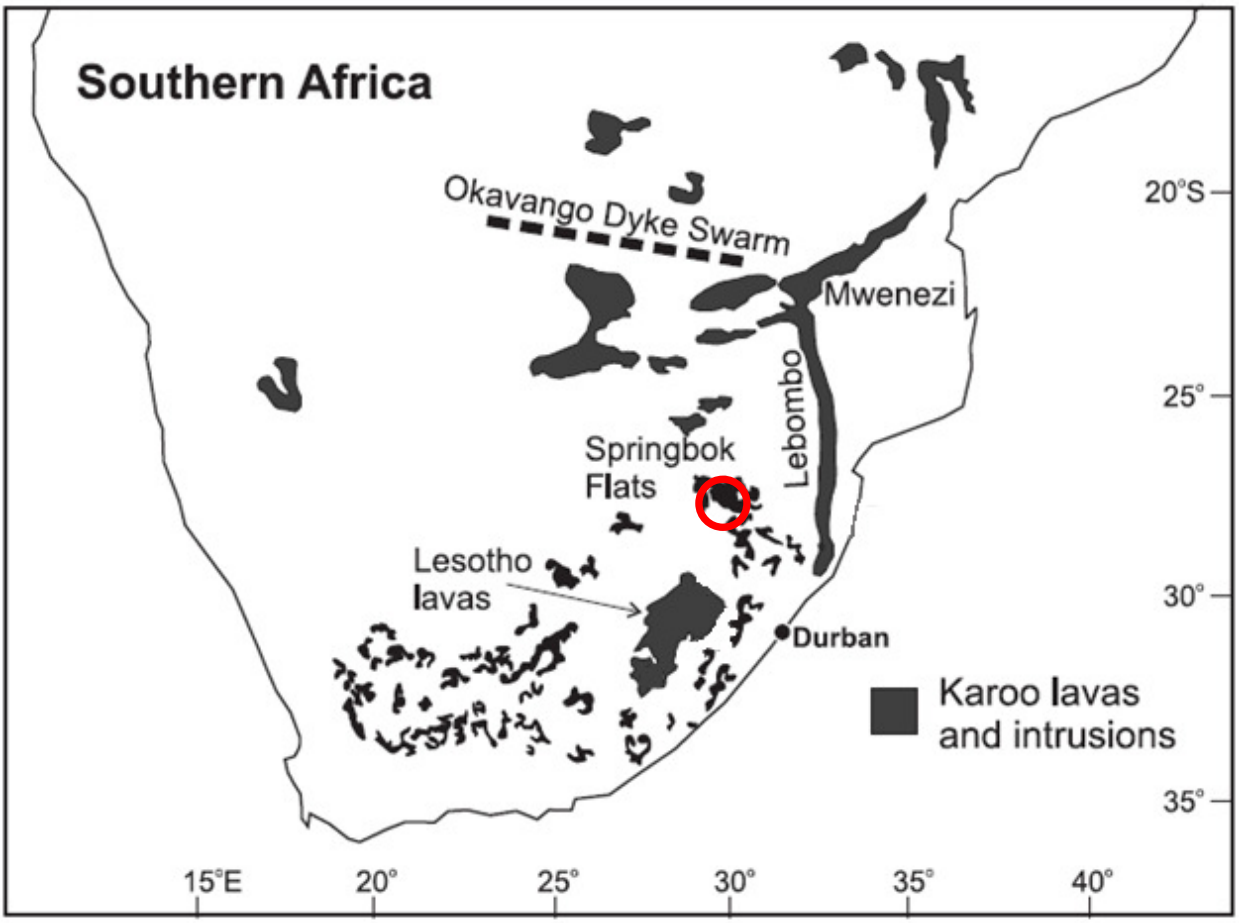

Figure 4: Karoo lavas and intrusions in Southern Africa. Highlighted in red is the Secunda study area (Adapted from Riley *et al.,* 2006*).*

1.2. Dolerite emplacement and propagation

The movement and propagation of dykes and sills is a complex and dynamic process. Experimental modelling by authors such as Cañón-Tapia & Merle (2006) can be used to describe this movement process, and factors affecting dyke emplacement(compiled from the works of McLeod and Tait, 1999; Kavanagh et al., 2006;; Cañón-Tapia and Merle, 2006; Poland et al., 2008) are listed below:

- The distance from the source the magma travels
- The density of the magma
- The piezometric pressure on the magma
- The flow rate of the magma
- The magma chamber overpressures
- The flow regime within the magma conduit
- Depth of emplacement
- Temperature of the magma
- Length of conduit

All of these properties influence the capacity of the magma to penetrate the surrounding country rock and define the way in which the thermal energy of the magma is transferred. From these parameters it can be proposed that the formational and propagation processes of dolerites will produce unique conduit specific metamorphic properties (McLeod and Tait, 1999; Kavanagh et al., 2006; Cañón-Tapia and Merle, 2006; Poland et al., 2008).

1.2.1 Magmatic properties: emplacement and propagation dynamics

The source magma properties define the propagation and emplacement dynamics of dolerite bodies and there are specific physical parameters of the source magma which greatly influence the propagation dynamics of the final intrusion. The most significant of these factors is magma chamber overpressure (Cañón-Tapia and Merle, 2006). This variable pressure within the magma chamber may be induced by influx of new magma, eruption, volatile exsolution or crystallization (Huppert and Woods, 2002; Cañón-Tapia and Merle, 2006; Dufek and Bachmann, 2010). These factors relate to the pervasive force induced by the leading edge of a dyke or sill at the initial stages of intrusion, and an increase in magmatic overpressure will result in an increase in the force applied at the leading edge of a dyke or sill (McLeod and Tait, 1999; Cañón-Tapia and Merle, 2006).

Pressure in the conduit during intrusive emplacement is fundamental to the way in which the intrusive propagates (McLeod and Tait, 1999; Kavanagh et al., 2006; Cañón-Tapia and Merle, 2006; Poland et al., 2008). The distance and height relationship (piezometric pressure) of a magma

conduit can also create variable flow forces within a magma conduit (Spiegelman and McKenzie, 1987; Kavanagh et al., 2006). Topographic gradients created by thermal upwelling will provide downhill slopes for gravitational flow (Yi-Gang Xu *et al.,* 2004), and the distance the magma must travel from the source, and the slope or incline on which the magma is forced to flow, will affect the rate at which the magma flows within the conduit.

The second component affecting the emplacement dynamics of an intruding magma is the flow of the magma within the conduit itself. This flow is controlled partially by the force provided by magma chamber pressures and piezometric pressures, but also by the physicochemical properties of the magma itself. The viscosity of the magma will define the resistance of the magma to flow, and magmas with high viscosity would require a greater force to induce flow, whereas magmas with lower viscosities would require less force.

The amalgamation of these factors defines the flow regime of the magma. Flow regime is divided into two main types, laminar and turbulent flow. Laminar flow defines non-turbulent fluids in which the particles in the fluid flow parallel to one another. Turbulent flow allows for the creation of vortexes or eddies within the fluid flow which disrupts the parallel flow of particles (Reynolds, 1883). The separation of these end members is defined by the Reynolds number of a specific fluid (Reynolds, 1883). The calculation of this number is explained by the following equation:

$$Re \equiv \frac{\rho_{liq} \bar{U} w}{\eta}$$

- $\bar{U}$ is the average velocity
- w is the half-thickness of the flow
- ρ_{liq} is the liquid density
- η is its viscosity

If the Reynolds number is higher than a threshold value, turbulent flow will occur, whereas if the Reynolds number is lower than the threshold value, laminar flow will occur (Kavanagh et al., 2006). The transition between laminar and turbulent flow can be anywhere in the range of Re= 10-1000, but within mafic magmas this value is ~28 (Kavanagh et al., 2006).

CHAPTER 2: PHYSICAL AND MINERALOGICAL PROPERITES OF SECUNDA DOLERITES

2.1. Stratigraphic distribution of dolerite sills

In the area mined by the Sasol Mining Company near Secunda, where coal is mined from the Ecca formation, several dolerite intrusions are commonly noted in the regional stratigraphy. The DO4, DO8 and DO10 dolerite intrusions were investigated in this study, owing to their stratigraphic positions (Figure 5), their continuity over the study region (Figure 6), and for their constant proximity to the C 4 lower coal seam. The DO4 sill crops out on surface (Figure 5) and four other sills (DO6, DO8, DOO, and DO12) are usually present in the area (van Niekerk, 1995).

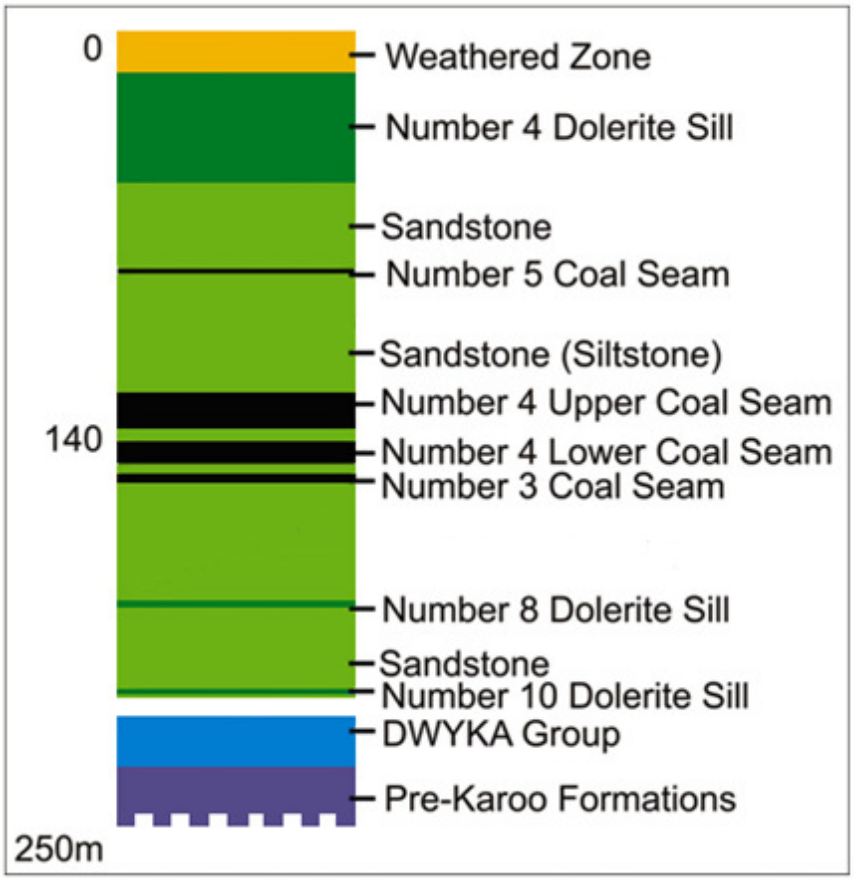

Figure 5: Generalized stratigraphy of the Secunda study area, as defined within the Sasol mining area

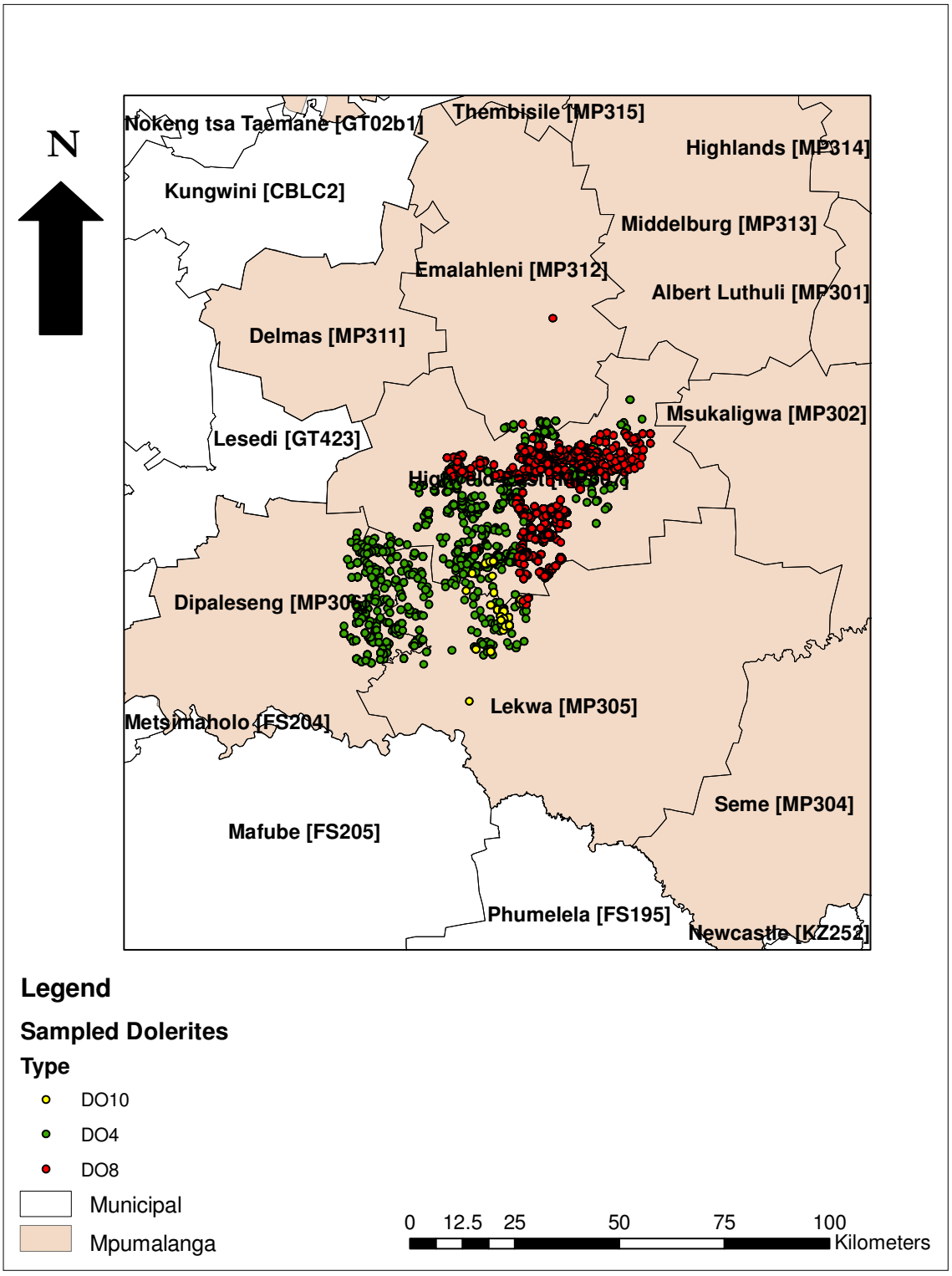

Figure 6: Borehole intersects of the three main dolerite sills of the Secunda study area. The points represent boreholes which intersect only one dolerite type. Note that the numbers following area names are the municipal area codes. Owing to the density of drilling in the area, some boreholes overlap with other borehole locations on the scale of the map.

2.2. Dolerite sampling methods

Samples were obtained from boreholes over the entire Sasol Secunda mining operation, where wireline diamond drill core with a diameter of 4.5 cm is drilled for mine planning purposes. The dolerite samples were taken within the central third of the sills to avoid contamination from surrounding country rock. All sampled core was cleaned to remove any remnant drilling lubricants.

2.2.1 Dolerite DO4

Figure 7: DO4 core sample with holocrystic texture

Figure 8: Photomicrograph of DO4 dolerite thin section under XPL.

Mineral assemblage: Plagioclase (80%), clinopyroxene (10%, with 5% inverted pigeonite), opaque minerals (5%)

Discussion: The geographically extensive DO4 dolerite sill is characterized by fine grained weathered mafic igneous material. The dolerite is found at a relatively constant stratigraphic position (see Figure 5) over the entire study area and is often in close proximity to the C 4 lower coal seam. In hand specimen no discernible fabric is visible (Figure 7). This sill shows highly variable thickness, ranging from 0.2m to 74.43m. In thin section, the DO4 dolerite samples exhibit a fine grained ophitic texture and are characterised by high degrees of weathering. The mineral assemblage is dominated by needle-like plagioclase grains with minor pigeonite, poikilitic clinopyroxene and interstitial opaque minerals. The pigeonite hosted in the DO4 dolerites has an inverted optical character with few of the examples showing fine augite lamella. Alteration of the DO4 dolerites is most prominent in the pyroxenes with plagioclase and the opaque minerals largely unaffected by alteration. Texturally the DO4 dolerite shows no preferred orientations or settling patterns.

Table 1: DO4 thin section descriptions

Section	Plagioclase grains properties	Pyroxene grains properties	Accessory minerals	Notable features within section
JB 1	Average grain size ~300µm, needle like shape and little to no alteration.	Minor augite lamella within inverted pigeonite. High levels of alteration noted in clinopyroxene.	Minor opaque minerals found interstitially between pyroxene grains	Ophitic texture
JB 2	Average grain size ~300µm, needle like shape and little to no alteration	Minor augite lamella within inverted pigeonite. High levels of alteration noted in clinopyroxene.	Minor opaque minerals found interstitially between pyroxene grains	Ophitic texture
JB 5	Average grain size ~300µm, needle like shape and little to no	Minor augite lamella within inverted pigeonite. High levels of alteration noted in	Minor opaque minerals found interstitially	Ophitic texture

	alteration	clinopyroxene.	between pyroxene grains	
JB 7	Average grain size ~300µm, needle like shape and little to no alteration	Minor augite lamella within inverted pigeonite. High levels of alteration noted in clinopyroxene.	Minor opaque minerals found interstitially between pyroxene grains	Finer grain size and larger amounts of plagioclase ~90%. Ophitic texture
JB 8	Average grain size ~300µm, needle like shape and little to no alteration	Minor augite lamella within inverted pigeonite. High levels of alteration noted in clinopyroxene.	Minor opaque minerals found interstitially between pyroxene grains	Ophitic texture
JB 9	Average grain size ~300µm, needle like shape and little to no alteration	Minor augite lamella within inverted pigeonite. High levels of alteration noted in clinopyroxene.	Minor opaque minerals found interstitially between pyroxene grains	Ophitic texture
JB 10	Average grain size ~300µm, needle like shape and little to no alteration	Minor augite lamella within inverted pigeonite. High levels of alteration noted in clinopyroxene.	Minor opaque minerals found interstitially between pyroxene grains	Ophitic texture
JB 14	Average grain size ~300µm, needle like shape and little to no alteration	Minor augite lamella within inverted pigeonite. High levels of alteration noted in clinopyroxene.	Minor opaque minerals found interstitially between pyroxene grains	Lesser degree of weathering, and slightly finer grain size. Ophitic texture
JB 15	Average grain size ~300µm, needle like shape and little to no alteration	Minor augite lamella within inverted pigeonite. High levels of alteration noted in clinopyroxene.	Minor opaque minerals found interstitially between pyroxene grains	Higher degree of alteration. Ophitic texture
JB 19	No signs of weathering	Minor augite lamella within	Minor opaque	Finer grain size,

	or alteration, average grain size ~300µm, needle like shape	inverted pigeonite. High levels of alteration noted in clinopyroxene.	minerals found interstitially between pyroxene grains	highly weathered pyroxenes. Ophitic texture
JB 20	Highly altered and greater amount ~90%, Average grain size ~300µm, needle like shape.	Minor augite lamella within inverted pigeonite. High levels of alteration noted in clinopyroxene.	Minor opaque minerals found interstitially between pyroxene grains	Finer grain size. Ophitic texture
JB 23	Average grain size ~300µm, needle like shape and little to no alteration, large phenocrysts similar to DO8 can be seen with grain sizes in excess of 1500µm	Larger clinopyroxene grain size of ~ 300µm. Minor augite lamella within inverted pigeonite.	Minor opaque minerals found interstitially between pyroxene grains	Larger grains that have much lesser degrees of weathering. Ophitic texture

2.2.2 Dolerite DO8

Figure 9: DO8 core sample with needle like phenocryst highlighted in red

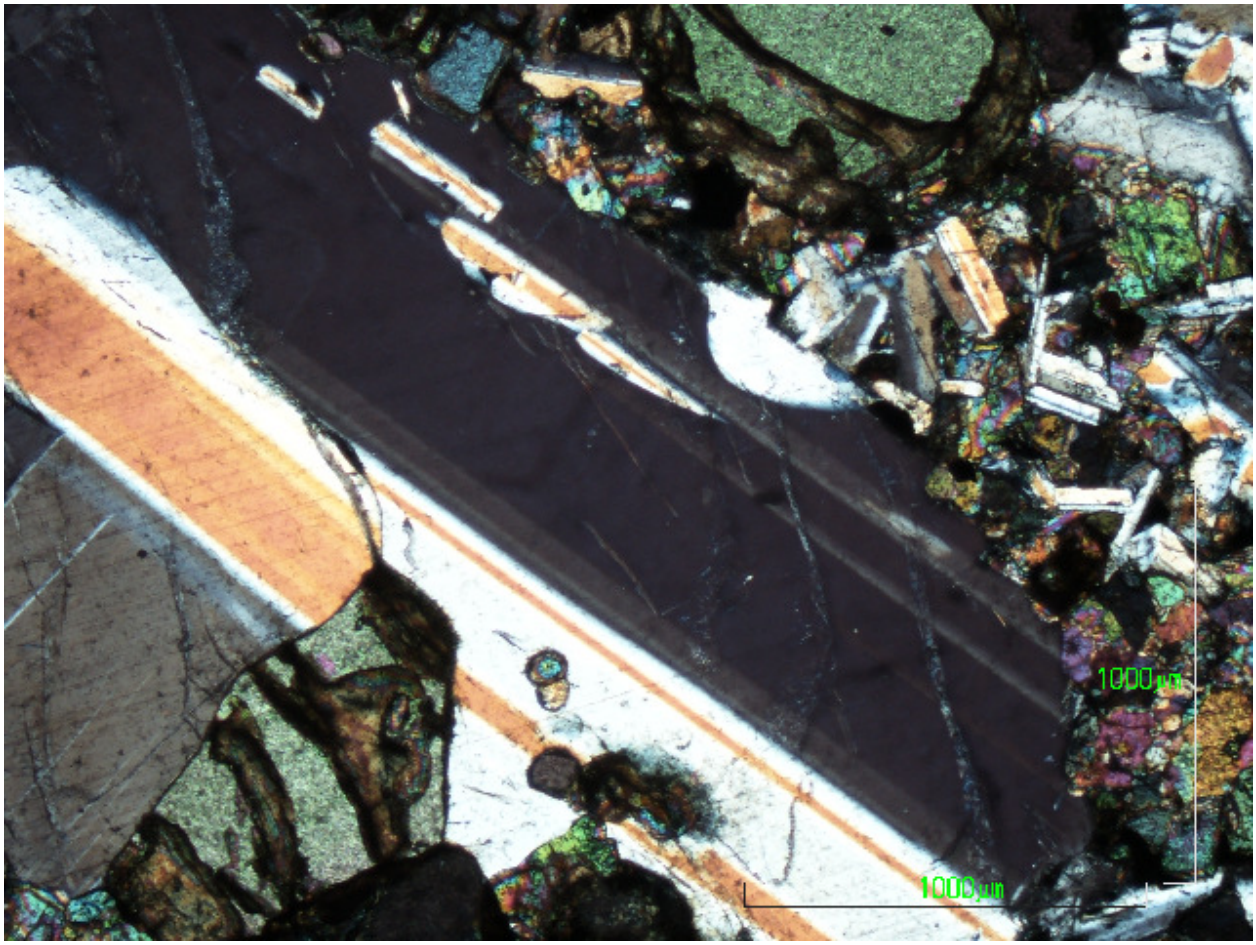

Figure 10: Photomicrograph of DO8 dolerite thin section under XPL.

Minerals: Plagioclase (80%), clinopyroxene (10%, with 5% inverted pigeonite), opaque minerals (3%), 2% olivine

Discussion: The DO8 dolerite sill is a coherent mafic igneous rock, characterized by needle-like phenocrysts visible in core samples (Figure 10). This dolerite sill type is geographically extensive

but with a noted concentration in the north-eastern zone of the study area as noted in Figure 6. It is often found at heights different to its generalized stratigraphic position (Figure 5) and often intersects the C 4 lower coal seam. It is also highly variable in thickness ranging from 0.01m to 44.65m. Within thin section no discernible fabric is visible although the plagioclase grains seem to cluster together in some instances. An example of the DO8 texture can be seen in Figure 10. The DO8 dolerites of the study area show a very uniform mineral assemblage throughout all the samples taken. Plagioclase dominates the mineralogy and there appears to be two generations of plagioclase growth, with the DO8 samples exhibiting phenocrysts of 4-8mm in length as well as matrix crystals of ~400µm. Olivine is rare in the samples but where present it is large in grain size, displaying high levels of alteration along its fracture plans. Clinopyroxene and inverted pigeonite form the majority of the matrix and are generally altered. Minor opaque minerals can be noted as interstitial grains within the matrix; most are amorphous. Texturally DO8 shows no settling patterns but a weak variolitic texture can occasionally be observed in the distribution of small plagioclase grains.

Table 2: DO8 thin section descriptions

Section	Plagioclase grains properties	Pyroxene grains properties	Accessory minerals	Notable features within section
JB 3	Two size variations with the smaller grains exhibiting weak variolitic textures.	Minor augite lamella within inverted pigeonite. Moderate to high levels of alteration of both clinopyroxene and inverted pigeonite	Minor opaques found interstitially between pyroxene grains	Two size variations of plagioclase possibly showing two generations of growth
JB 11	Two size variations with the smaller grains exhibiting weak variolitic textures.	Minor augite lamella within inverted pigeonite. Moderate to high levels of alteration of both clinopyroxene and inverted pigeonite	Minor opaques found interstitially between pyroxene grains. Large olivine grains with high levels of alteration along fractures	Very low degrees of weathering and two size variations of plagioclase possibly showing two generations of growth

JB 18	Two size variations with the smaller grains exhibiting weak variolitic textures.	Minor augite lamella within inverted pigeonite. Moderate to high levels of alteration of both clinopyroxene and inverted pigeonite	Minor opaques found interstitially between pyroxene grains. Large olivine grains with high levels of alteration along fractures	Two size variations of plagioclase possibly showing two generations of growth
JB 21	Two size variations with the smaller grains exhibiting weak variolitic textures.	Minor augite lamella within inverted pigeonite. Moderate to high levels of alteration of both clinopyroxene and inverted pigeonite	Minor opaques found interstitially between pyroxene grains. Large olivine grains with high levels of alteration along fractures	Very low degrees of alteration, two size variations of plagioclase possibly showing two generations of growth
JB 22	Two size variations with the smaller grains exhibiting weak variolitic textures.	Minor augite lamella within inverted pigeonite. Moderate to high levels of alteration of both clinopyroxene and inverted pigeonite	Minor opaques found interstitially between pyroxene grains	Very low degrees of alteration. Two size variations of plagioclase possibly showing two generations of growth
JB 24	Two size variations with the smaller grains exhibiting weak variolitic textures.	Minor augite lamella within inverted pigeonite. Moderate to high levels of alteration of both clinopyroxene and inverted pigeonite	Minor opaques found interstitially between pyroxene grains. Large olivine grains with high levels of alteration along fractures	Very low degrees of alteration. Two size variations of plagioclase possibly showing two generations of growth

2.2.3 DO10 Dolerite physical properties

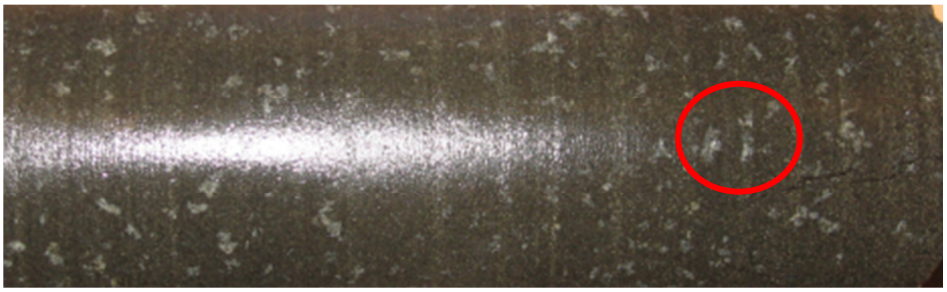

Figure 11: DO10 core sample with star shaped of nodular orientation of phenocrysts highlighted in red

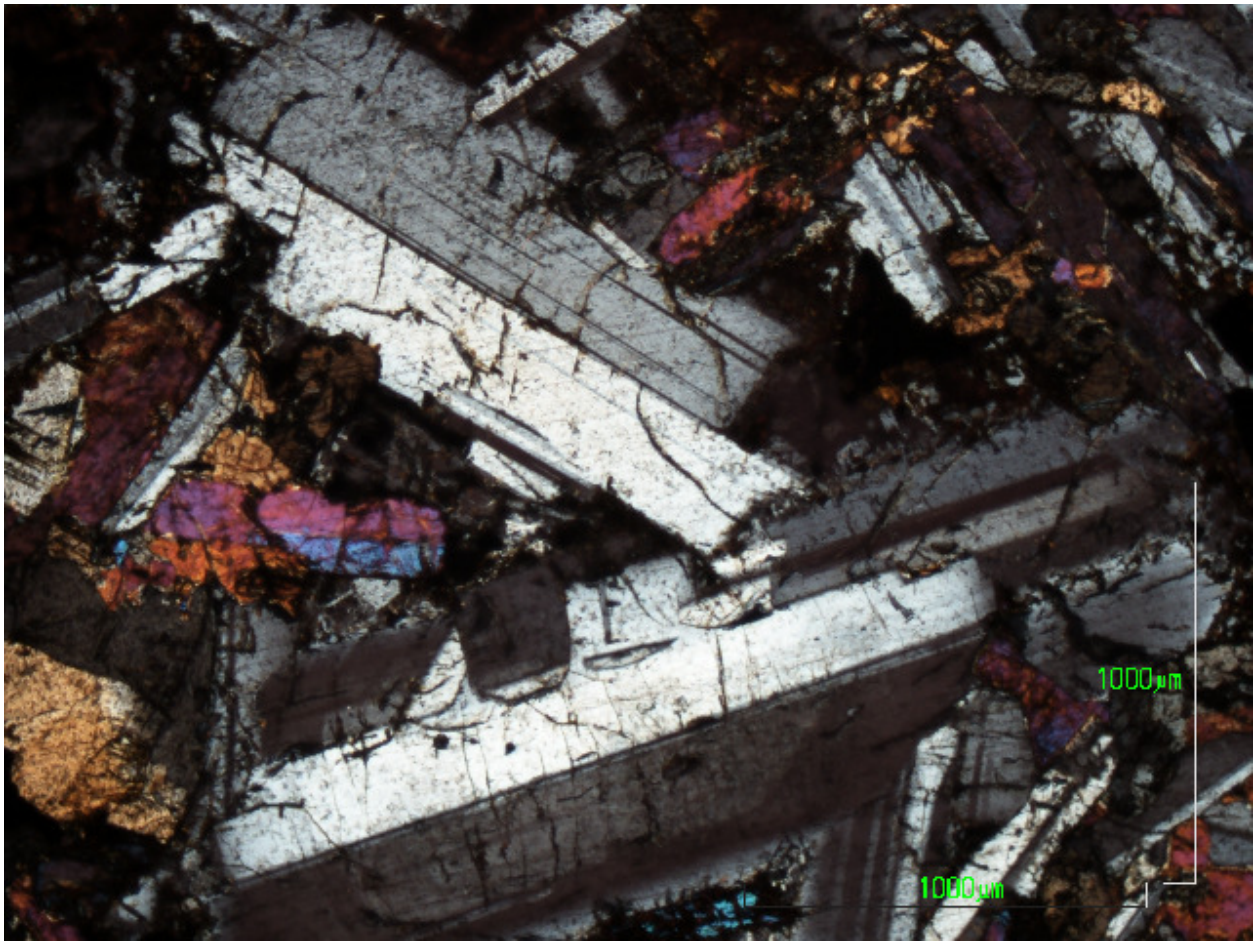

Figure 12: Photomicrograph of DO10 dolerite thin section under XPL.

Minerals: Plagioclase (80%), clinopyroxene (10%, with 5% inverted pigeonite), opaque minerals (5%)

Discussion: The DO10 dolerite sills show much lower degrees of alteration and high levels of competency compared to the DO4 dolerite sill. Star-shaped or nodular clusters of phenocrysts are visible in core samples (Figure 12). Amongst the sampled dolerites the DO10 is the least continuous and is found mainly within the south-eastern zone of the sampled area. The DO10 dolerites are relatively constant in their stratigraphic position below the C 4 lower seam, but they do intrude upwards into close proximity of the seam in several places. Within thin section the dolerites do not display any discernible fabric of any kind, although the plagioclase grains do orientate themselves into cross- or star- shapes which can be identified in core samples; an example of this texture can be seen in Figure 12. The DO10 dolerite samples have a mineral assemblage dominated by plagioclase grains with two distinct size variations; the larger grains display a weak radial texture with the smaller grains showing weak variolitic textures. Inverted pigeonite and clinopyroxene are hosted in the matrix and display no visible preferred orientations or settling patterns; the grains are amorphous and show higher levels of alteration than the surrounding plagioclase or opaque minerals. The minor opaque minerals occur as interstitial grains with no defined crystallographic features and occur most often interstitially between the pyroxenes of the matrix.

Table 3: DO10 thin section descriptions

Section	Plagioclase grains properties	Pyroxene grains properties	Accessory minerals	Notable features within section
JB 4	Two size variations, with the large grains exhibiting a weak radial texture and the smaller grains showing a weak variolitic texture.	Minor augite lamella within inverted pigeonite	Minor opaques found interstitially between pyroxene grains	Two size variations of plagioclase possibly showing two generations of growth
JB 6	Two size variations, with the large grains exhibiting	Minor augite lamella within	Minor opaques found interstitially	Two size variations of plagioclase

	a weak radial texture and the smaller grains showing a weak variolitic texture	inverted pigeonite	between pyroxene grains	possibly showing two generations of growth
JB 12	Two size variations, with the large grains exhibiting a weak radial texture and the smaller grains showing a weak variolitic texture	Minor augite lamella within inverted pigeonite	Minor opaques found interstitially between pyroxene grains	Two size variations of plagioclase possibly showing two generations of growth
JB 13	Weathered and finer grain size, no phenocrysts present.	Fine grained and highly weathered	Minor opaques found interstitially between pyroxene grains	Section is highly weathered and shows no phenocrysts
JB 16	Two size variations, with the large grains exhibiting a weak radial texture and the smaller grains showing a weak variolitic texture	Minor augite lamella within inverted pigeonite	Minor opaques found interstitially between pyroxene grains	Two size variations of plagioclase possibly showing two generations of growth
JB 17	Weathered and finer grain size, no phenocrysts present.	Fine grained and highly weathered	Minor opaques found interstitially between pyroxene grains	Section is highly weathered and shows no phenocrysts

2.2. Summary

All sampled dolerites were no less than 3m thick, and all samples were obtained within the central third of the sill, to minimise any potential contamination by the host sediments. The DO4, DO8 and DO10 dolerites have varying general physical character in core samples. The DO4 dolerite is altered, fine grained and contains no visible phenocrysts, whereas the DO8 and DO10 dolerites contain needle-like and star-shaped or nodular phenocrysts respectively, together with a more coherent nature than DO4. The occasional appearance of olivine within the DO8 dolerite sets it apart from the DO10 and DO4 mineral assemblages, but the presence of two size variations of plagioclase in DO8 is comparable to that in the DO10 dolerites. Inverted pigeonite can be seen in all the dolerite samples with minor augite lamella occasionally visible.

CHAPTER 3: DOLERITE GEOCHEMISTRY

3.1. Introduction

Though the petrographic description of the dolerites in the field area revealed only minor mineralogical differences between the three dolerite intrusions, it was necessary to analyse the dolerites chemically to check for geochemical variation. XRF results of the sampled Secunda dolerites were then used to investigate the relationship between the DO4, DO8 and DO10 dolerites and the formations within the Drakensberg and Lebombo Groups of the Karoo Igneous Province.

3.2. Methodology

The sampled Secunda dolerites were prepared for XRF by the crushing of ~40cm of sampled core to a gravel size. This coarse gravel-sized sample was then milled to <75mm in a tungsten carbide milling vessel, with the resulting powder being roasted at 1000ºC to remove volatile components such as water. The roasted powders melting temperature is reduced by adding 1g sample to 6g $Li_2B_4O_7$ and this mixture is then fused into a glass bead. These beads were analysed for the major elements using the ARL9400XP+ spectrometer at the University of Pretoria. A second portion of the milled powder was used to produce pressed powder briquettes to analyse for trace elements. All the analyses were done with blank and certified reference materials to ensure accurate results.
The results below display data produced from the XRF analysis, both absolute abundances and inter-elemental ratios are displayed to aid in the identification of any variations or trends within the magmatic sequences. All data displayed has been normalized from the data tables 4-6.

Table 4: Unnormalised major and trace element data for the Secunda dolerites.

	std dev[1]	LOD[1]	GSN cert[1]	GSN[1]	JB25	JB26	JB27	JB28	JB29	JB30	JB31	JB32	JB33	JB35	JB36	JB39
SiO_2	0.40	0.02	65.80	65.02	51.05	48.80	50.56	51.22	49.19	51.84	51.93	48.49	51.40	43.68	48.92	53.08
TiO_2	0.0300	0.0032	0.6800	0.7133	1.1811	1.9100	1.2523	1.3514	1.7378	1.2106	0.9729	0.9713	0.9667	1.1590	2.0138	1.4292
Al_2O_3	0.30	0.01	14.67	15.06	14.10	14.79	15.17	13.74	13.18	14.48	14.97	11.74	15.25	15.40	13.76	12.87
Fe_2O_3	0.3000	0.0097	3.7500	3.9329	12.6731	15.6483	11.8185	13.2563	14.8341	12.5655	10.9730	13.3177	10.6595	11.3765	17.0088	13.4382
MnO	0.0065	0.0013	0.0560	0.0595	0.1961	0.2188	0.1679	0.1806	0.1897	0.1829	0.1638	0.1907	0.1583	0.1780	0.2179	0.1843
MgO	0.1000	0.0118	2.3000	1.9347	7.1057	4.6994	5.7342	6.9151	6.1384	5.3467	7.4544	12.0726	7.3671	3.5592	4.7924	4.9849
CaO	0.07	0.01	2.50	2.71	9.51	11.31	9.86	9.72	9.33	10.80	10.27	8.03	10.29	11.22	10.39	9.45
Na_2O	0.1100	0.0265	3.7700	3.2751	2.4692	1.8962	1.9166	1.9333	3.2721	1.3094	1.5830	1.4382	2.2468	1.8666	2.1426	2.5922
K_2O	0.0600	0.0050	4.6300	4.8990	0.8877	0.3398	0.8059	0.8696	0.9374	0.7726	0.7497	0.7005	0.8407	0.8733	0.4399	1.0298
P_2O_5	0.08	0.01	0.28	0.22	0.14	0.14	0.22	0.10	0.18	0.15	0.13	0.22	0.07	0.22	0.10	0.27
Cr_2O_3	0.0053	0.0006	0.0080	0.0285	0.0485	0.0186	0.0497	0.0525	<0.01	0.0228	0.0551	0.0977	0.0486	0.0189	0.0191	0.0307
NiO	0.0100	0.0013	0.0043	0.0818	0.0190	<0.01	0.0137	0.0184	0.0337	0.0157	0.0172	0.0655	0.0165	0.0175	<0.01	0.0054
V_2O_5	0.0018	0.0008	0.0116	0.0120	0.0445	0.0655	0.0320	0.0427	0.0312	0.0433	0.0386	0.0164	0.0708	0.0615	0.1100	0.0819
ZrO_2	0.0050	0.0009	0.0317	0.0122	0.0079	<0.01	<0.01	<0.01	<0.01	<0.01	<0.01	0.0114	<0.01	<0.01	0.0076	0.0096
SO_3	NA	NA	NA	0.22	0.02	<0.01	<0.01	0.02	0.03	<0.01	0.01	0.06	0.03	0.16	<0.01	<0.01
WO_3	NA	NA	NA	0.05	<0.01	<0.01	<0.01	<0.01	<0.01	<0.01	<0.01	<0.01	<0.01	<0.01	<0.01	<0.01
BaO	NA	NA	NA	0.28	<0.01	<0.01	<0.01	<0.01	<0.01	<0.01	<0.01	<0.01	<0.01	<0.01	<0.01	<0.01
Cl	NA	NA	NA	0.04	<0.01	<0.01	<0.01	<0.01	<0.01	<0.01	<0.01	<0.01	<0.01	<0.01	<0.01	<0.01
CuO	0.0037	0.0003	NA	0.02871	<0.01	0.02782	0.0176	0.0246	0.03183	0.01437	0.0249	<0.01	0.01641	0.01812	0.05123	0.01723
ZnO	NA	NA	NA	0.01	<0.01	0.02	0.01	0.01	<0.01	0.02	0.01	0.02	<0.01	0.02	0.02	0.03
Rb_2O	NA	NA	NA	0.02	<0.01	<0.01	<0.01	<0.01	<0.01	<0.01	<0.01	<0.01	<0.01	<0.01	<0.01	<0.01
SrO	NA	NA	NA	0.07	0.03	0.02	0.03	0.03	0.03	0.03	0.02	0.03	0.01	0.05	0.03	0.03
LOI	NA	NA	1.32	1.32	0.53	0.09	2.33	0.50	0.86	1.20	0.62	2.53	0.56	10.13	-0.02	0.47
Total	NA	NA	99.82	100.00	100.00	100.00	100.00	100.00	100.00	100.00	100.00	100.00	100.00	100.00	100.00	100.00

ppm	std dev[1]	LOD[1]	GSN cert[1]	GSN[1]	JB25	JB26	JB27	JB28	JB29	JB30	JB31	JB32	JB33	JB35	JB36	JB39
Cu	3	2	20	85	71	218	81	75	95	101	69	52	71	108	216	88
Ga	2	2	22	19	19	22	20	19	19	19	17	15	16	16	23	21
Mo	1	1	1	1	3	5	3	3	4	3	2	2	2	1	5	2
Nb	3	2	21	22	8	8	8	9	10	10	6	7	6	8	9	8
Ni	6	3	34	35	107	54	75	85	52	55	82	293	85	52	46	40
Pb	3	3	53	55	8	4	11	11	12	10	9	13	3	3	3	18
Rb	4	2	185	186	25	14	24	23	26	21	24	23	24	23	17	27
Sr	4	3	570	582	272	197	307	268	261	209	190	251	186	365	215	276
Th	2	3	42	41	6	8	3	4	8	8	5	4	3	4	11	4
U	2	3	8	8	3	8	3	3	7	3	3	3	3	5	8	4
Y	4	3	19	9	30	38	29	32	37	33	29	27	28	36	43	36
Zn	4	4	48	69	101	104	105	97	116	102	91	107	94	105	109	110
Zr	6	10	235	215	134	122	138	139	162	122	110	114	111	125	140	162
Co	6	3	65	56	43	42	43	44	43	43	45	62	47	47	44	37
Cr	40	15	55	42	336	49	287	278	102	119	325	455	331	183	39	132
Sc	5	1	7	8	22	24	24	22	23	26	22	18	21	33	25	23
V	10	1	65	48	246	380	288	253	290	246	200	178	207	345	421	280
Cs	5	10	5	9	10	9	9	12	9	9	9	9	9	9	9	9
Ba	14	5	1400	1117	324	92	232	237	361	172	196	447	185	270	72	286
La	24	5	75	53	12	4	12	10	10	15	18	15	18	17	4	11
Ce	14	6	135	119	6	5	5	5	11	7	7	5	9	5	5	12

Table 5: Unnormalised major and trace element data for the Secunda dolerites.

	std dev[1]	LOD[1]	GSN cert[1]	GSN[1]	JB1	JB2	JB3	JB4	JB5	JB7	JB8	JB9	JB10	JB11	JB13	JB14	JB15	JB18	JB19
SiO_2	0.40	0.02	65.80	65.80	51.39	51.10	46.67	51.48	51.46	52.38	52.41	52.35	52.08	48.70	50.40	48.47	51.95	48.80	51.10
TiO_2	0.0300	0.0032	0.6800	0.6758	1.3425	0.9556	1.8623	1.2417	0.9440	0.9703	1.2244	1.3334	0.9609	2.0964	1.1610	1.0737	0.9676	2.1401	1.0073
Al_2O_3	0.30	0.01	14.67	15.33	13.39	15.97	12.17	15.12	15.24	16.16	15.07	14.88	16.13	14.35	15.49	14.60	15.90	12.09	15.39
Fe_2O_3	0.3000	0.0097	3.7500	3.7570	12.9454	10.0178	20.0371	12.7257	12.1129	10.1477	11.3688	11.9345	10.1805	16.5474	12.0607	13.1376	10.0440	19.0303	12.3889
MnO	0.0065	0.0013	0.0560	0.0555	0.1911	0.1585	0.2823	0.1991	0.1872	0.1660	0.1736	0.1735	0.1641	0.2363	0.1901	0.2124	0.1593	0.2809	0.1712
MgO	0.1000	0.0118	2.3000	2.2774	7.8312	6.8544	4.4246	5.7152	6.4245	6.8136	6.7851	6.4853	7.1862	5.1056	5.6914	6.5780	6.9222	4.3673	6.5361
CaO	0.07	0.01	2.50	2.68	8.33	9.79	11.39	10.29	10.54	10.00	9.22	9.31	9.91	10.00	10.45	12.16	9.82	10.54	10.80
Na_2O	0.1100	0.0265	3.7700	3.9632	2.4390	2.5868	2.2769	2.4728	1.7701	2.4440	2.6811	2.7337	2.3096	2.6766	2.4395	2.1146	2.3278	2.1468	1.3148
K_2O	0.060	0.005	4.630	4.569	0.776	0.728	0.469	0.778	0.691	0.825	0.874	0.842	0.759	0.451	0.744	0.929	0.767	0.423	0.651
P_2O_5	0.08	0.01	0.28	0.30	0.21	0.12	0.22	0.20	0.09	0.12	0.19	0.20	0.13	0.20	0.19	0.09	0.13	0.12	0.10
Cr_2O_3	0.0053	0.0006	0.0080	0.0272	0.0549	0.0556	0.0143	0.0227	0.0540	0.0511	0.0668	0.0500	0.0547	0.0126	0.0220	0.0662	0.0558	0.0134	0.0673
NiO	0.0100	0.0013	0.0043	0.0478	0.0163	0.0052	0.0278	0.0019	0.0162	0.0053	0.0132	0.0065	0.0077	0.0036	0.0024	0.0456	0.0077	0.0265	0.0184
V_2O_5	0.0018	0.0008	0.0116	0.0121	0.0483	0.0389	0.0746	0.0503	0.0581	0.0403	0.0448	0.0478	0.0398	0.0746	0.0466	0.0429	0.0395	0.0839	0.0894
ZrO_2	0.0050	0.0009	0.0317	0.0169	0.0137	0.0102	0.0031	0.0136	0.0007	0.0108	0.0130	0.0137	0.0111	0.0135	0.0118	0.0000	0.0100	0.0000	0.0000
SO_3	NA	NA	NA	NA	NA	NA	NA	NA	NA	NA	NA	NA	NA	NA	NA	NA	NA	NA	NA
WO_3	NA	NA	NA	NA	NA	NA	NA	NA	NA	NA	NA	NA	NA	NA	NA	NA	NA	NA	NA
BaO	NA	NA	NA	NA	NA	NA	NA	NA	NA	NA	NA	NA	NA	NA	NA	NA	NA	NA	NA
Cl	NA	NA	NA	NA	NA	NA	NA	NA	NA	NA	NA	NA	NA	NA	NA	NA	NA	NA	NA
CuO	NA	NA	NA	NA	NA	NA	NA	NA	NA	NA	NA	NA	NA	NA	NA	NA	NA	NA	NA
ZnO	NA	NA	NA	NA	NA	NA	NA	NA	NA	NA	NA	NA	NA	NA	NA	NA	NA	NA	NA
Rb_2O	NA	NA	NA	NA	NA	NA	NA	NA	NA	NA	NA	NA	NA	NA	NA	NA	NA	NA	NA
SrO	NA	NA	NA	NA	NA	NA	NA	NA	NA	NA	NA	NA	NA	NA	NA	NA	NA	NA	NA
LOI	NA	NA	1.32	1.29	0.59	0.36	-0.01	0.52	0.35	0.38	0.24	0.29	0.40	-0.18	1.22	0.41	0.34	-0.16	0.32
Total	NA	NA	99.82	100.80	99.57	98.75	99.91	100.83	99.93	100.52	100.37	100.66	100.33	100.29	100.13	99.93	99.44	99.91	99.94

ppm	std dev[1]	LOD[1]	GSN cert[1]	GSN[1]	JB1	JB2	JB3	JB4	JB5	JB7	JB8	JB9	JB10	JB11	JB13	JB14	JB15	JB18	JB19
Cu	3	2	20	34	189	170	684	257	139	167	165	181	148	671	237	156	163	688	157
Ga	2	2	22	12	13	12	18	13	10	13	14	15	12	18	11	12	13	14	11
Mo	1	1	1	1	5	4	7	7	5	5	5	5	4	7	5	4	4	8	5
Nb	3	2	21	21	8	7	8	10	6	7	8	8	7	9	10	6	6	9	7
Ni	6	3	34	34	138	65	54	53	72	62	96	76	73	48	59	78	77	49	81
Pb	3	3	53	66	30	23	19	30	17	16	22	21	22	17	26	23	17	19	19
Rb	4	2	185	183	23	25	19	24	24	26	26	23	23	17	23	23	22	17	23
Sr	4	3	570	575	242	229	218	213	172	199	270	267	198	201	213	189	189	193	175
Th	2	3	42	49	13	11	18	14	14	11	11	14	12	16	14	9	11	17	12
U	2	3	8	12	11	8	17	10	9	9	10	11	9	15	12	7	10	15	8
Y	4	3	19	10	34	30	45	35	29	29	30	34	29	43	34	28	31	45	30
Zn	4	4	48	46	94	68	99	90	69	72	88	83	78	89	86	75	75	102	76
Zr	6	10	235	213	149	110	142	129	112	111	139	143	109	139	123	107	113	145	113
Co	6	3	65	68	58	45	53	45	48	51	49	53	48	49	50	65	54	52	53
Cr	40	15	55	145	405	464	182	237	444	439	484	394	440	162	247	472	440	159	446
Sc	5	1	7	5	25	29	30	30	26	31	26	25	28	31	32	28	27	34	27
V	10	1	65	47	267	226	438	271	201	232	258	274	213	430	260	220	215	458	225
Cs	5	10	5	11	9	9	9	9	9	9	9	12	9	9	9	9	9	9	9
Ba	14	5	1400	1345	322	479	187	238	271	297	377	379	272	146	233	247	267	118	246
La	24	5	75	60	4	4	4	4	4	4	4	4	4	4	4	4	4	4	4
Ce	14	6	135	142	40	39	32	35	39	39	49	48	34	29	40	34	39	23	32

Table 6: Unnormalised major and trace element data for the Secunda dolerites.

	std dev[1]	LOD[1]	GSN cert[1]	GSN[1]	JB12	JB20
SiO_2	0.40	0.02	65.80	65.76	44.02	47.17
TiO_2	0.0300	0.0032	0.6800	0.6763	2.3918	1.0382
Al_2O_3	0.30	0.01	14.67	15.07	12.46	14.68
Fe_2O_3	0.3000	0.0097	3.7500	3.7354	23.1782	14.4632
MnO	0.0065	0.0013	0.0560	0.0538	0.3048	0.2049
MgO	0.1000	0.0118	2.3000	2.2145	4.2290	7.4819
CaO	0.07	0.01	2.50	2.65	10.41	11.89
Na_2O	0.1100	0.0265	3.7700	3.8338	1.8403	1.3348
K_2O	0.060	0.005	4.630	4.622	0.366	0.760
P_2O_5	0.08	0.01	0.28	0.29	0.12	0.12
Cr_2O_3	0.0053	0.0006	0.0080	0.0144	0.0108	0.0985
NiO	0.0100	0.0013	0.0043	0.0163	0.0419	0.0592
V_2O_5	0.0018	0.0008	0.0116	0.0124	0.0941	0.0312
ZrO_2	0.0050	0.0009	0.0317	0.0200	<0.01	<0.01
SO_3	NA	NA	NA	NA	NA	NA
WO_3	NA	NA	NA	NA	NA	NA
BaO	NA	NA	NA	NA	NA	NA
Cl	NA	NA	0.00	0.00	0.15	0.14
CuO	NA	NA	NA	NA	NA	NA
ZnO	NA	NA	NA	NA	NA	NA
Rb_2O	NA	NA	NA	NA	NA	NA
SrO	NA	NA	NA	NA	NA	NA
LOI	NA	NA	1.32	1.29	0.19	0.41
Total	NA	NA	99.82	100.26	99.83	99.88

ppm	std dev[1]	LOD[1]	GSN cert[1]	GSN[1]	JB12	JB20
Cu	3	2	20	28	236	73
Ga	2	2	22	19	23	15
Mo	1	1	1	1	7	4
Nb	3	2	21	21	9	6
Ni	6	3	34	38	40	98
Pb	3	3	53	56	26	17
Rb	4	2	185	181	19	22
Sr	4	3	570	577	211	168
Th	2	3	42	46	17	9
U	2	3	8	9	17	6
Y	4	3	19	10	49	29
Zn	4	4	48	48	88	63
Zr	6	10	235	221	155	108
Co	6	3	65	69	50	51
Cr	40	15	55	57	145	433
Sc	5	1	7	7	29	29
V	10	1	65	55	443	205
Cs	5	10	5	9	35	61
Ba	14	5	1400	1408	162	272
La	24	5	75	55	4	4
Ce	14	6	135	143	35	41

[1]Standard deviation from limit of detection (std dev), Limit of detection (LOD), GSN cert: is the certified standard values, GSN: is the values produced when the certified sample was analysed during the specific analysis run

1

3.3. Results

3.3.1 Major element analysis

Tables 4-6 show the major element data obtained by XRF for the Secunda dolerites. In Figure 13 it can be seen that TiO_2 concentrations of the DO8 dolerites are enriched above those of the DO4 and DO10 dolerites which have similar concentrations. DO4 shows the greatest variation in SiO_2, possibly related to the high levels of alteration observed in thin section.

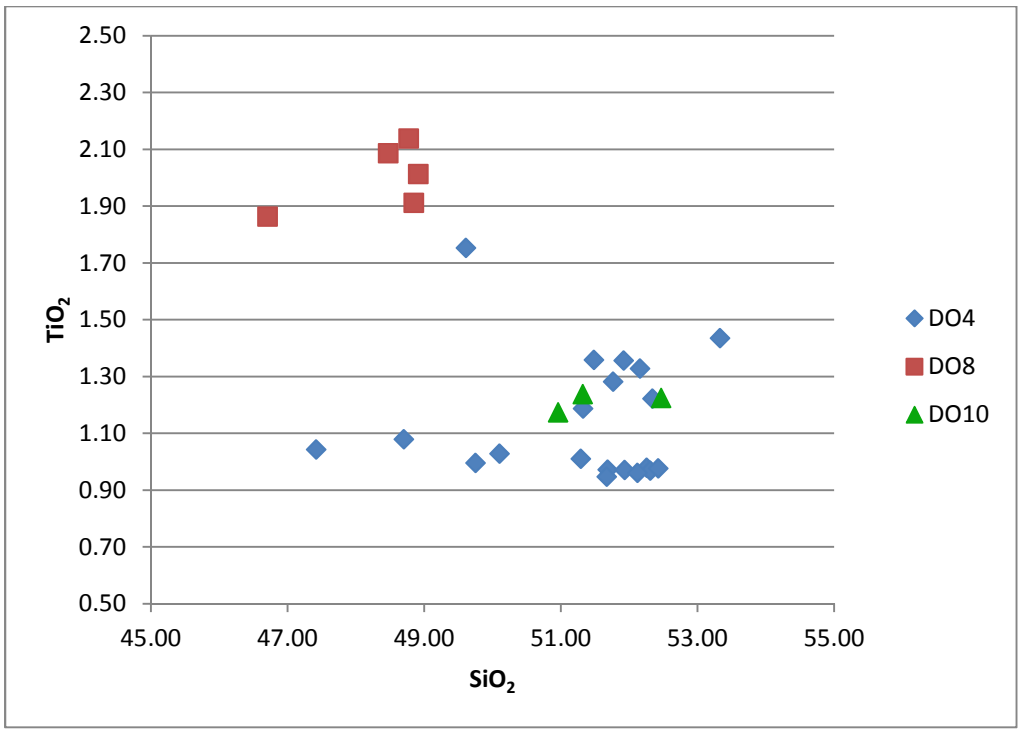

Figure 13: Plot of TiO_2 against SiO_2 for the Secunda dolerites

Figure 14 displays a Harker diagram of MgO for the Secunda dolerites; the diagram shows the DO8 dolerites have the lowest MgO concentrations, despite being olivine-bearing. There appears to be two groups of data within the DO4 data set, caused by the variation in SiO_2; specifically, a clustering of data points within the DO4 data can be seen between 51-53 wt % SiO_2. This grouping may again reflect the less than pristine nature of the DO4 samples. The DO8 dolerites are clearly seperable from the other two dolerites.

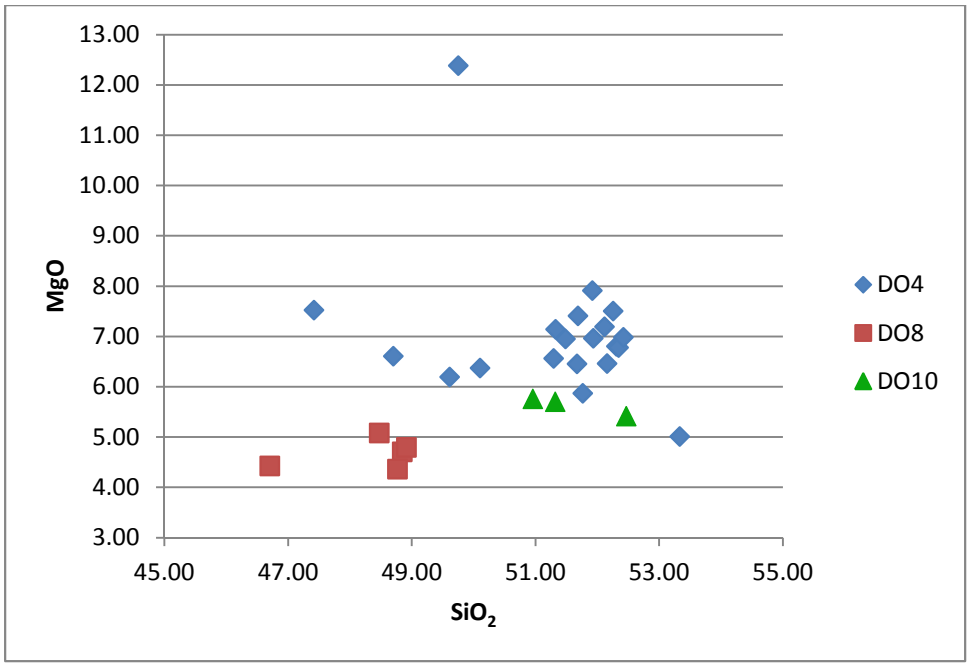

Figure 14: Plot of MgO against SiO_2 for the Secunda dolerites

Considerable scatter within the Al_2O_3 concentrations of all three Secunda dolerites (Figure 15) can be noted. The lower abundance of plagioclase in the olivine-bearing DO8 rocks is reflected in lower Al_2O_3 values, but little differentiation between the DO4 and DO10 dolerites can be made. The data does depict an increase in Al_2O_3 concentrations with increasing SiO_2 values.

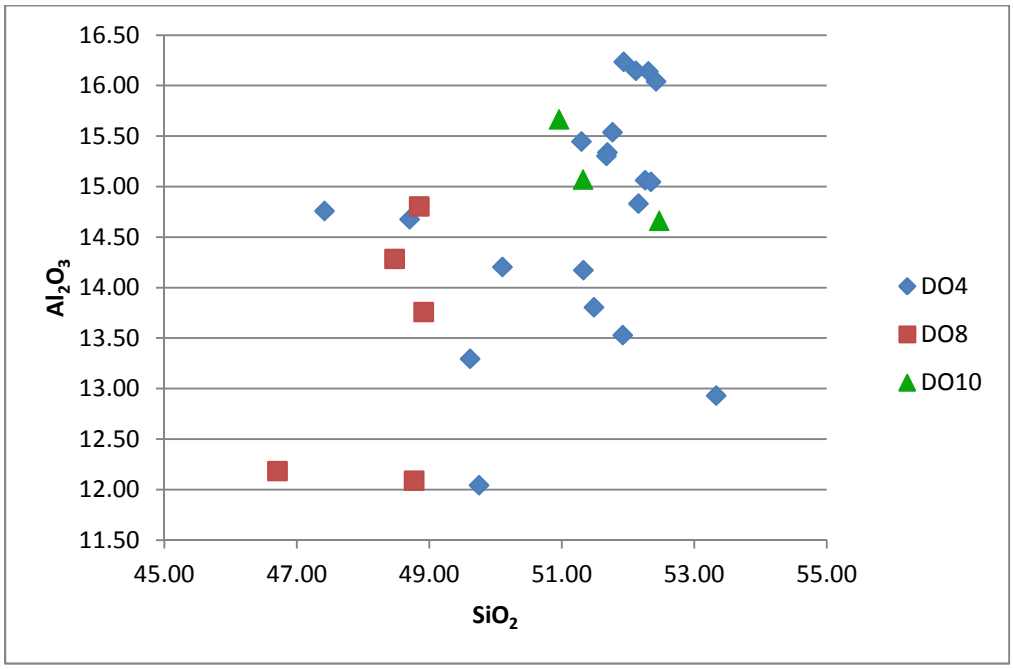

Figure 15: Plot of Al_2O_3 against SiO_2 of the Secunda dolerites

3.3.2 Trace element analysis

The trace elemental analysis is approached using the same methodology as seen in the major elemental analysis, although trace elemental data can allow insight into the evolution of mafic magmatic series. The use of both compatible and incompatible trace elements was applied to aid in the identification of possible unique magma types within the Secunda dolerites.

In Figure 17, Nb and Zr, two incompatible elements are plotted against one another. DO4 shows a large scatter in this diagram, with a cluster of data points at the lowest concentrations for both Nb and Zr. The DO8 dolerite shows concentrations of Zr between 120-150ppm, similar to the upper concentrations of the DO4 dolerite. The DO10 dolerite shows enriched concentrations of Nb relative to the other two dolerites, with the majority of the data plotting above 9ppm. Figure 17 showing Nb against Y shows similar groupings to Zr vs. Nb, but there is greater separation between the DO8 data and the DO4 data.

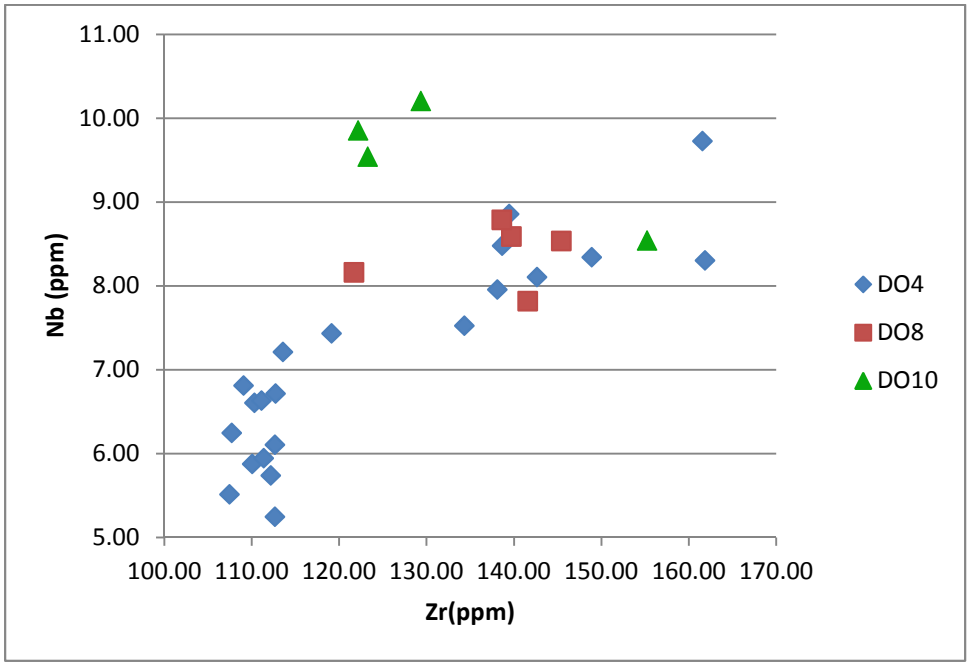

Figure 16: Plot of Nb against Zr of the Secunda dolerites

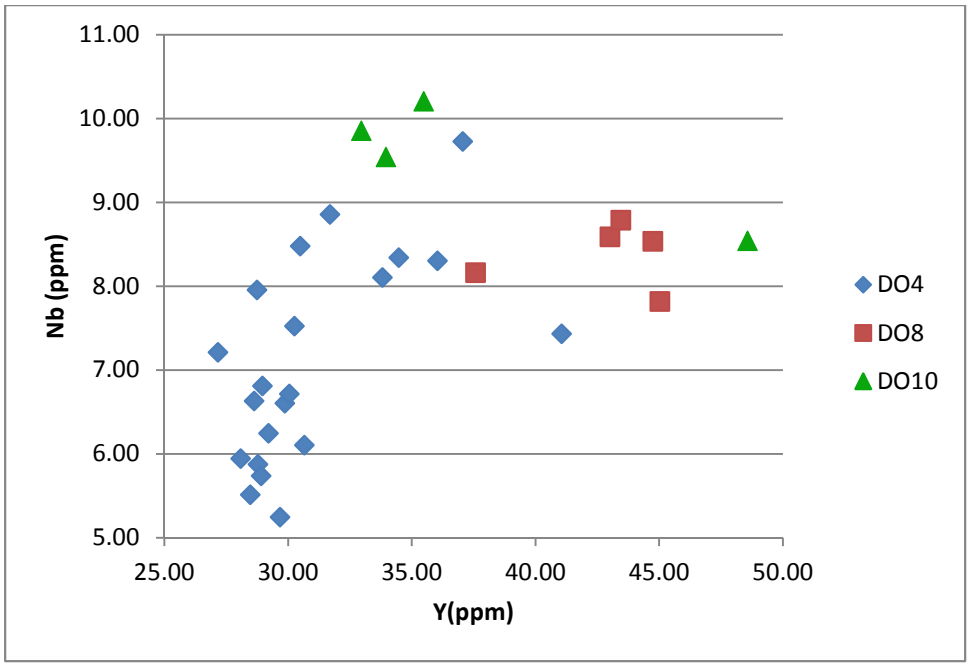

Figure 17: Plot of Nb against Y of the Secunda dolerites

Figure 18 shows Zr vs Y for the Secunda dolerites. The DO4 dolerite shows two groupings of data, one with low levels of Zr and Y approximately 110ppm and 28ppm respectively. The second group shows a greater spread of data within both Zr and Y, with a Zr range of ~135-160ppm and Y range of ~28-37ppm. The DO4 and DO8 display similar data spreads in both Zr and Y.

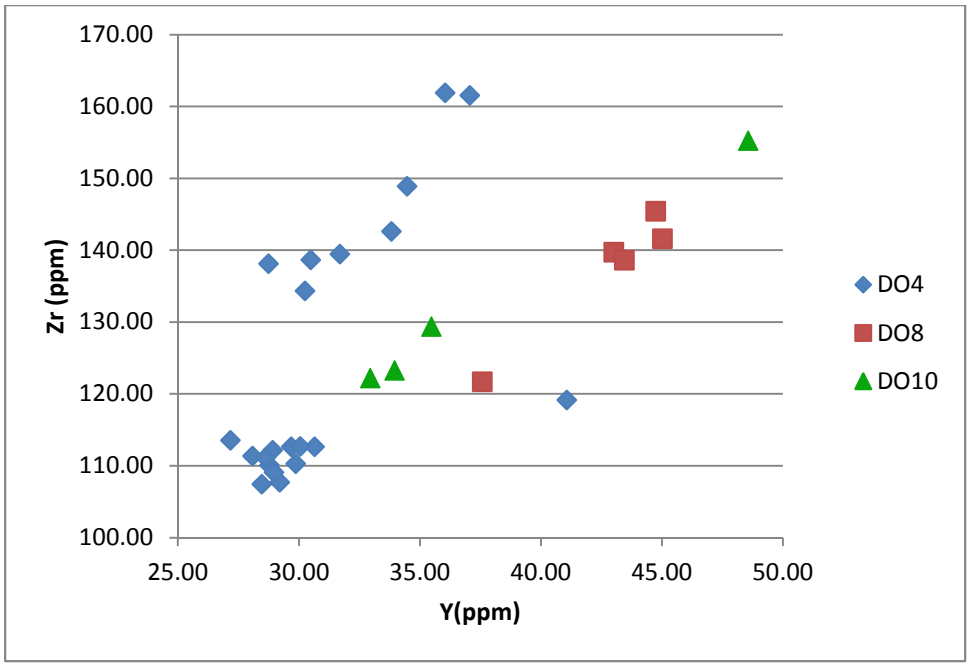

Figure 18: Plot of Zr against Y of the Secunda dolerites

3.4. Comparison with published Karoo dolerite data

The location of the study area (Figure 2) between the Drakensberg and Lebombo volcanic groups of the Karoo Igneous Province makes it crucial to understand the relationship between the DO4, DO8 and DO10 dolerites and these two volcanic terrains. The Drakensberg and Lebombo igneous sequences are most commonly referred to as a singular entity (the "Karoo Igneous Province"), although this flood basalt province has been divided into separate magma types based mainly on Ti content (Elburg and Goldberg, 2000; Mitha, 2006). High Ti material ("Lebombo") occurs in the central and western Lebombo-Save-Mwenezi monocline (see Figure 2), and low Ti material ("Drakensberg") is found in the Northern Lebombo-Save-Mwenezi monocline and the Southern and central Karoo regions (Elburg and Goldberg, 2000; Mitha, 2006).

The mineralogical composition of each magma type is nearly identical, containing plagioclase and pyroxene (Elburg and Goldberg, 2000; Mitha, 2006). The subtle variations are marked by the presence of minor olivine and apatite in the Karoo and Lebombo respectively (Elburg and Goldberg, 2000; Mitha, 2006). Thus, based solely on mineralogical parameters, both

the Karoo and Lebombo dolerites would be indistinguishable from the Secunda dolerites as described in chapter 2.

The Karoo and Lebombo groups have been subdivided into formations as seen in Table 7. The formations have unique geochemical characteristic and are most commonly separated by Ti-Zr enrichment and trace element ratios (Elburg and Goldberg, 2000; Duncan and Marsh, 2006 and Jourdan *et al.,* 2004). Average geochemical characteristics and groupings are shown in Tables 8 and 9 (after Duncan and Marsh, 2006), although it must be noted that the Sabie River, Lesotho, Barkly East and Letaba Formations are stratigraphically comparable but show unique geochemical characteristics

Table 7: Stratigraphic units of the Karoo Igneous province after Duncan and Marsh (2006)

Karoo Igneous Province			
Drakensberg Group		**Lebombo Group**	
Formation	*Rock type*	*Formation*	*Rock type*
		Movene	Basalt
		Mbuluzi	Rhyolite
		Jozini	Rhyodacite
Lesotho	Basalt	Sabie River	Basalt
Barkly East	Basalt	Letaba	Picritic Basalt
		Mashikiri	Nephelinite

Table 8: Average geochemical characteristics of the Drakensberg Group and its Fromations after Duncan and Marsh (2006)

Drakensberg Group									
	Barkly East Formation				**Lesotho Formation**				
n	(23)	(21)	(16)	(21)	(120)	(43)	(164)	(15)	(5)
SiO_2	54.69	52.95	52.67	53.28	51.74	51.80	51.67	52.10	51.31
TiO_2	0.88	1.03	1.01	1.04	0.95	0.96	1.06	1.30	1.53
Al_2O_3	15.37	16.13	16.03	15.29	15.67	15.53	15.62	14.51	14.12
FeO_{tot}	9.15	9.29	9.28	10.17	9.96	10.46	10.77	12.12	13.53
CaO	10.16	10.60	10.95	10.21	10.70	10.83	10.85	10.20	10.53
MgO	6.66	6.04	6.79	6.59	7.93	7.51	6.81	6.29	5.53
MnO	0.21	0.18	0.16	0.17	0.17	0.18	0.19	0.22	0.24
K_2O	0.54	1.06	0.69	0.71	0.58	0.64	0.67	0.83	0.51
Na_2O	2.14	2.47	2.26	2.38	2.14	2.16	2.17	2.22	2.51
P_2O_5	0.15	0.21	0.17	0.15	0.16	0.17	0.18	0.22	0.19

Ti/Y	0.03	0.04	0.04	0.04	0.04	0.04	0.04	0.04	0.05
Ti/Zr	0.01	0.01	0.01	0.01	0.01	0.01	0.01	0.01	0.01
Nb/Zr	0.04	0.11	0.11	0.03	0.08	0.08	0.07	0.07	0.05
TOTAL	99.95	99.96	100.01	99.99	100.00	100.24	99.99	100.01	100.00
Sc (ppm)	33	28	32	28	32	35	36	39	35
Cr (ppm)	269	279	353	265	322	255	211	180	104
Ni (ppm)	52	73	99	95	107	93	70	62	66
Rb (ppm)	20	19	52	19	11	12	12	18	12
Sr (ppm)	217	308	231	183	197	191	190	181	186
Y (ppm)	28	27	26	29	25	27	28	35	32
Zr (ppm)	119	145	107	138	81	98	98	121	118
Nb (ppm)	4.8	16.4	11.7	3.5	6.4	7.7	6.9	8.4	5.70
Ba (ppm)	173	250	194	281	183	207	218	260	35

Table 9: Average geochemical characteristics of the Lebombo Group and its Formations after Duncan and Marsh (2006)

Lebombo Group							
	Mashikiri Formation	**Letaba Formation**	**Sabie River Formation**			**Jozini Formation**	**Mbuluzi Formation**
			LTZ	HTZ	HTZ.HF		
n	(21)	(77)	(96)	(106)	(41)	(70)	(23)
SiO_2	44.90	50.11	52.35	52.95	50.88	70.47	71.46
TiO_2		2.86	1.74	3.19	3.72	0.55	0.52
Al_2O_3	13.23	8.73	14.61	13.39	12.87	12.84	12.53
FeO_{tot}	12.65	11.30	11.98	11.24	14.88	5.85	5.18
CaO	9.18	7.40	9.53	8.50	7.99	1.70	1.84
MgO	6.56	15.38	5.84	5.68	4.12	0.40	0.39
MnO	0.22	0.15	0.18	0.16	0.23	0.12	0.12
K_2O	2.05	1.83	0.74	1.99	1.63	4.65	4.45
Na_2O	6.92	1.60	2.76	2.36	2.76	3.27	3.40
P_2O_5	0.94	0.44	0.25	0.52	0.92	0.15	0.12
Ti/Y	0.00	0.11	0.05	0.08	0.06	0.00	0.00
Ti/Zr	0.00	0.01	0.01	0.01	0.01	0.00	0.00
Nb/Zr	0.58	0.06	0.06	0.06	0.09	0.08	0.09
TOTAL	96.65	99.80	99.98	99.98	100.00	100.00	100.01
Sc(ppm)	19	21	32	24	29	13	<5

Cr(ppm)	84	911	150	166	24	8	<5
Ni(ppm)	56	787	90	102	33	7	<5
Rb(ppm)	60	41	19	43	40	128	134
Sr(ppm)	1416	924	345	888	513	177	138
Y(ppm)	24	27	32	39	58	116	130
Zr(ppm)	226	352	144	384	402	1094	867
Nb(ppm)	131	20	8.3	22	36	85	74
Ba(ppm)	1757	849	260	836	678	1479	1268

The comparison between the major element compositions for the Karoo formations and the Secunda dolerites (Figures 20-22) show that the DO4 and DO10 Secunda dolerites can generally be grouped with the Barkly East, Lesotho and Sabie (LTZ) Formations. The DO8 dolerite Ti concentrations are relatively enriched, and plot at an intermediate level between the Lesotho and Letaba Formations of the Karoo Province, whereas the low MgO concentrations in the DO8 are comparable to that of the Sabie (HTZ-HF) Group's average value. Figure 22 shows that the DO8 dolerites are also low in Al_2O_3 relative to most of the Karoo data. The data points with low silica values in the DO4 dolerites do not match with any Karoo data.

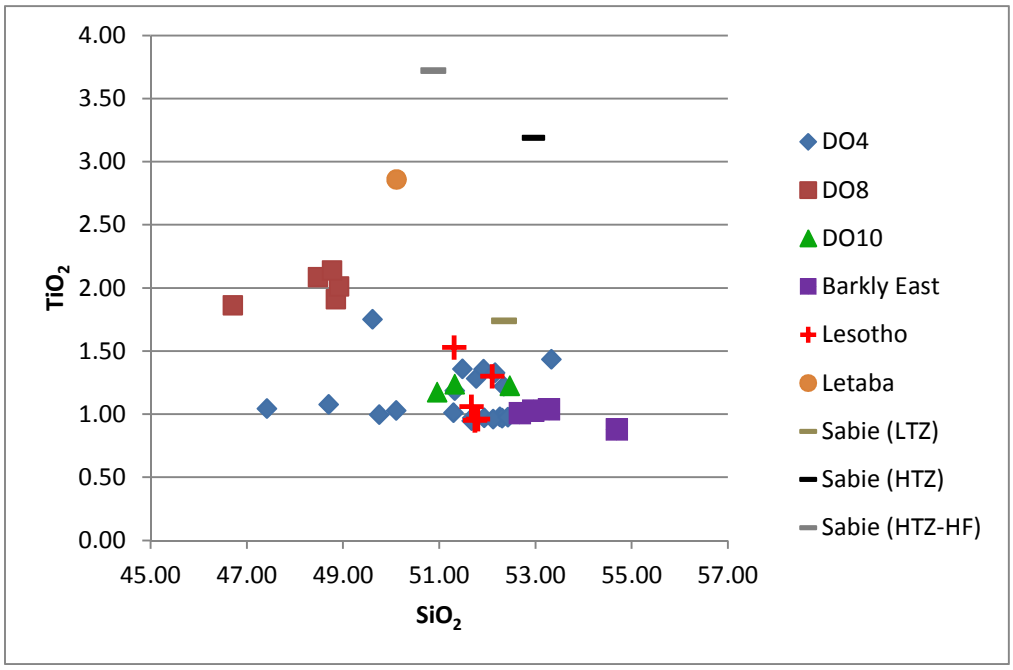

Figure 19 : Plot of TiO_2 against SiO_2 for the basaltic and picritic formations of the Karoo Igneous Province in relation to the Secunda dolerites.

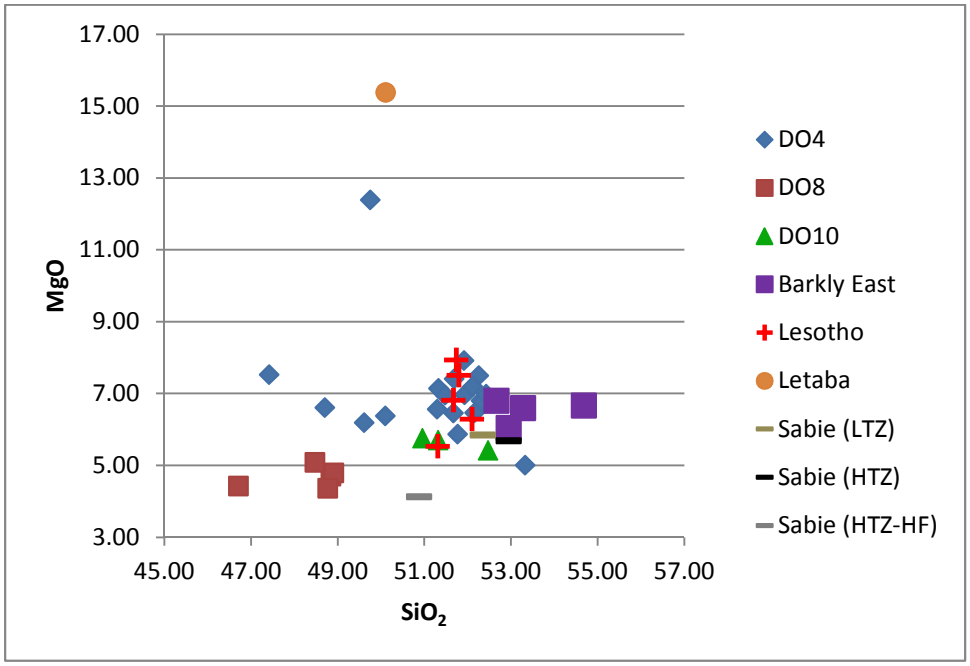

Figure 20: Plot of MgO against SiO_2 for the basaltic and picritic formations of the Karoo Igneous Province in relation to the Secunda dolerite

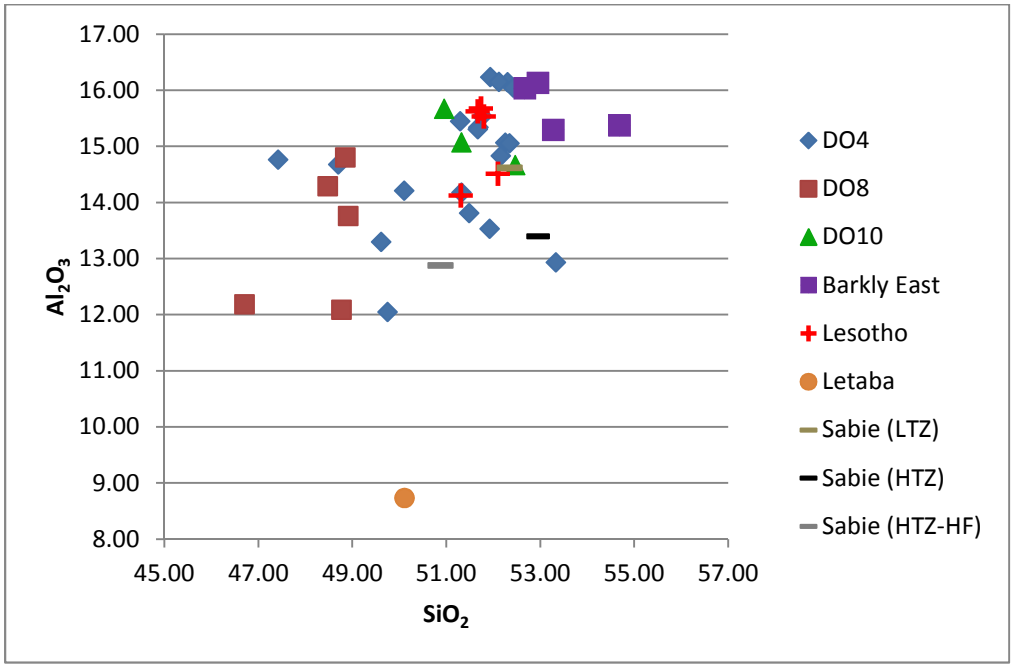

Figure 21: Plot of Al_2O_3 against SiO_2 for the basaltic and picritic formations of the Karoo Igneous Province in relation to the Secunda dolerites.

Trace element data from the different Karoo formations is plotted in Figures 23-25. These incompatible element variation diagrams can briefly be summarised as showing little variation between the Secunda dolerites and the Karoo formations, with only the DO8 dolerite showing relatively higher Y and Zr concentrations comparable to the Sabie (HTZ). The DO4 and DO10 dolerites show closer concentrations to that of the Lesotho, Sabie (LTZ) and Barkley East Formations.

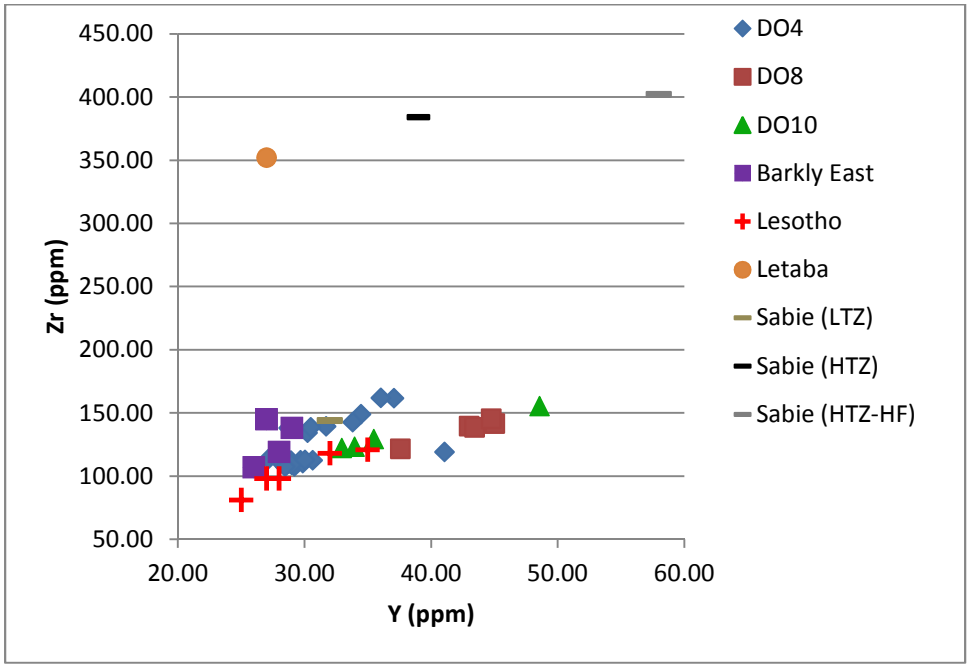

Figure 22: Plot of Zr against Y for the basaltic and picritic formations of the Karoo Igneous Province in relation to the Secunda dolerites.

.

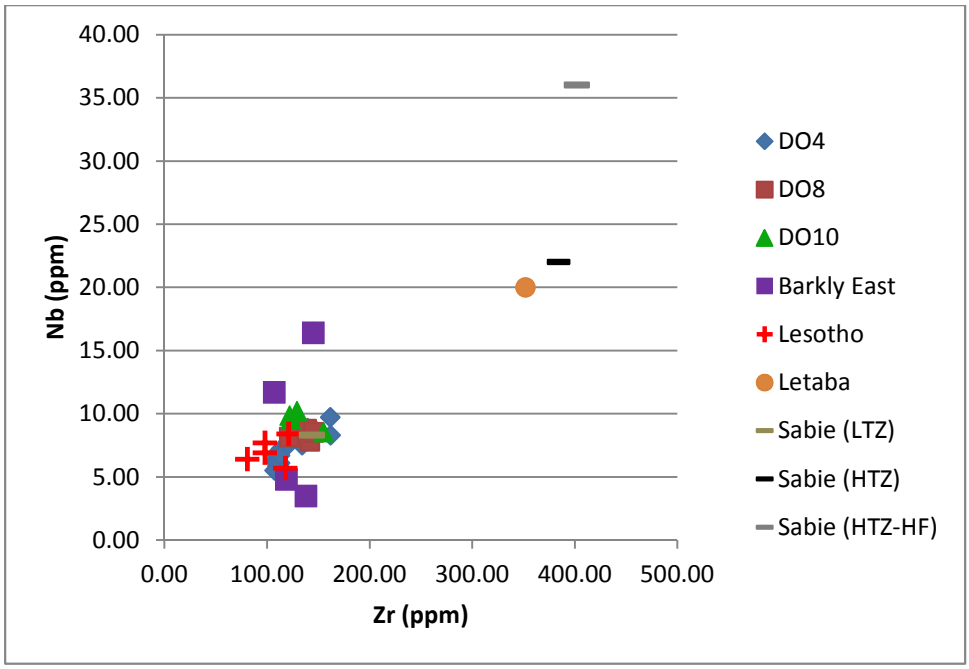

Figure 23: Plot of Nb against Zr for the basaltic and picritic formations of the Karoo Igneous Province in relation to the Secunda dolerites.

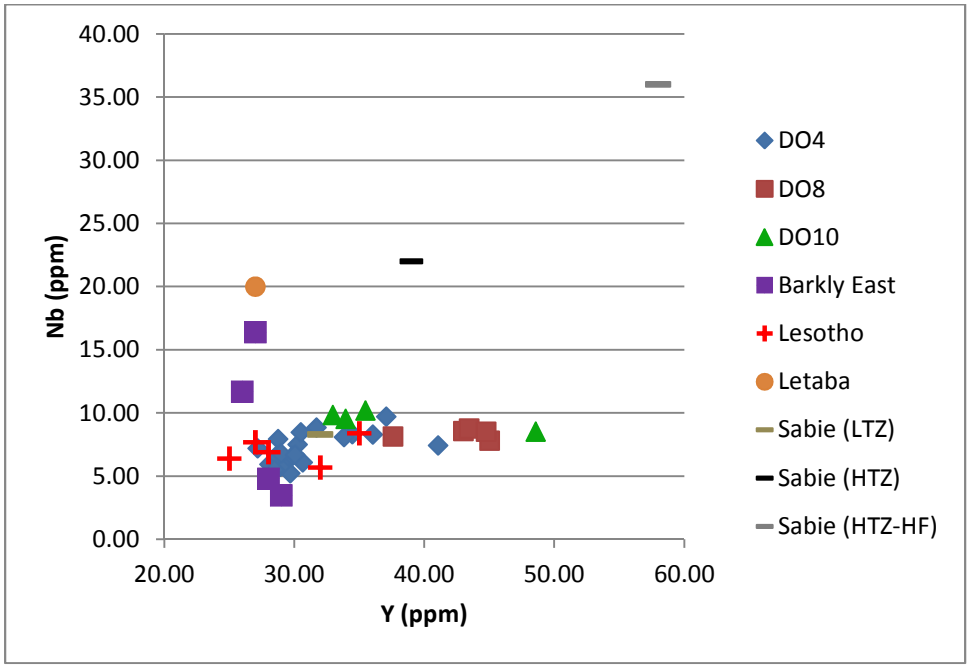

Figure 24: Plot of Nb against Y for the basaltic and picritic formations of the Karoo Igneous Province in relation to the Secunda dolerites.

One tool regularly used in dolerite geochemistry is the use of elemental ratios to improve the discrimination between magma types which have crystallised very similar mineralogy (Duncan & Marsh, 2006). Several of these diagrams are plotted here (Figures 26-29). The inter-element plots

shown in Figures 26 and 27 shows the Secunda dolerites having an increasing TiO_2/Y ratio as we move from DO4 to DO10 to DO8. The comparative plot in Figure 27 shows that the Secunda dolerite plot in line with the TiO_2/Y and MgO values of the Lesotho, Barkley East and Sabie (LTZ) Formations. The bivariant plots of Figures 28 and 29 show the DO8 dolerite with distinctly higher TiO_2/Zr values compared to both the Secunda dolerites and the Karoo Formations. The Zr/Nb values show interesting results in Figure 28, where the DO4, DO8 and DO10 show unique groupings. These groups are present in Figure 29 but are all comparable to the Zr/Nb values of the Lesotho and Sabie (LTZ) Formations.

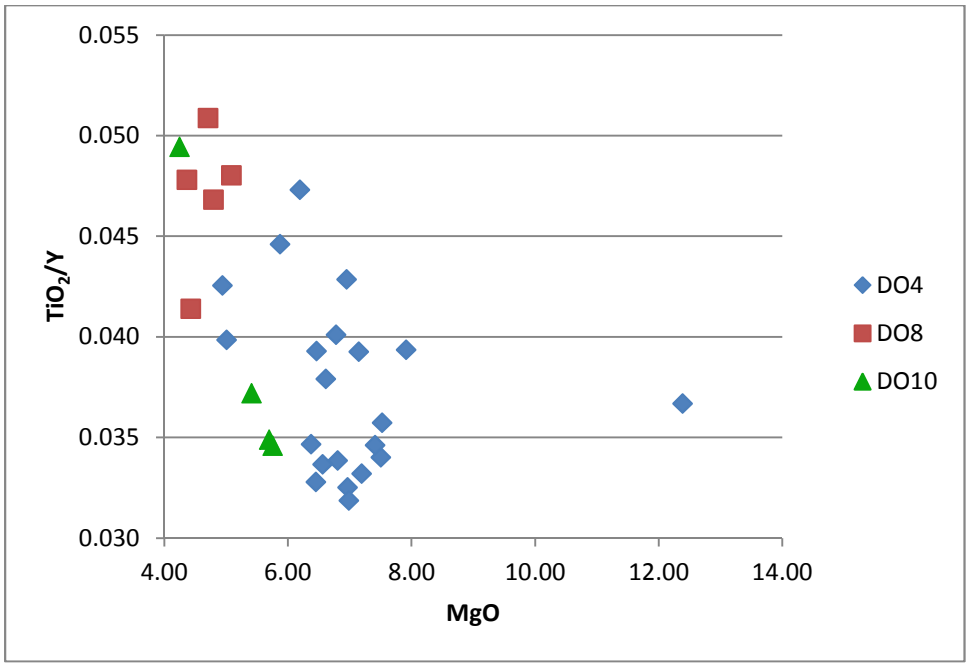

Figure 25: Plot of TiO_2/Y against MgO of the Secunda dolerites

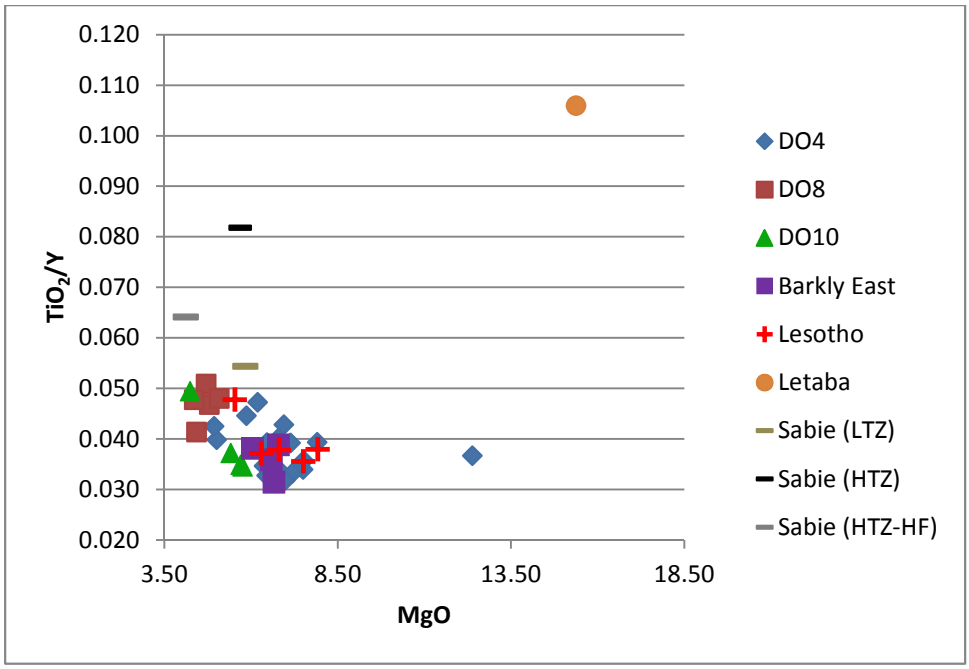

Figure 26: Plot of TiO_2/Y against MgO for the basaltic and picritic formations of the Karoo Igneous Province in relation to the Secunda dolerites.

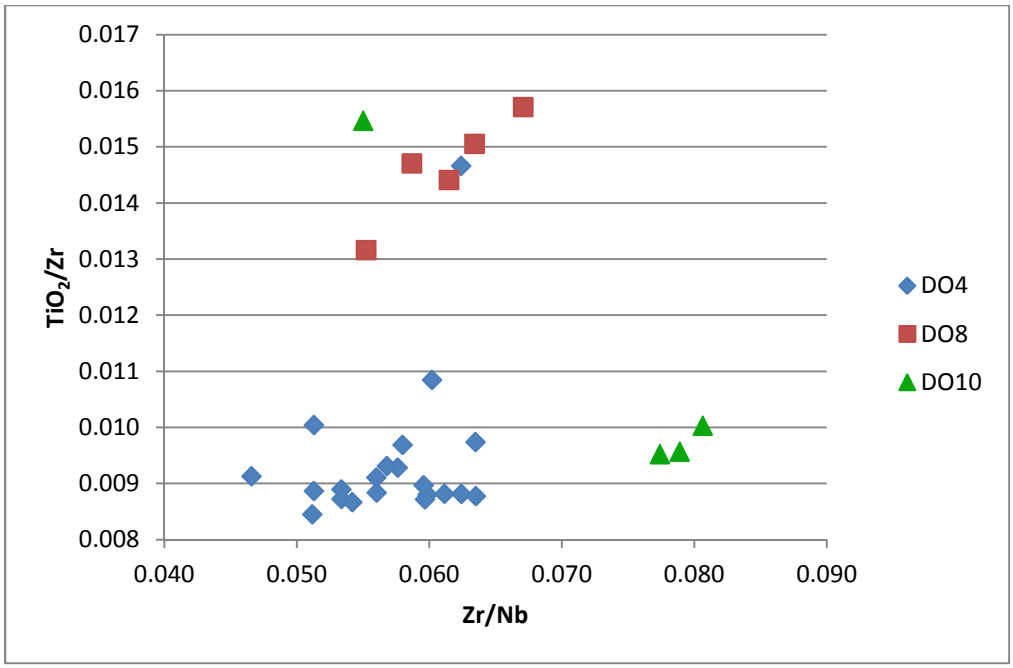

Figure 27: Plot of TiO_2/Zr against Zr/Nb of the Secunda dolerites

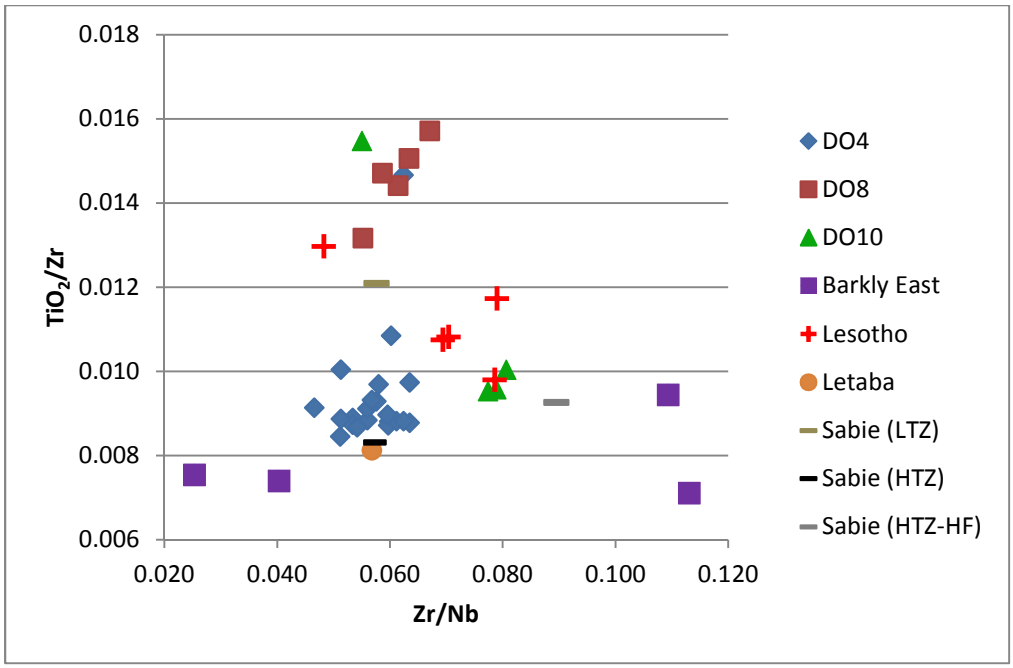

Figure 28: Plot of TiO_2/Zr against Zr/Nb for the basaltic and picritic formations of the Karoo Igneous Province in relation to the Secunda dolerites.

3.5. Conclusions

In summary, the major and trace element data are sufficient to distinguish between the three different dolerites in the Sasol Mining Area in Secunda. Major elements show that the DO8 dolerites are readily distinguishable from the DO4 and DO10 dolerites, whereas the DO4 and DO10 dolerites are inseparable on their major element geochemistry. The DO4 dolerites are the most variable, possibly owing to surficial alteration. Incompatible trace elements are able to distinguish between the DO4 and DO10 dolerites, on the basis of low Nb, Zr, and Yr concentrations in the DO4 dolerites. The geochemical relationship of the Secunda dolerites shows that the three dolerites have some unique geochemical characteristics but these characteristics are in line with the average geochemistry of the Karoo Igneous Province. The analysis showed the DO4 and DO10 Secunda dolerites are conformable with the Barkley East, Sabie (LTZ) and Lesotho Formations, whereas the DO8 dolerites plot slightly differently to all known Karoo dolerites.

CHAPTER 4: COAL QUALITY AND DOLERITE PROXIMITY

The metamorphic effect of Karoo-aged igneous intrusions on coal has previously been studied by authors such as Fredericks *et al.,* (1985); Golad and Carr, (2004) and many others, in which the thermal metamorphic effects of a single intrusive contact with coal was studied intensively. The approach adopted in this study is one where three specific dolerite types were selected to investigate their effect on a single coal seam over a large area.

4.1. Dolerite selection and sampling

Evaluation of the possible effects of dolerite proximity on the main C4 lower coal seam was approached by identifying trends within existing data. An initial data set was obtained from Sasol Secunda, which contained ~15 000 borehole logs listing:

- Dolerite type
- Dolerite thickness
- Dolerite position
- Coal seam thickness
- Coal seam position
- Proximate analysis values for DAFV, Vols and Ash
- Geographic coordinates

The data set was filtered and modelled to obtain parameters specific to the DO4, DO8 and DO10 dolerites. The filtering process removed all logs where coal was intercalated with sediments to obtain a representative value for the effect of the dolerites on the coal. The initial ~15 000 boreholes were filtered to ~8000 which contained only the three dolerites under investigation. Each borehole contained only one of the dolerite types under investigation. The filtered data set was separated as follows:

- 3145 Holes intersecting only D04
- 4663 Holes intersecting only DO8
- 116 Holes intersecting only DO10

4.2. Dolerite and coal evaluation

The effect of intrusive dolerites have on the coal seam is represented by the proximate analysis of coal samples and with three main parameters used to define the level of devolatilization:

1. Ash content (Ash)

   The ash content value represents the volumetric amount of inorganic material within the coal after combustion (Speight, 2005). This value is highly affected by intercalations of other sedimentary material which raises the value.

2. Volatile content (Vols)

   The volatile content value is the percentage of volatile products excluding water vapour released during the combustion of the coal under specific conditions (Speight, 2005). This measures the amount of volatile content within the coal. Thus if the volatile products have been expelled prior to this test the coal can be termed as devolatilized (Speight, 2005).

3. Dry ash free volatile value (DAFV)

   The DAFV value is a measure of the heating value of the coal with all moisture removed; this value is easily affected by dolerite thermal interaction (Speight, 2005).

In the coal mining industry in South Africa, dolerites are held to have a thermo-metamorphic effect on coal which decreases the DAFV value, and thus this parameter is a good value to estimate the possible relationship between coal quality and dolerite proximity, what is often termed the "level of devolatilization" caused by the dolerite intrusion. Quantitative values for the three quality parameters have been classified by Sasol as follows:

- DAFV: < 26 = Devolatilized 28 > DAFV >26 dependent on other parameters
- Vols: < 16 = Devolatilized when not intercalated with other sedimentary material
- Ash: > 36% = Devolatilized when not intercalated with other sedimentary material

A note must be made that the DAFV value is the most diagnostic value as it is independent of the sedimentary intersections or inclusions within the coal seam as some samples may include sedimentary boundaries which dramatically affect the ash and volatile content.

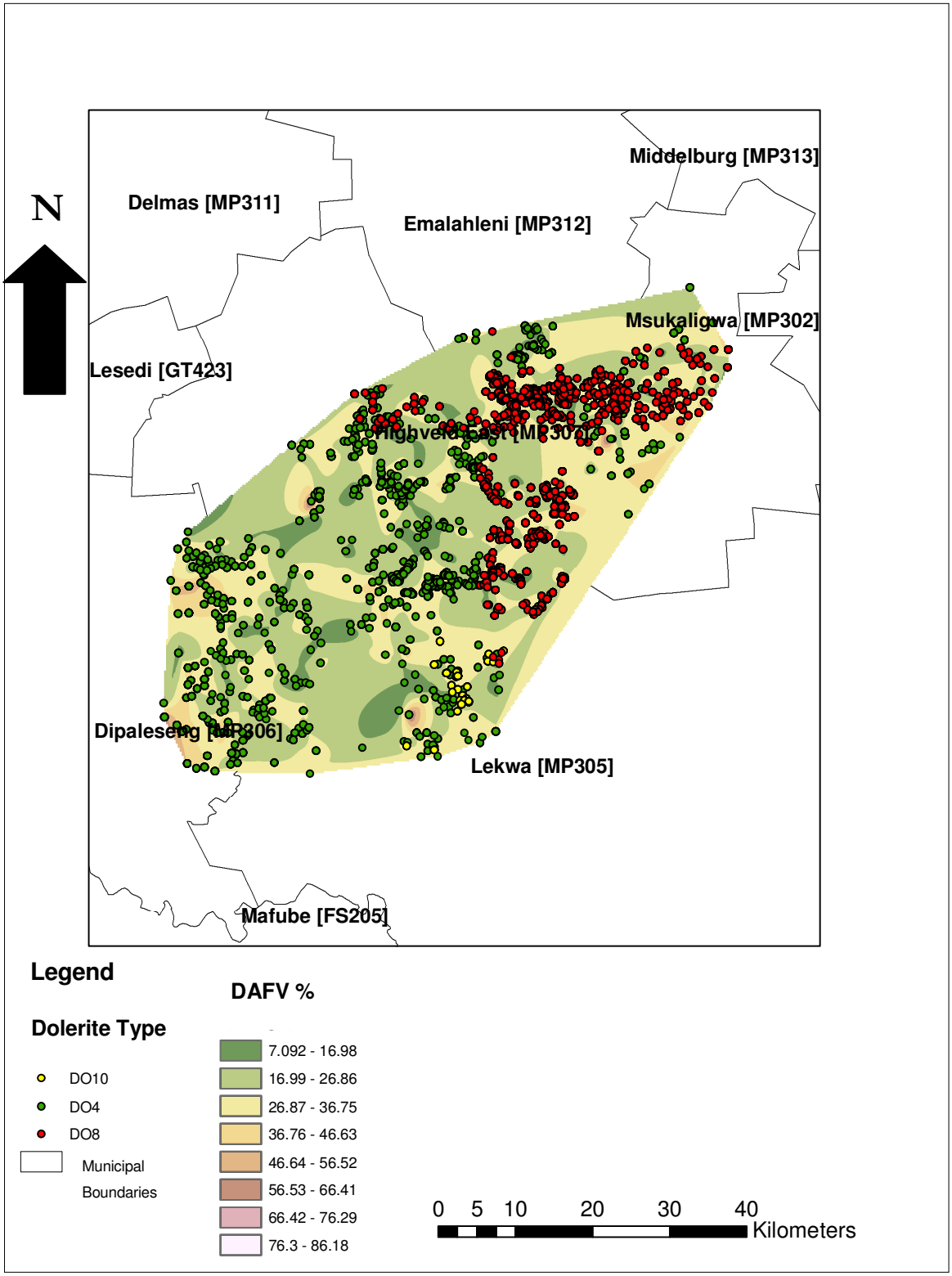

Figure 29: DAFV concentration of the C4 Lower coal seam in comparison to dolerite type and geographic position. Note that the numbers following area names are the municipal area codes.

4.2.1 Coal quality and the proximity of dolerite intrusions

The map above (Figure 30) was compiled using ARC GIS 9.3, with the spatial analyst tool box. The map data is derived from the Sasol coal and dolerite data tables in the Appendix. All interpolated surfaces use the Natural Neighbour interpolation function and display surfaces which are resampled from nearest neighbour (for discrete data).

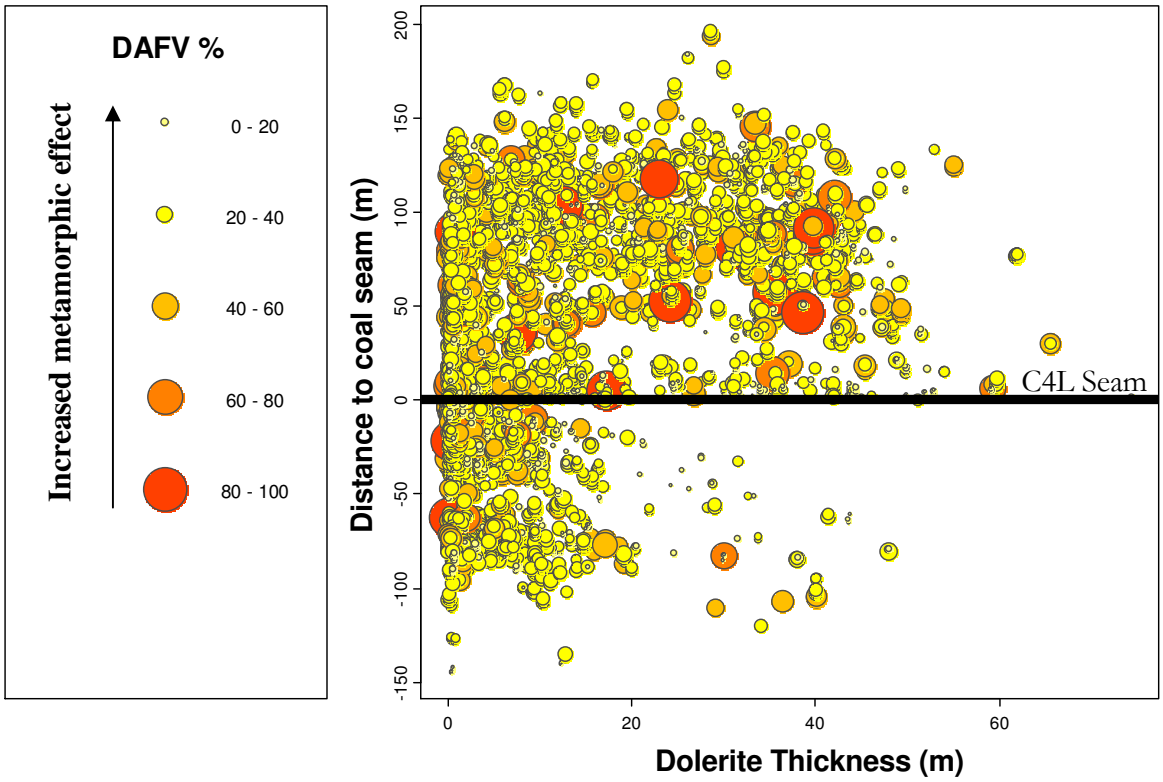

Figure 30: Coal dry ash free volatile percentage in relation to the thickness of dolerite and the interval between the dolerite and the coal seam for the DO4, DO8 and DO10 dolerite types

Figure 31 and 32 are graphical representations of the three components DAFV, distance from the C 4 lower coal seam and the thickness of the dolerite sill at that point. Figure 32 displays DAFV values at progressively smaller intervals away from the C4L coal seam. The DAFV value is represented by the size and colour of the circles on the plot with the smaller lighter colours representing lower quality coal. Figures 31 and 32 display no trends with regard to DAFV value, thickness of dolerite or distance between the dolerite and the coal seam.

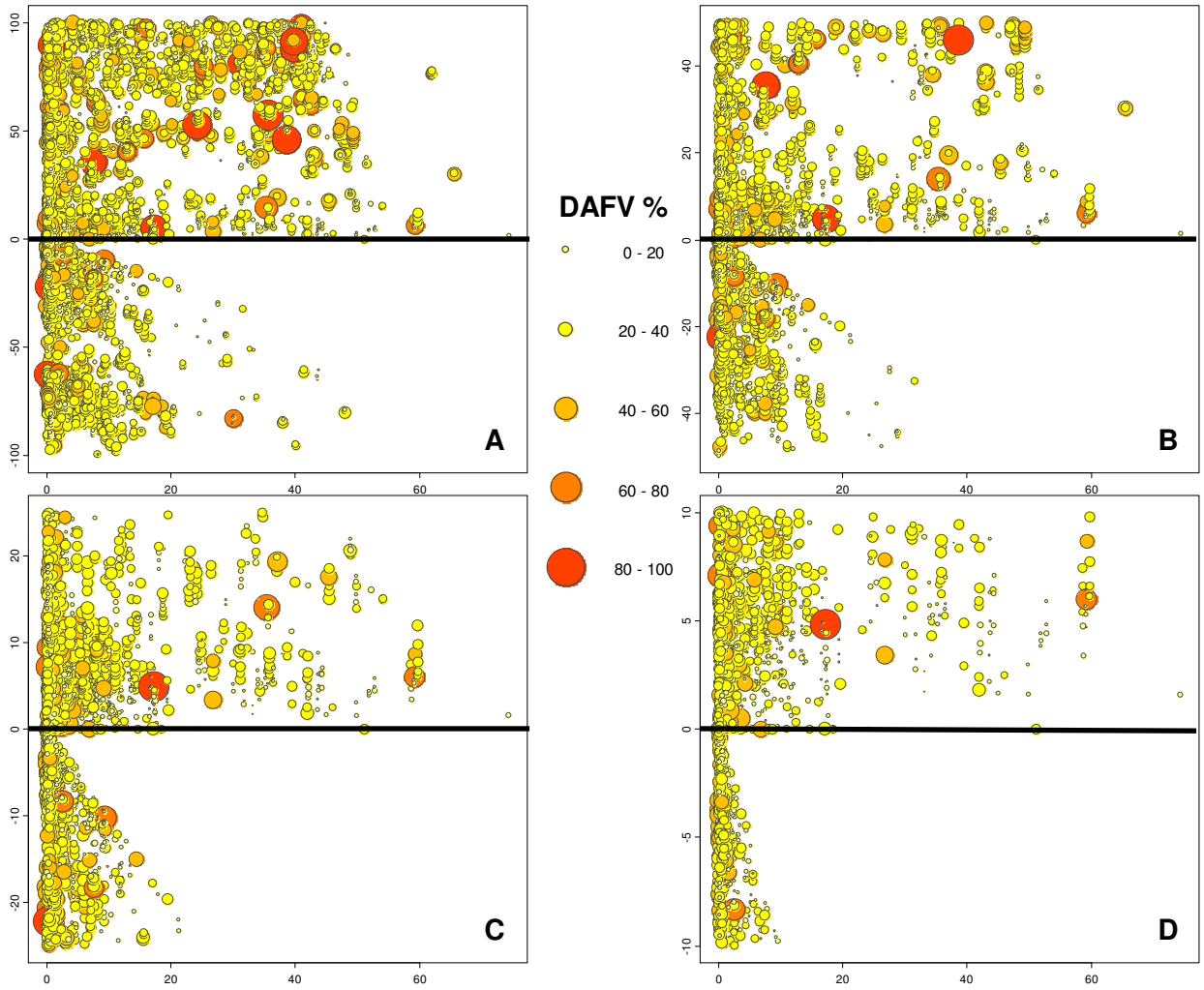

Figure 31: Coal DAFV percentage in relation to the thickness of dolerite and the interval between the dolerite and the coal seam for the DO4, DO8 and DO10 dolerite types. A shows data for dolerites within a maximum of 100m, B shows data for dolerites within a maximum of 50m, C shows data for dolerites within a maximum of 25m and C shows data for dolerites within a maximum of 10m

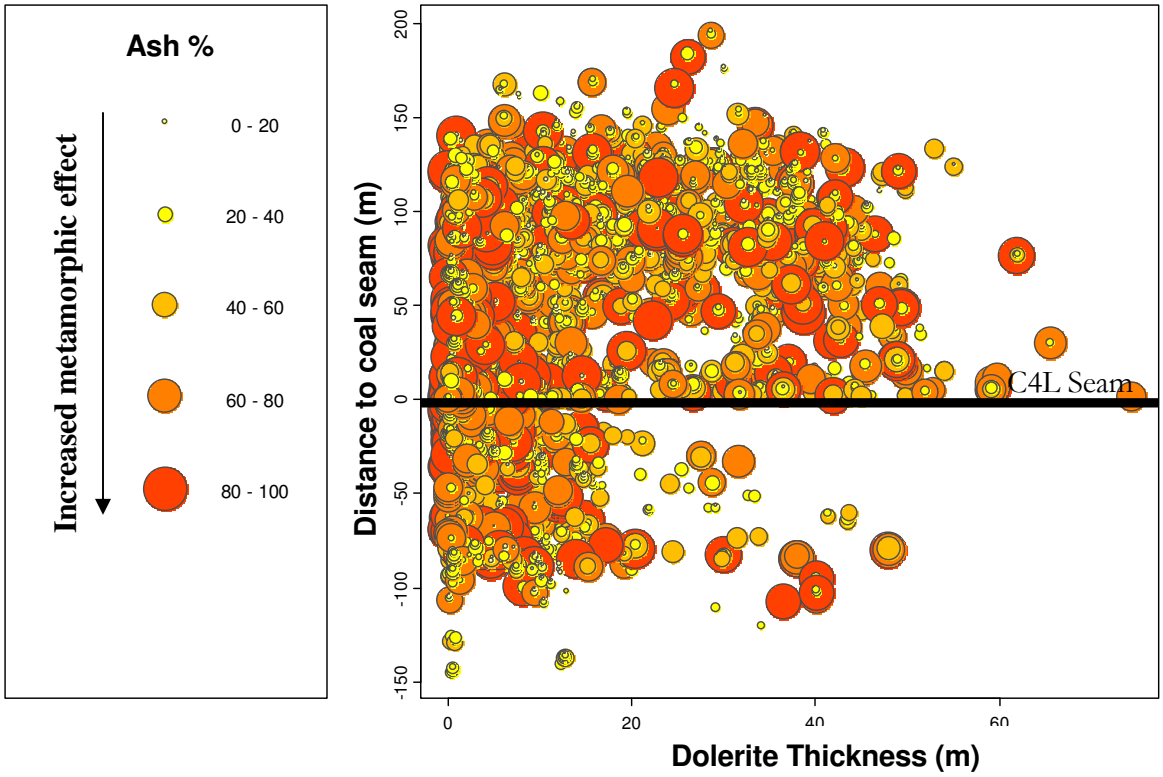

Figure 32: Coal ash percentage in relation to the thickness of dolerite and the interval between the dolerite and the coal seam for the DO4, DO8 and DO10 types

Figures 33 and 34 display the ash content of the coal in relation to the position and thickness a dolerite is from the C 4 lower coal seam. Figure 34 displays ash values at progressively smaller intervals away from the C4L coal seam. The larger and darker circles in the plots reflect increases of inorganic matter percentage within the coal samples. Figures 33 and 34 display no trends with regard to ash value, thickness of dolerite or distance the dolerite is from the coal seam.

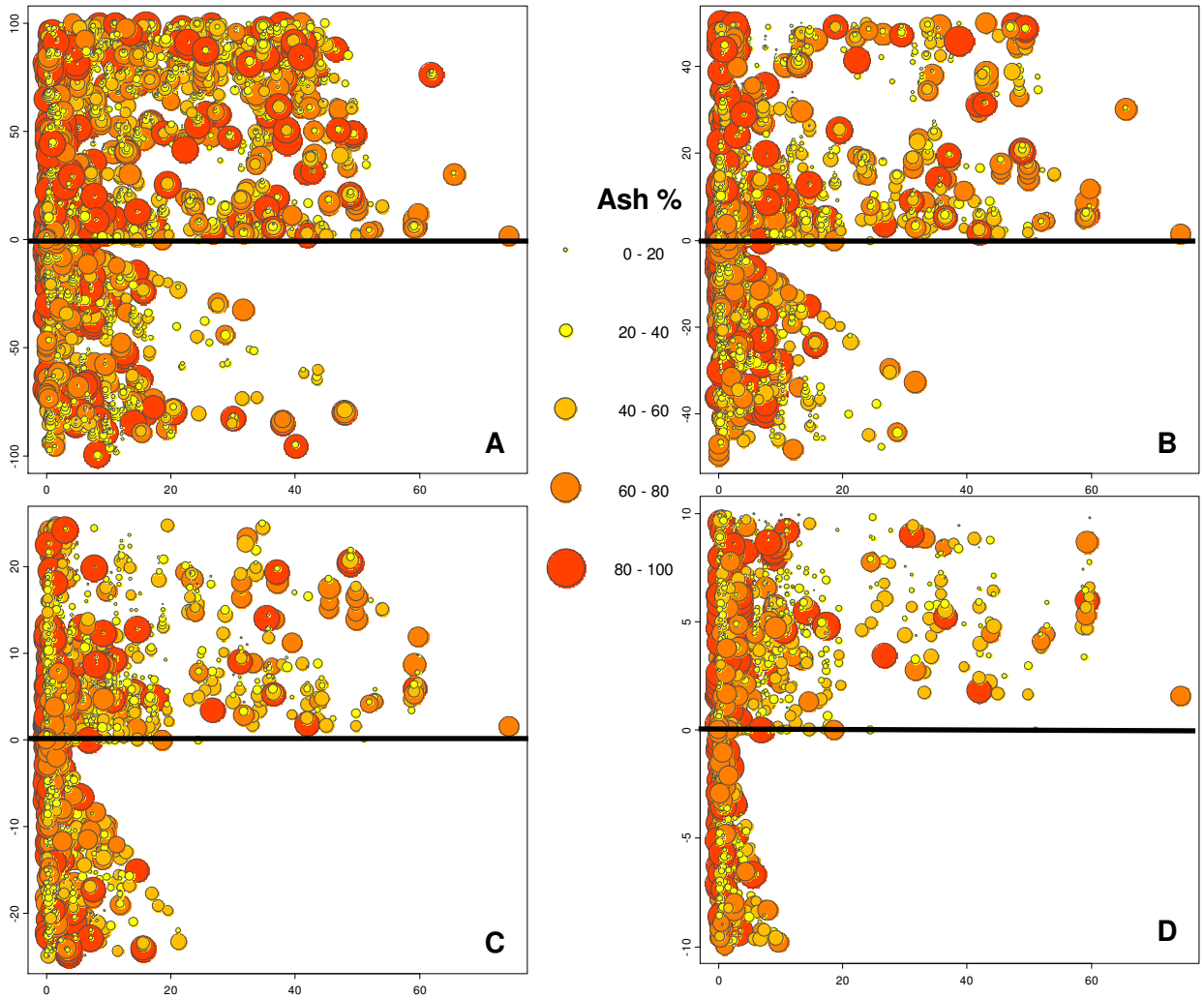

Figure 33: Coal Ash percentage in relation to the thickness of dolerite and the interval between the dolerite and the coal seam for the DO4, DO8 and DO10 types. A shows data for dolerites within a maximum of 100m, B shows data for dolerites within a maximum of 50m, C shows data for dolerites within a maximum of 25m and C shows data for dolerites within a maximum of 10m

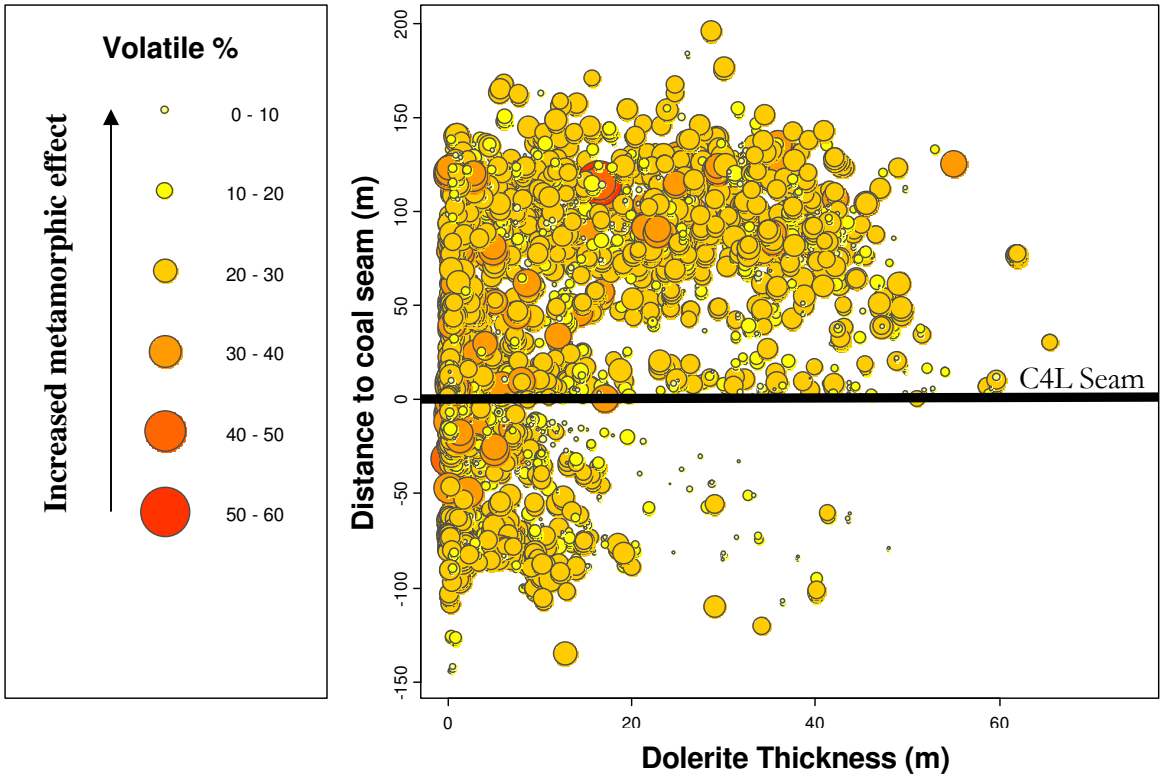

Figure 34: Coal Volatile percentage in relation to the thickness of dolerite and the interval between the dolerite and the coal seam for the DO4, DO8 and DO10 types.

Figures 35 and 36 graphically display the volatile content within coal samples in relation to the position and thickness a dolerite is from the C 4 lower coal seam with Figure 36 displaying volatile values at progressively smaller intervals away from the C4L coal seam. The smaller and lighter the circles within the plot, the lower the quality of coal the coal. Figures 35 and 36 display no trends with regard to the volatile content value, thickness of dolerite or distance the dolerite is from the coal seam.

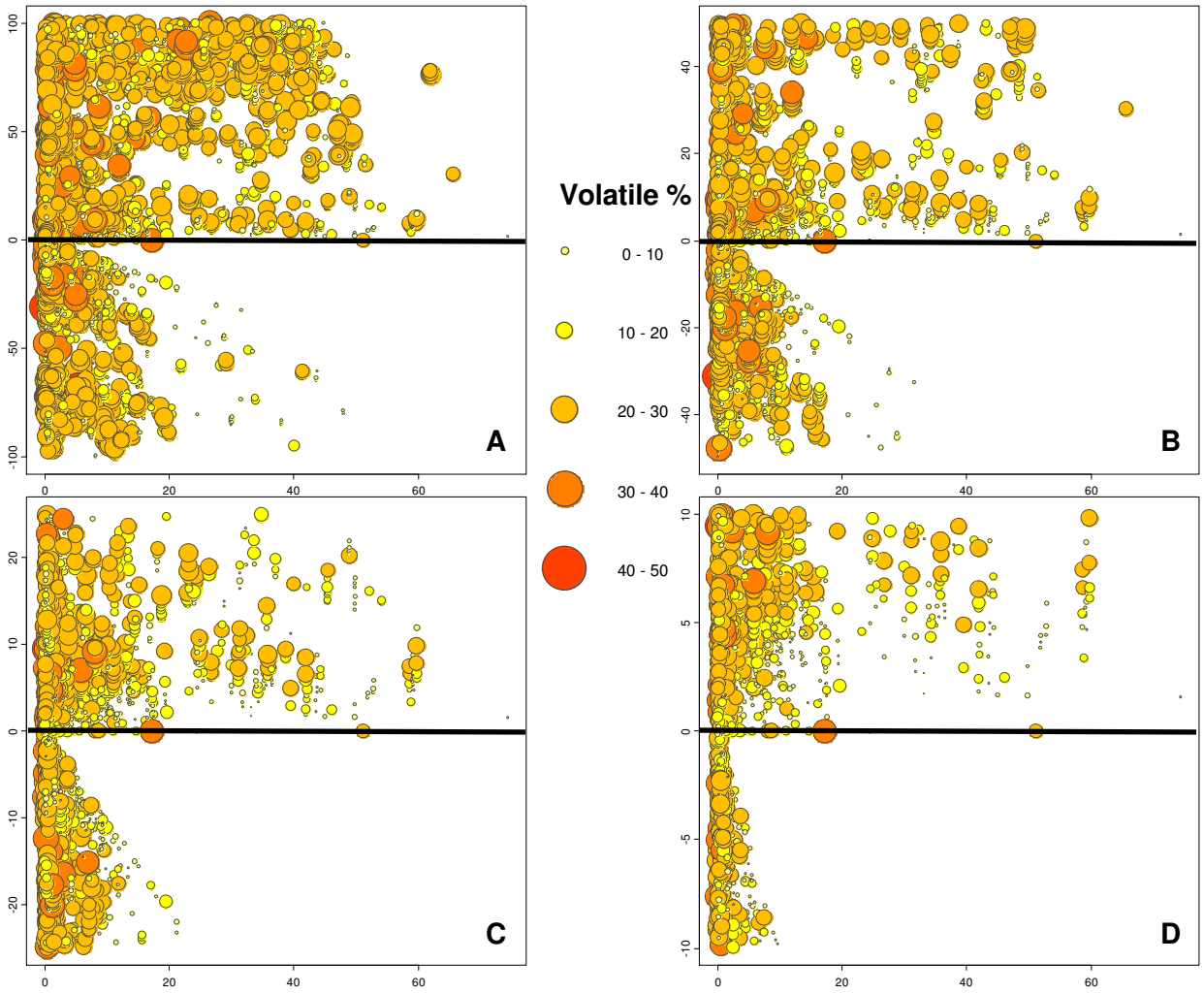

Figure 35: Coal volatile percentage in relation to the thickness of dolerite and the interval between the dolerite and the coal seam for the DO4, DO8 and DO10 types. A shows data for dolerites within a maximum of 100m, B shows data for dolerites within a maximum of 50m, C shows data for dolerites within a maximum of 25m and C shows data for dolerites within a maximum of 10m

4.2.3 The DO4 dolerite and coal quality

The data plotted below shows only the coal quality data associated with DO4 dolerites.

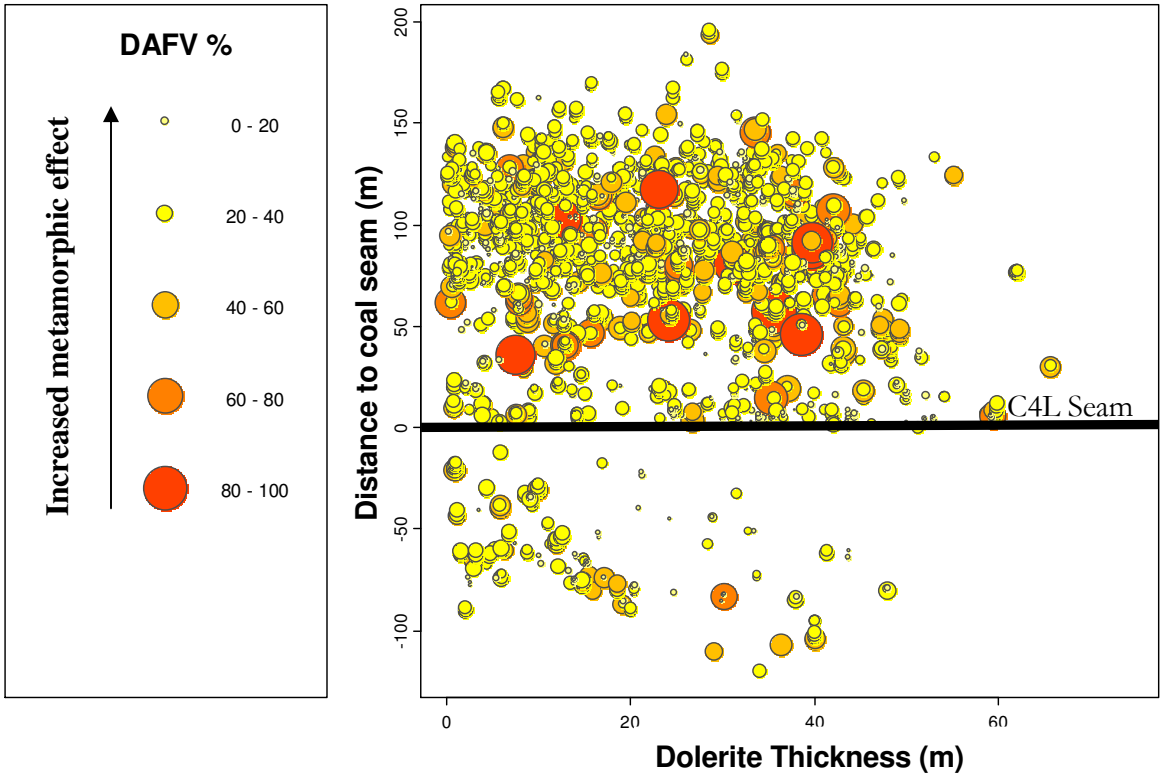

Figure 36: Coal dry ash free volatile percentage in relation to the thickness of dolerite and the interval between the dolerite and the coal seam for the DO4 dolerite

Figure 37 is a graphical representation of the three components DAFV, distance from the C 4 lower coal seam and the thickness of the dolerite sill at that point. The DAFV value is represented by the size and colour of the circles on the plot with the smaller lighter colours representing lesser quality coal. The DO4 dolerite is concentrated above the coal seam, but the figure displays no trends with regard to DAFV value, thickness of dolerite or distance the dolerite is from the coal seam.

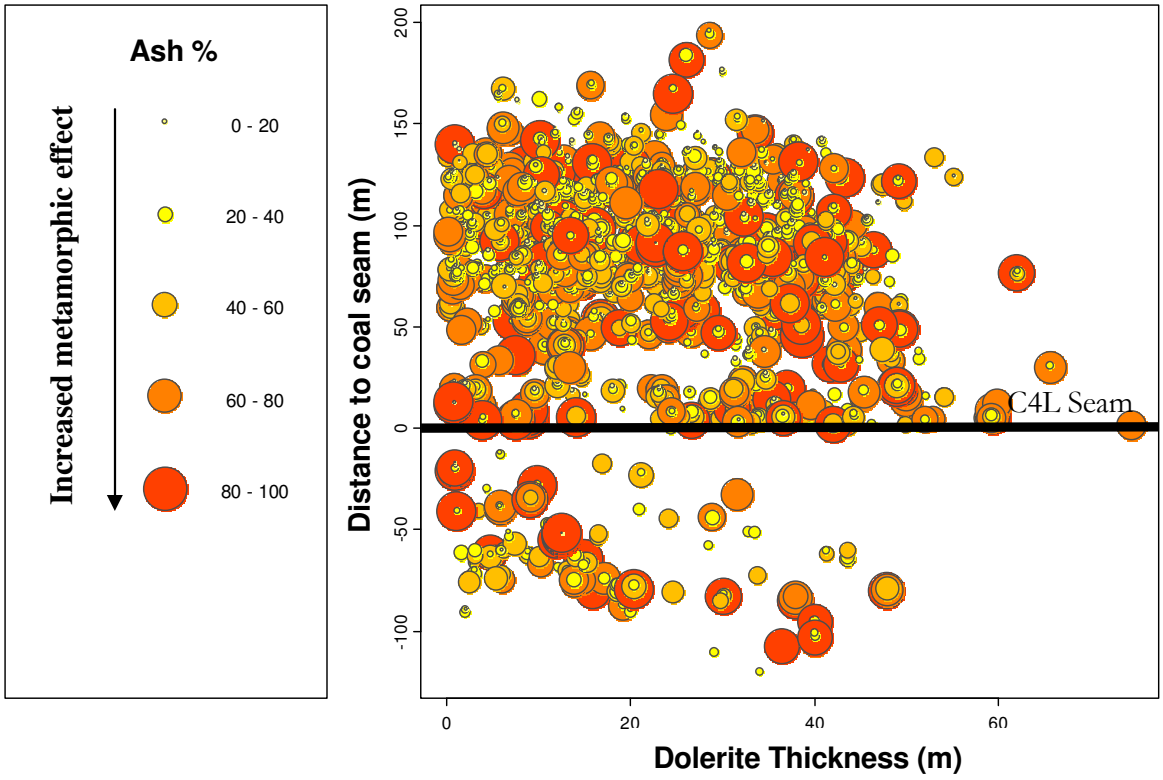

Figure 37: Coal Ash percentage in relation to the thickness of dolerite and the interval between the dolerite and the coal seam for the DO4 dolerite

Figure 38 displays the ash content of the coal in relation to the position and thickness a dolerite is from the C 4 lower coal seam. The larger and darker the circle in the plot reflects a greater increase of inorganic matter percentage within the coal sample. The figure displays no trends with regard to ash value, thickness of dolerite or distance the dolerite is from the coal seam.

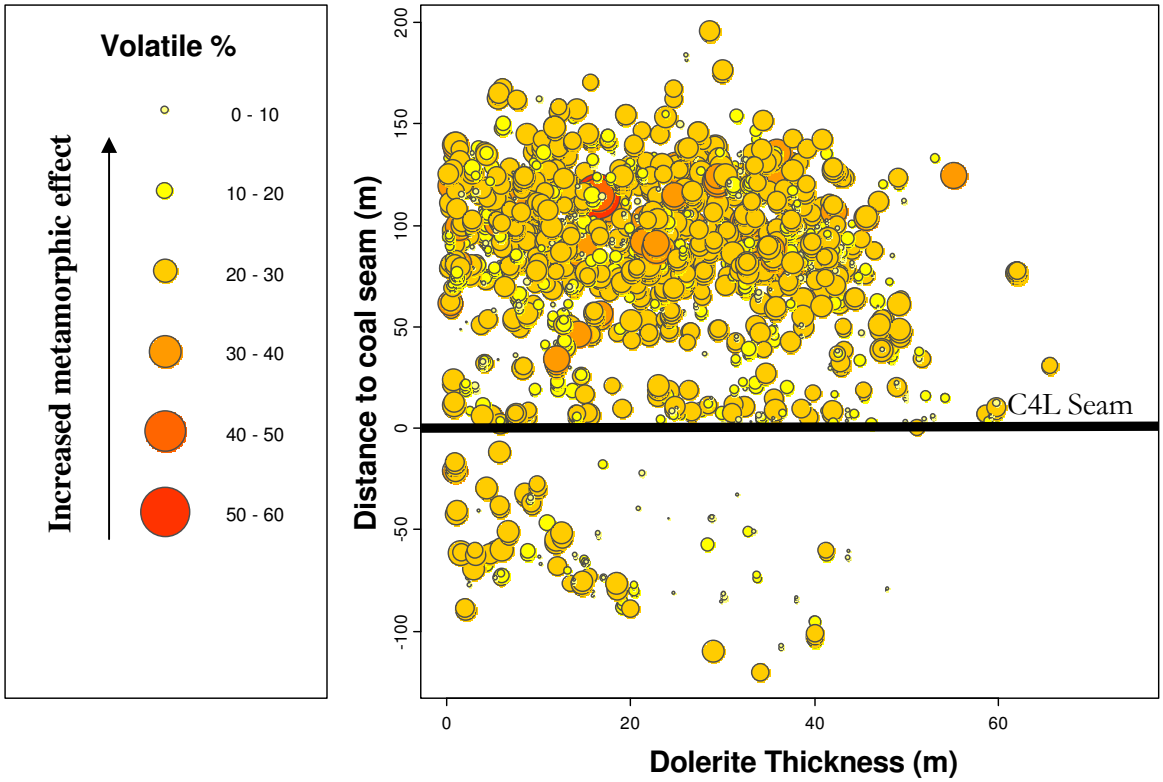

Figure 38: Coal volatile percentage in relation to the thickness of dolerite and the interval between the dolerite and the coal seam for the DO4 dolerite

Figure 39 graphically displays the volatile content within coal samples in relation to the position and thickness a dolerite is from the C 4 lower coal seam. The smaller and lighter the circles within the plot, the lesser the quality of coal the coal. The figure displays no trends with regard to volatile content value, thickness of dolerite or distance the dolerite is from the coal seam.

4.2.4 The DO8 dolerite and coal quality

The data plotted below shows only the coal quality data associated with DO8 dolerites.

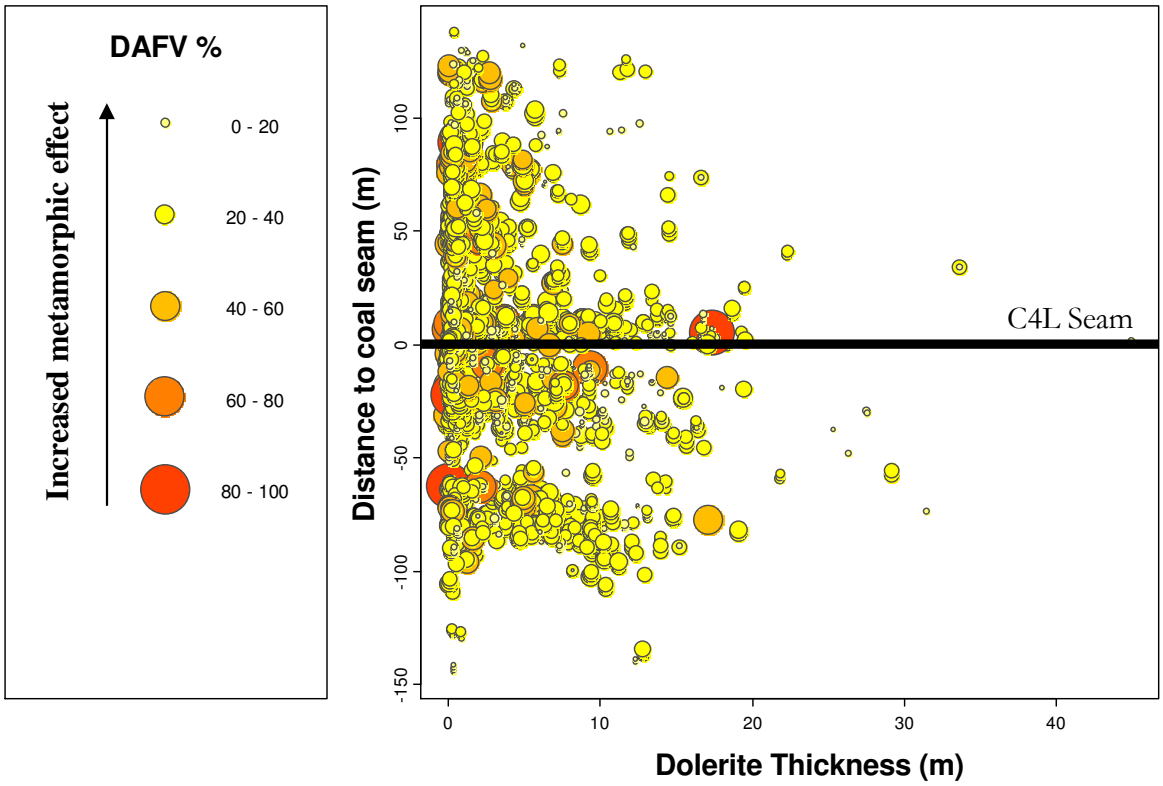

Figure 39: Coal dry ash free volatile percentage in relation to the thickness of dolerite and the interval between the dolerite and the coal seam for the DO8 dolerite

Figure 40 is a graphical representation of the three components DAFV, distance from the C 4 lower coal seam and the thickness of the dolerite sill at that point. The DAFV value is represented by the size and colour of the circles on the plot with the smaller lighter colours representing lesser quality coal. The DO8 dolerite has a highly variable position occurring both above and below the coal seam. However the figure displays no trends with regard to DAFV value, thickness of dolerite or distance the dolerite is from the coal seam.

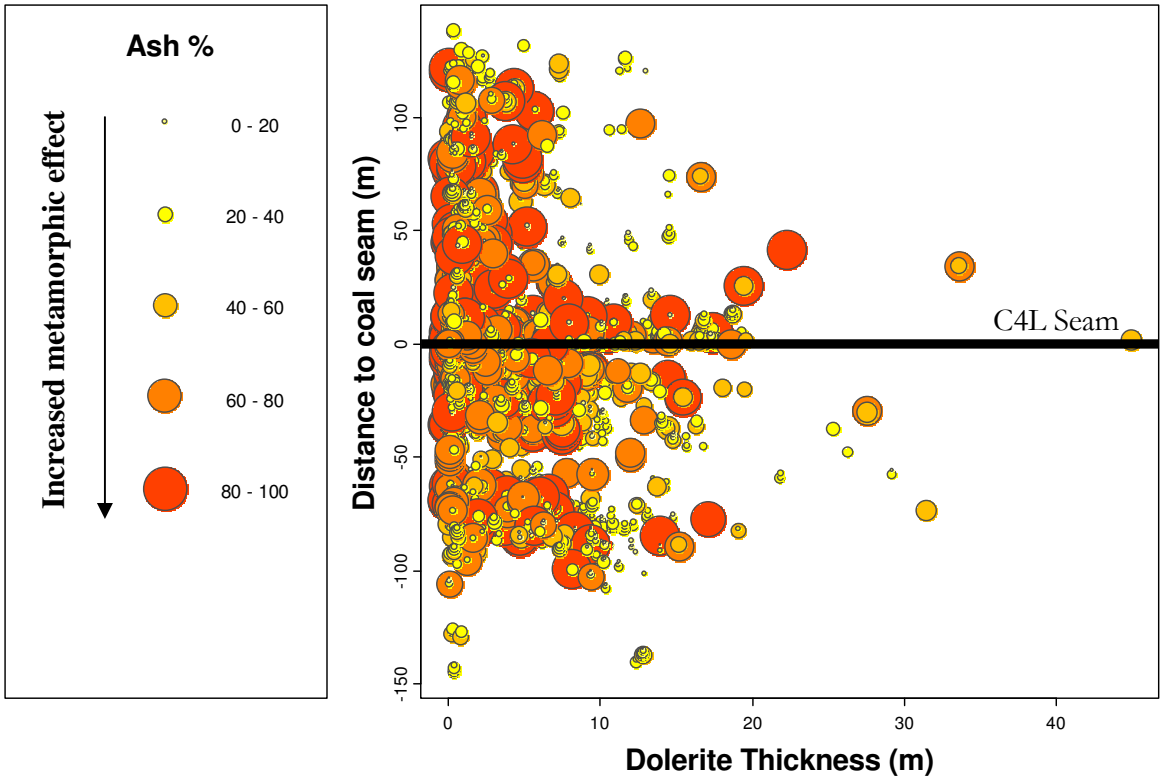

Figure 40: Coal ash percentage in relation to the thickness of dolerite and the interval between the dolerite and the coal seam for the DO8 dolerite

Figure 41 displays the ash content of the coal in relation to the position and thickness a dolerite is from the C4 lower coal seam. The larger and darker the circle in the plot reflects a greater increase of inorganic matter percentage within the coal sample. The figure displays no trends with regard to ASH value, thickness of dolerite or distance the dolerite is from the coal seam.

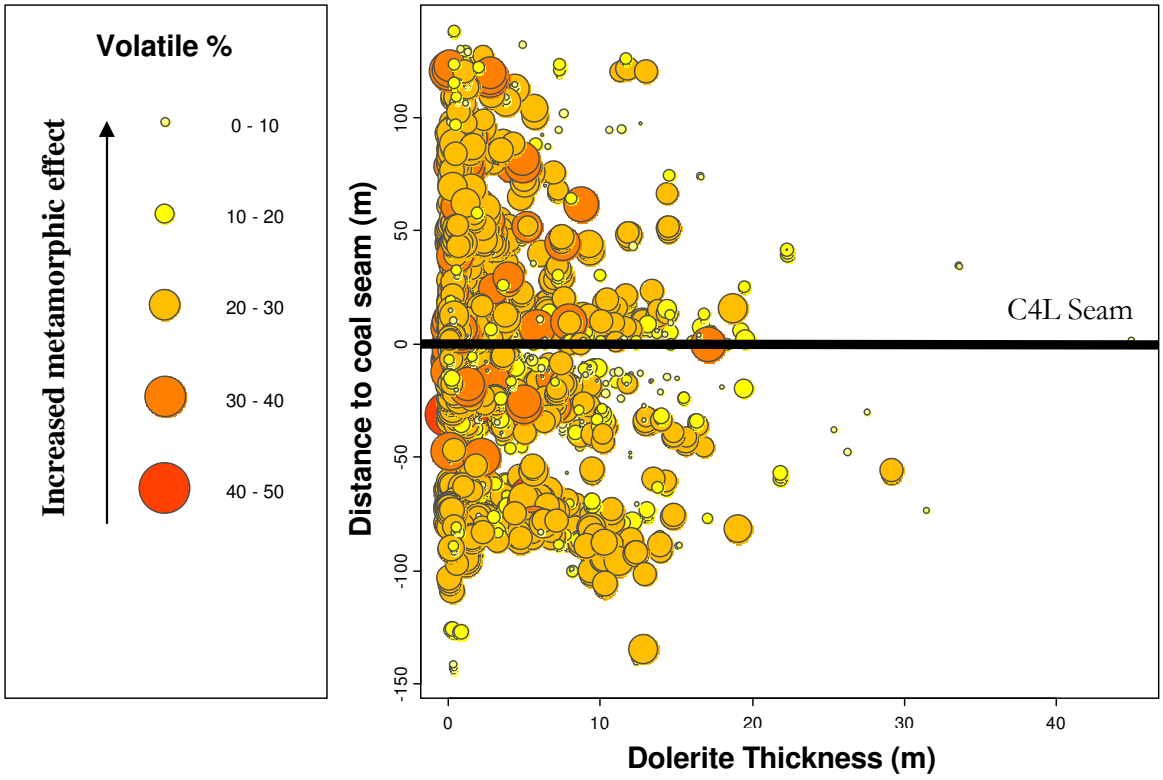

Figure 41: Coal Volatile percentage in relation to the thickness of dolerite and the interval between the dolerite and the coal seam for the DO8 dolerite

Figure 42 graphically displays the volatile content within coal samples in relation to the position and thickness a dolerite is from the C 4 lower coal seam. The smaller and lighter the circles within the plot, the lesser the quality of coal the coal. The figure displays no trends with regard to the Vols value, thickness of dolerite or distance the dolerite is from the coal seam.

4.2.5 The DO10 dolerite and coal quality

The data plotted below shows only the coal quality data associated with DO10 dolerites.

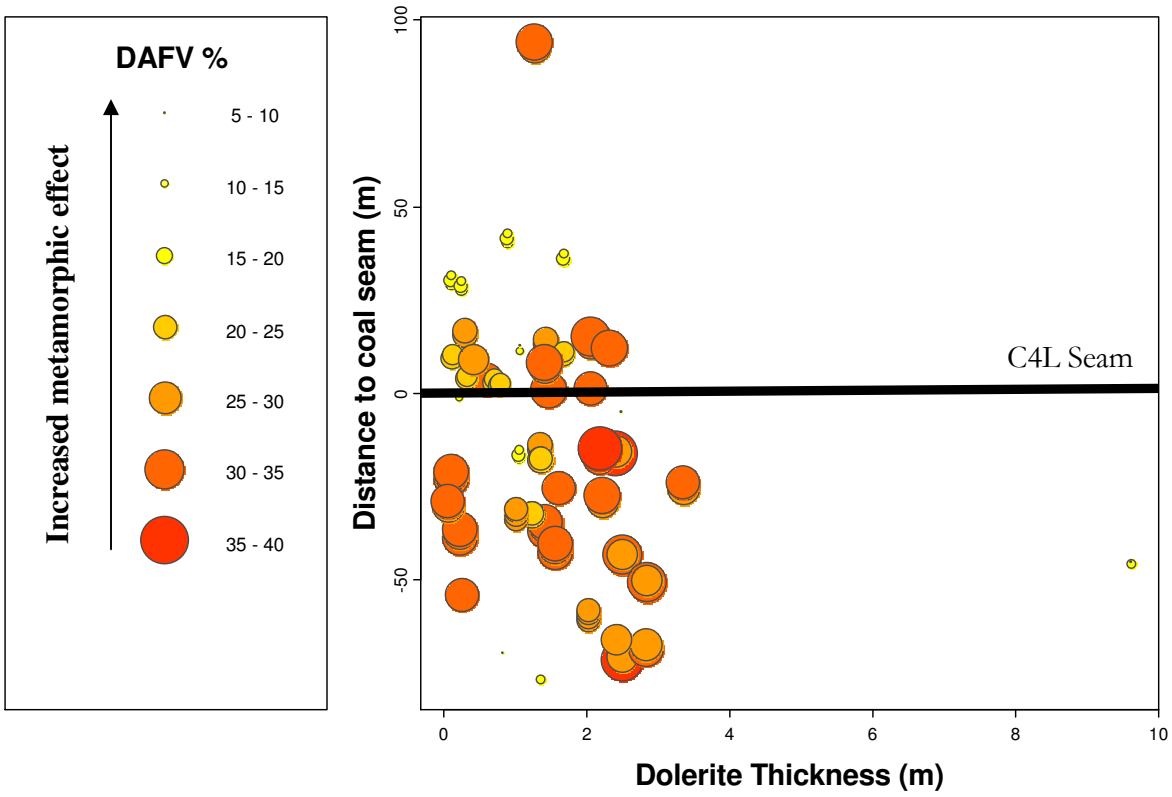

Figure 42: Coal dry ash free volatile percentage in relation to the thickness of dolerite and the interval between the dolerite and the coal seam for the DO10 dolerite

Figure 43 is a graphical representation of the three components DAFV, distance from the C 4 lower coal seam and the thickness of the dolerite sill at that point. The DAFV value is represented by the size and colour of the circles on the plot with the smaller lighter colours representing lesser quality coal. The DO10 dolerite is concentrated below the coal seam with the majority of occurrences within 50m of the coal. The plot displays no trends with regard to DAFV value, thickness of dolerite or distance the dolerite is from the coal seam.

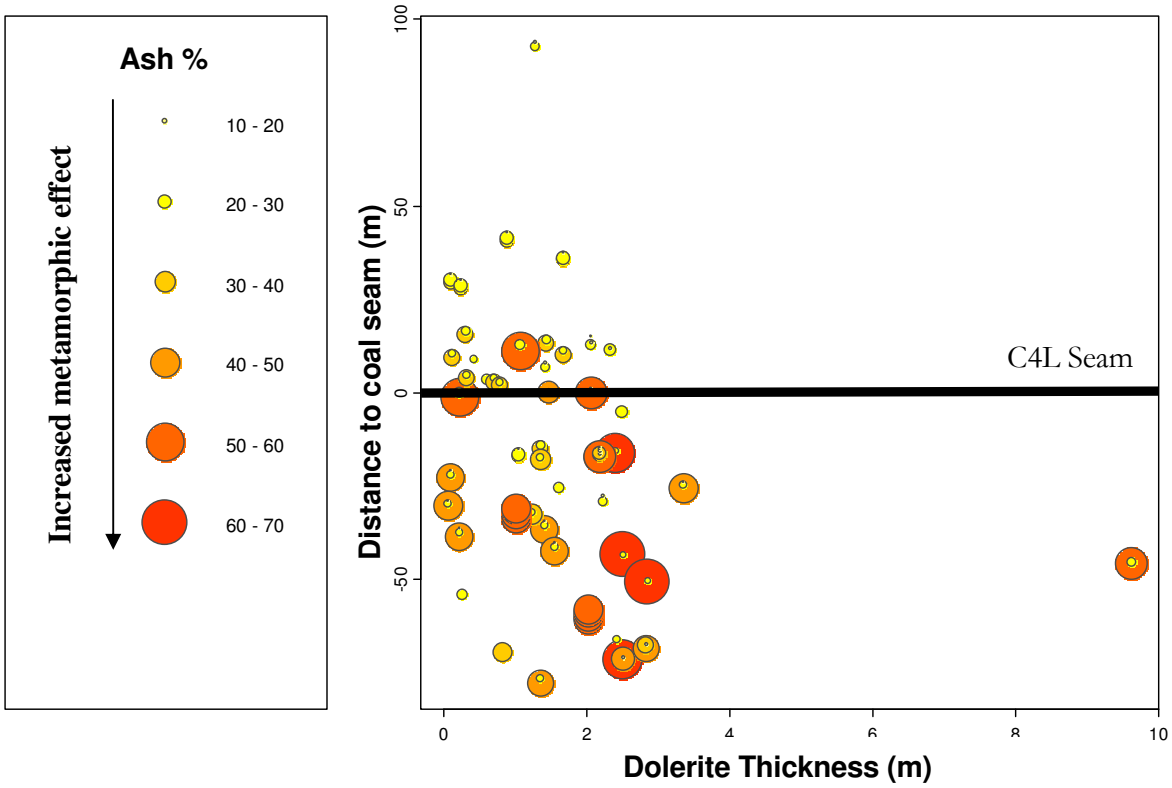

Figure 43: Coal Ash percentage in relation to the thickness of dolerite and the interval between the dolerite and the coal seam for the DO10 dolerite

Figure 44 displays the ash content of the coal in relation to the position and thickness a dolerite is from the C 4 lower coal seam. The larger and darker the circle in the plot reflects a greater increase of inorganic matter percentage within the coal sample. The figure displays no trends with regard to ash value, thickness of dolerite or distance the dolerite is from the coal seam.

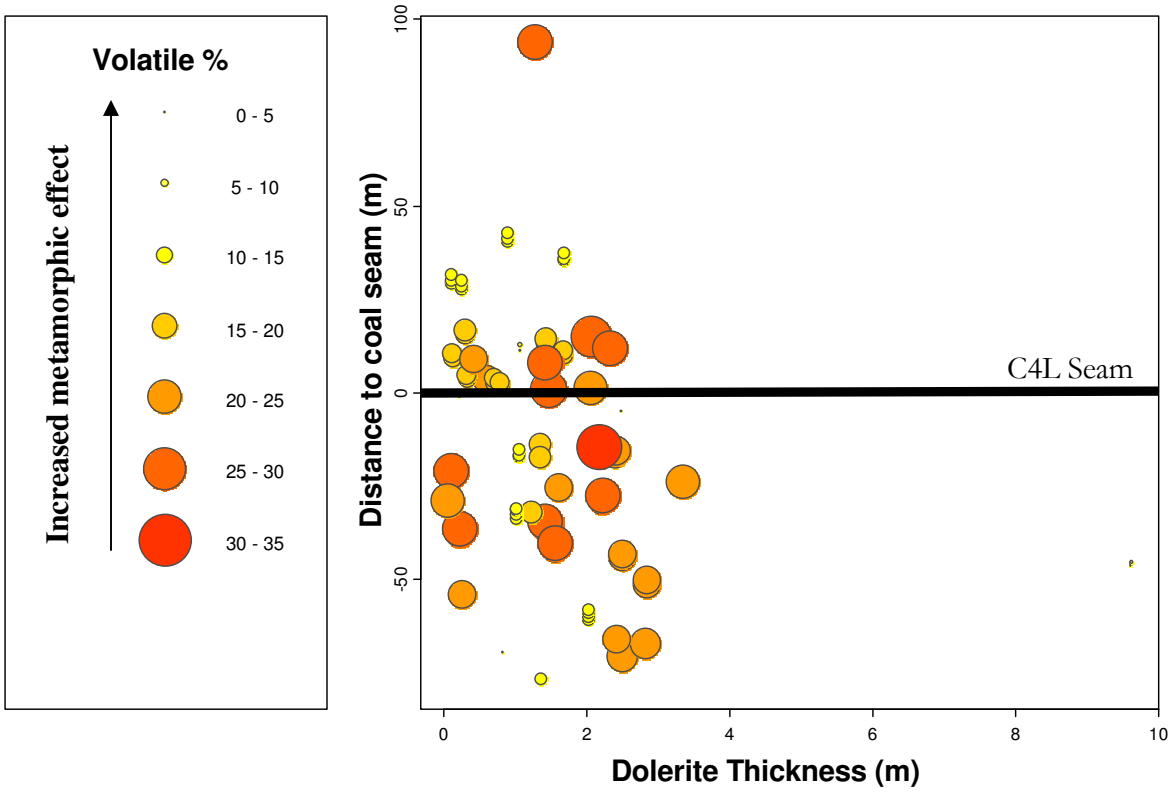

Figure 44: Coal Volatile percentage in relation to the thickness of dolerite and the interval between the dolerite and the coal seam for the DO10 dolerite

Figure 45 graphically displays the volatile content within coal samples in relation to the position and thickness a dolerite is from the C4 lower coal seam. The smaller and lighter the circles within the plot, the lesser the quality of coal the coal. The figure displays no trends with regard to Vols value, thickness of dolerite or distance the dolerite is from the coal seam.

4.3. Statistical Analysis

Statistical analysis of the metamorphic effects of the Secunda dolerites was performed to identify any sub-groups or trends within the data. The analysis is based on the coal quality data derived from the Sasol Secunda data base with focus on the three main devolatilization parameters. The approach to the statistical analysis was to initially describe all the dolerite types in focus and then to separate them out into the three types, namely DO4, DO8 and DO10. This was done to once

again identify whether there are any fundamental differences between the dolerites themselves with regard to their metamorphic effect. To do this two methods are employed, firstly a graphical representation of the data is produced using histograms, box plots, density plots and violin plots to identify groups in the data, and secondly numerical summary statistics are used to look for comparability between dolerite types. Both methods were employed on all three main metamorphic parameters *i.e.* DAFV %, Volatile % and Ash %.

Figures 46, 47 and Table 10 display the graphical and descriptive statistics for the entire data set of DO4, DO8 and DO10 dolerites. Within Figures 49 the image to the right contains the graphical statistical data for the devolatilization parameter DAFV %. To be noted here is the high kurtosis level of 2.52 (note that all exact figures are obtained from Table 10) shown in the histogram and the large number of "outliers" indicated within the box-plot. The histogram shows a slight skewness to the right of 0.60, well displayed in the violin plot. The density plot shows two main peaks in a narrow range ~0-40, but the complete range of data for the DAFV parameter covers the interval 0-100 when all 7924 samples are considered.

The right portion of Figure 48 depicts the graphical statistics for the Ash % for the entire data set. Immediately identifiable in the histogram is the high level of skewness (1.33 to the right), coupled with large numbers of "outliers" as indicated in the box-plot. Also to be noted are the three peaks identifiable in the density plot. The ash data shown in table 10 shows a wide sample range of 92.10, coupled with a large sample variance as seen in the violin plot.

Figure 47 contains the graphical statistics data for the Volatile % parameter. The histogram and box plot show a near normal distribution with a small number of "outliers". The density plot shows three peaks over a narrow range of ~0-30. The indicators of location show 16.11%, 16.60% and 12.00% Volatiles for the mean, median and mode respectively.

Within the 7924 boreholes in which the three dolerites occur, devolatilization of the C4 lower seam occurs in 19.70% of the boreholes. This value is derived by identifying all instances where the values of DAFV, Vols and Ash are beyond the levels set by Sasol for devolatilized coal, and then dividing this number of samples by the total number of boreholes studied within the study area.

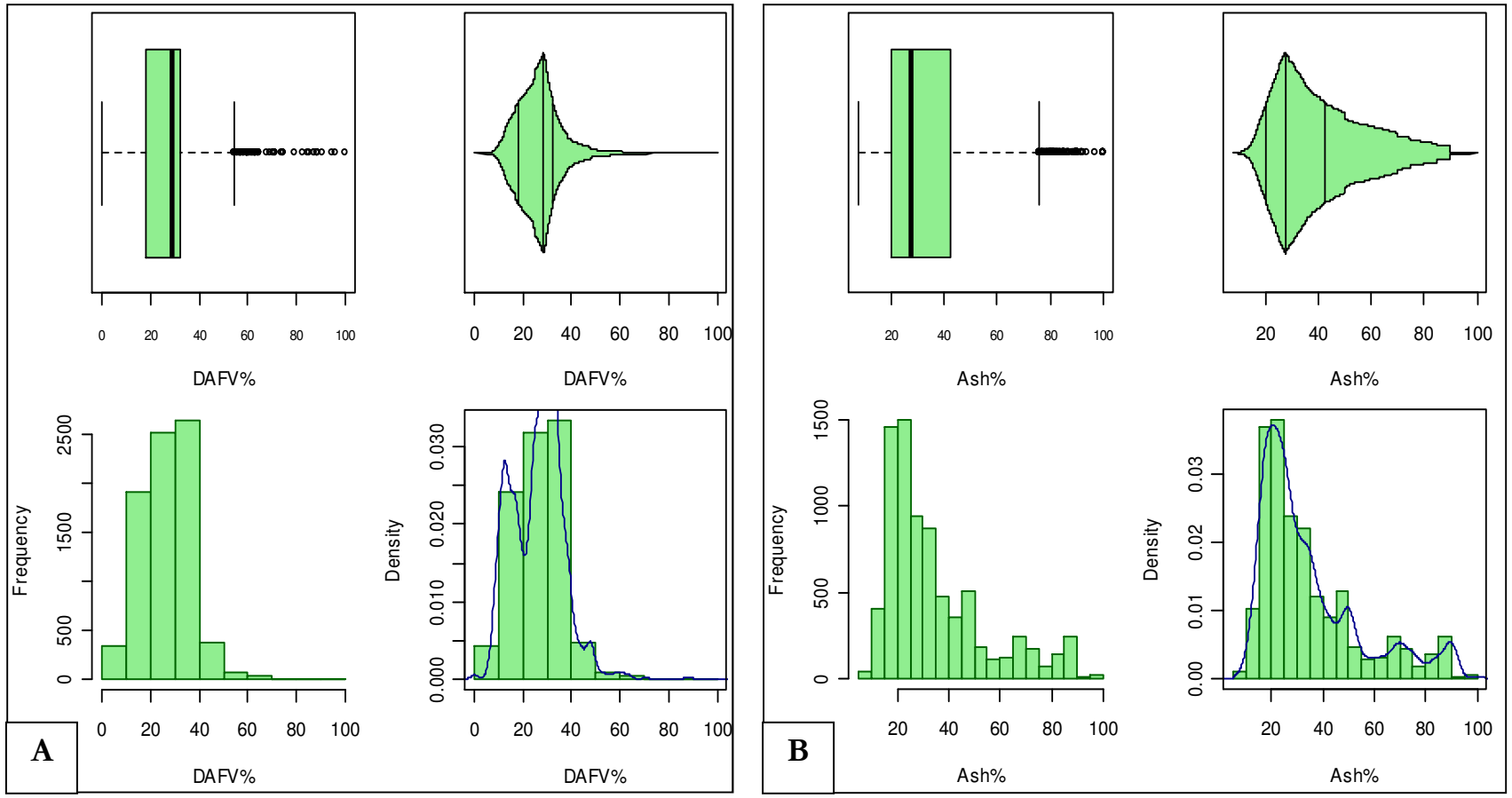

Figure 45: A: Dry ash free volatile percentage % graphical statistics on DO4, DO8 and DO10 dolerite samples. B: Ash % graphical statistics on DO4, DO8 and DO10 dolerite samples.

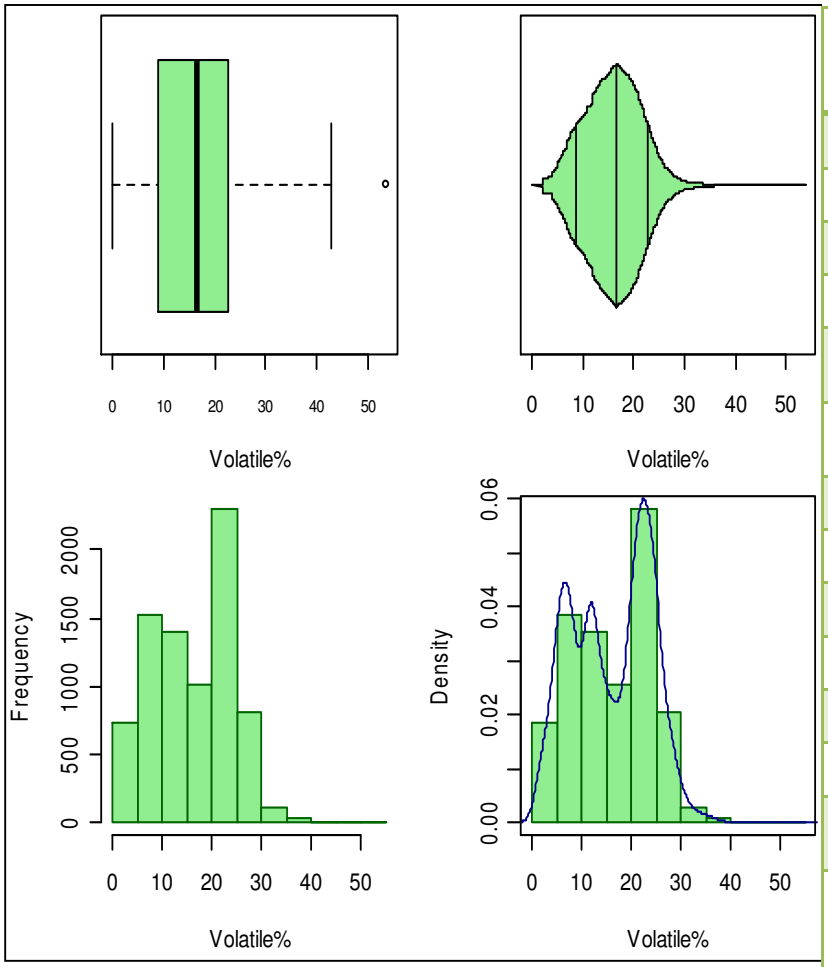

Figure 46: Volatile % graphical statistics on DO4, DO8 and DO10 dolerite samples.

Table 10: Summary statistics of DAFV, Ash and Volatile parameters for DO4, DO8 and DO10 dolerites

Statistical Measure	DAFV %	Ash %	Volatile %	Devolatilization %
Mean	26.55	34.77	16.11	
Standard Error	0.12	0.23	0.09	
Median	28.46	27.70	16.60	
Mode	25.00	50.00	12.00	
Standard Deviation	10.52	20.03	7.97	
Sample Variance	110.71	401.37	63.54	
Kurtosis	2.52	0.96	-1.01	
Skewness	0.60	1.33	-0.02	
Range	100.00	92.10	53.70	
Minimum	0.00	7.90	0.00	
Maximum	100.00	100	53.70	
Sample size	7924	7924	7924	
Confidence Level (95.0%)	0.23	0.44	0.18	
Devolatilization %				19.70

4.3.1 DO4: Statistical analysis of coal qualities

Figures 48, 49 and table 11 display the graphical and descriptive statistics for all the occurrences of the DO4 dolerite within the study area. Within Figure 48 the image to the left contains the graphical statistical data for the devolatilization parameter DAFV %. To be noted here is the high kurtosis level of 3.98 (note that all exact figures are obtained from table 11) within the histogram and the large number of "outliers" indicated within the boxplot. The histogram shows skewness of 0.89 to the right which is well displayed in the violin plot. The density plot shows two main peaks in a narrow range ~0-40, but it must be noted that the data range for the DAFV parameter is from 0 to 100 over the 3145 sample set.

The right portion of Figure 48 depicts the graphical statistics for the Ash %. Within the histogram a high level of skewness of 1.24 to the right can be noted as well as a large numbers of "outliers" indicated in the box-plot. Four peaks are viable in the density plot over the full range of the plot. The summary statistics for the Ash % data in table 11 shows a wide sample range of 92.10, which is coupled with a large sample variance that can best be seen in the violin plot.

Figure 49 contains the graphical statistics data for the Volatile % parameter, the histogram and box plot show a near normal distribution with a small quantity of "outliers" and indicators of location with values of 16.39%, 17.60% and 12.00% Volatiles for the mean,median and mode respectively.. The density plot shows three peaks over a narrow range of ~0-30.

Within the 3125 occurrences of the DO4 dolerite type, devolatilization of the C4 lower seam occurs 18.16 % of the time. This value is derived by identifying all instances that the values of DAFV, Vols and Ash are beyond the levels set by Sasol for devolatilized coal and then dividing it by the total samples or occurrences of the dolerites within the study area.

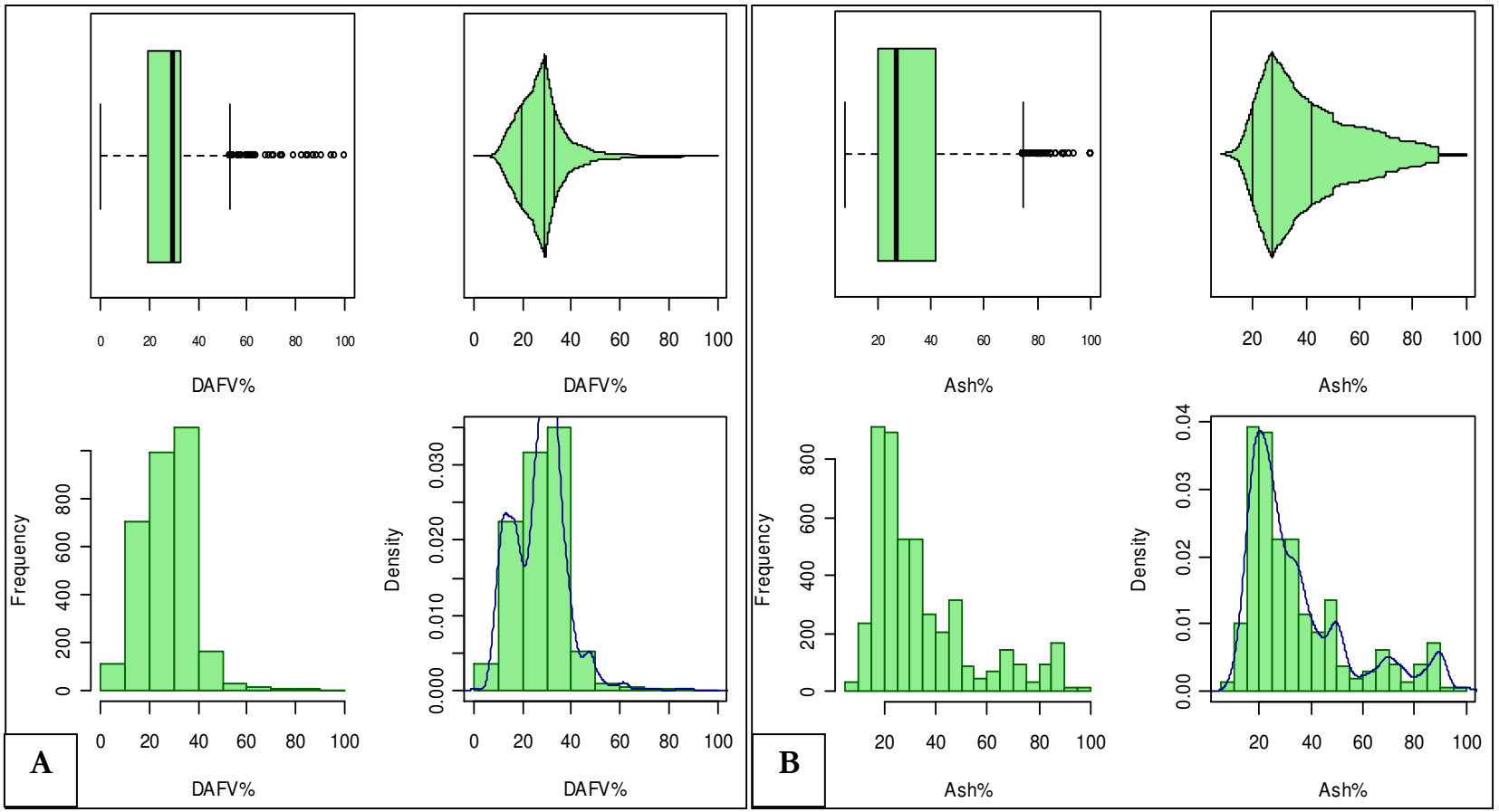

Figure 47: A: Dry ash free volatile percentage % graphical statistics on DO4 dolerite samples. B: Ash % graphical statistics on DO4 dolerite samples.

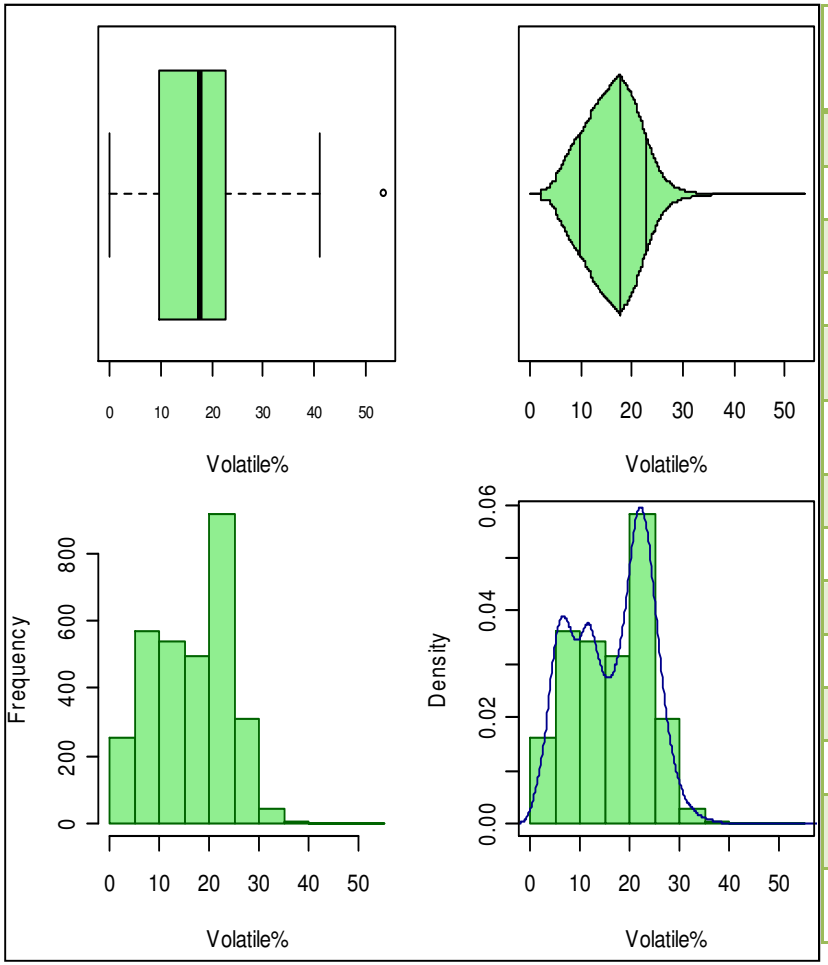

Figure 48: Volatile % graphical statistics on DO4 dolerite samples.

Table 11: Summary statistics of DAFV, Ash and Volatile parameters for the DO4 dolerite

Statistical Measure	DAFV %	Ash %	Volatile %	Devolatilization %
Mean	27.38	35.17	16.39	
Standard Error	0.19	0.35	0.14	
Median	29.16	28.40	17.60	
Mode	25.00	50.00	12.00	
Standard Deviation	10.79	19.71	7.69	
Sample Variance	116.46	388.42	59.11	
Kurtosis	3.98	0.72	-0.86	
Skewness	0.89	1.24	-0.06	
Range	100.00	92.10	53.70	
Minimum	0.00	7.90	0.00	
Maximum	100.00	100.00	53.70	
Sample size	3145	3145	3145	
Confidence Level (95.0%)	0.38	0.69	0.27	
Devolatilization %				18.16

4.3.2 DO8: Statistical analysis of coal qualities

Figures 50, 51 and Table 12 display the graphical and descriptive statistics for all the occurrences of the DO8 dolerite within the study area. In Figure 50 the image to the left contains the graphical statistical data for the devolatilization parameter DAFV %. It can be seen that the histogram has a high a near normal distribution with the values for the indicators of location being 26.02%, 27.83% and 25.00% DAFV for the mean, median and mode respectively (note that all exact figures are obtained from table 12). A large number of "outliers" are indicated within the box-plot and the histogram shows skewness of 0.38 to the right, which can also be note in the violin plot. The density plot shows two main peaks in a narrow range of ~0-40, but it must be noted that the data range for the DAFV parameter is from 0 to 100 over the 4663 sample set.

The right portion of Figure 50 depicts the graphical statistics for the Ash %. Within the histogram a high level of skewness of 1.38 to the right can be noted as well as a large numbers of "outliers" indicated in the box-plot. Four peaks are visible in the density plot over the full range of the plot. The summary statistics for the Ash % data in table 12 shows a wide sample range of 92.00, which is coupled with a large sample variance of 415.26 that can best be seen in the violin plot.

Figure 51 contains the graphical statistics data for the Volatile % parameter. The histogram and box plot show a near normal distribution with no "outliers" and indicators of location with values of 15.91 %, 15.80 % and 12.00% Volatiles for the mean, median, and mode respectively. The density plot shows three peaks over a narrow range of ~0-30.

The 4663 occurrences of the DO8 dolerite type are associated with devolatilization of the C4 lower seam 20.89 % of the time. This value is derived by identifying all instances that the values of DAFV, Vols and Ash are beyond the levels set by Sasol for devolatilized coal and then dividing it by the total samples or occurrences of the dolerites within the study area.

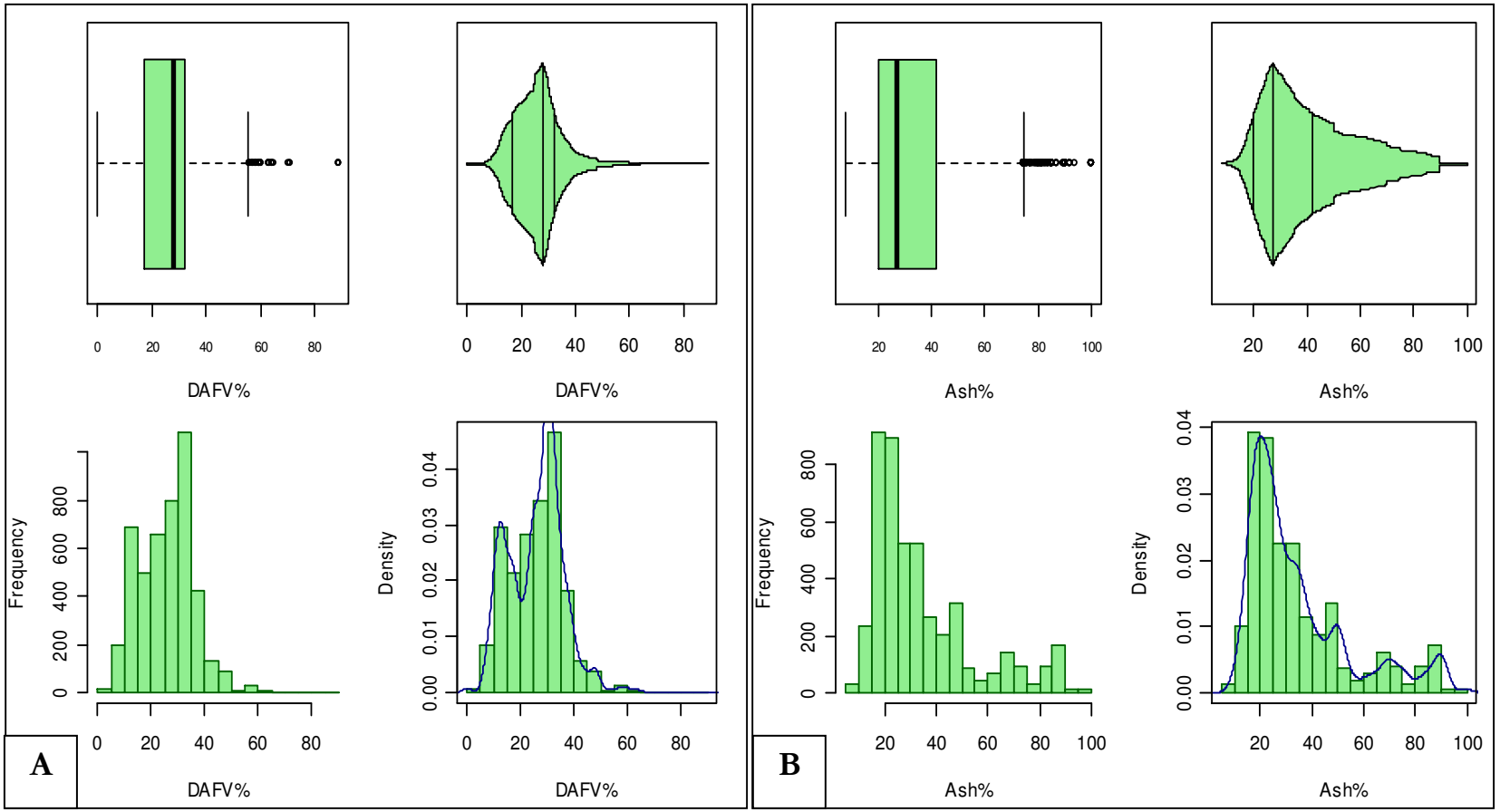

Figure 49: A: Dry ash free volatile percentage % graphical statistics on DO8 dolerite samples. B: Ash % graphical statistics on DO8 dolerite samples.

Table 12: Summary statistics of DAFV, Ash and Volatile parameters for the DO8 dolerite

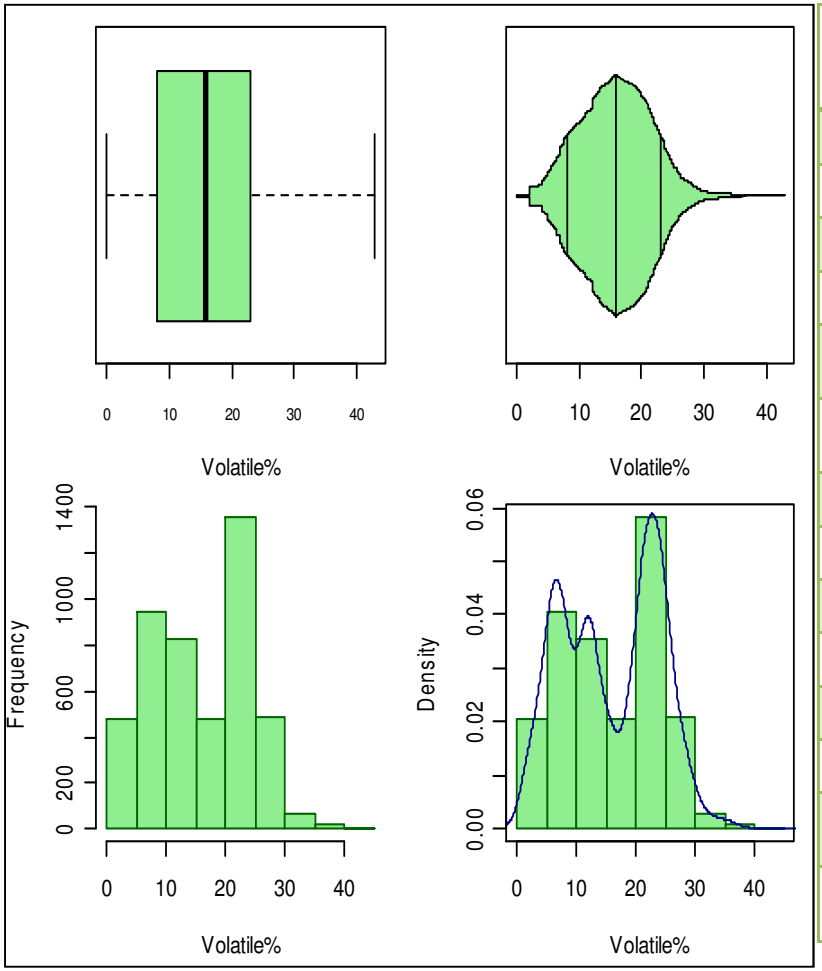

Statistical Measure	DAFV %	Ash %	Volatile %	Devolatilization %
Mean	26.02	34.60	15.91	
Standard Error	0.15	0.30	0.12	
Median	27.83	27.20	15.80	
Mode	25.00	50.00	12.00	
Standard Deviation	10.38	20.38	8.20	
Sample Variance	107.73	415.26	67.22	
Kurtosis	1.22	1.08	-1.10	
Skewness	0.38	1.38	0.01	
Range	88.71	92.00	42.80	
Minimum	0.00	8.00	0.00	
Maximum	87.71	100.00	42.80	
Sample size	4663	4663	4663	
Confidence Level (95.0%)	0.30	0.59	0.24	
Devolatilization %				20.89

Figure 50: Volatile % graphical statistics on DO8 dolerite samples.

4.3.3 DO10: Statistical analysis of coal qualities

Figures 52, 53 and table 13 display the graphical and descriptive statistics for the all the occurrences of the DO10 dolerite within the Secunda study area. The left portion of Figure 52 contains the graphical statistical data for the devolatilization parameter DAFV %. To be noted here is the near normal distribution in the histogram and the lack of "outliers" in the box-plot. The histogram shows skewness of -0.68to the left which is well displayed in the violin plot. The density plot shows two main peaks in a narrow range ~5-40.

The right portion of Figure 52 depicts the graphical statistics for the Ash %. The histogram is skewed to the right with a skewness value of 0.82 (note that all exact Figures are obtained from table 13). A note should be made of the small number of "outliers" indicated in the box-plot. Two peaks are visible in the density plot over the full range of the plot. The summary statistics for the Ash % data in table 13 shows a large sample variance of 180.62 that can best be seen in the violin plot.

Figure 53 contains the graphical statistics data for the Volatile % parameter. The histogram and box plot show a near normal distribution with no "outliers" and indicators of location with values of 16.64, 16.10 and 12.00 for the mean median and mode respectively. The density plot show three peaks over a narrow range ~0-30.

Within the 116 occurrences of the DO10 dolerite type devolatilization of the C4 lower seam occurs 13.79 % of the time. This value is derived by identifying all instances that the values of DAFV, Vols and Ash are beyond the levels set by Sasol for devolatilized coal and then dividing it by the total samples or occurrences of the dolerites within the study area.

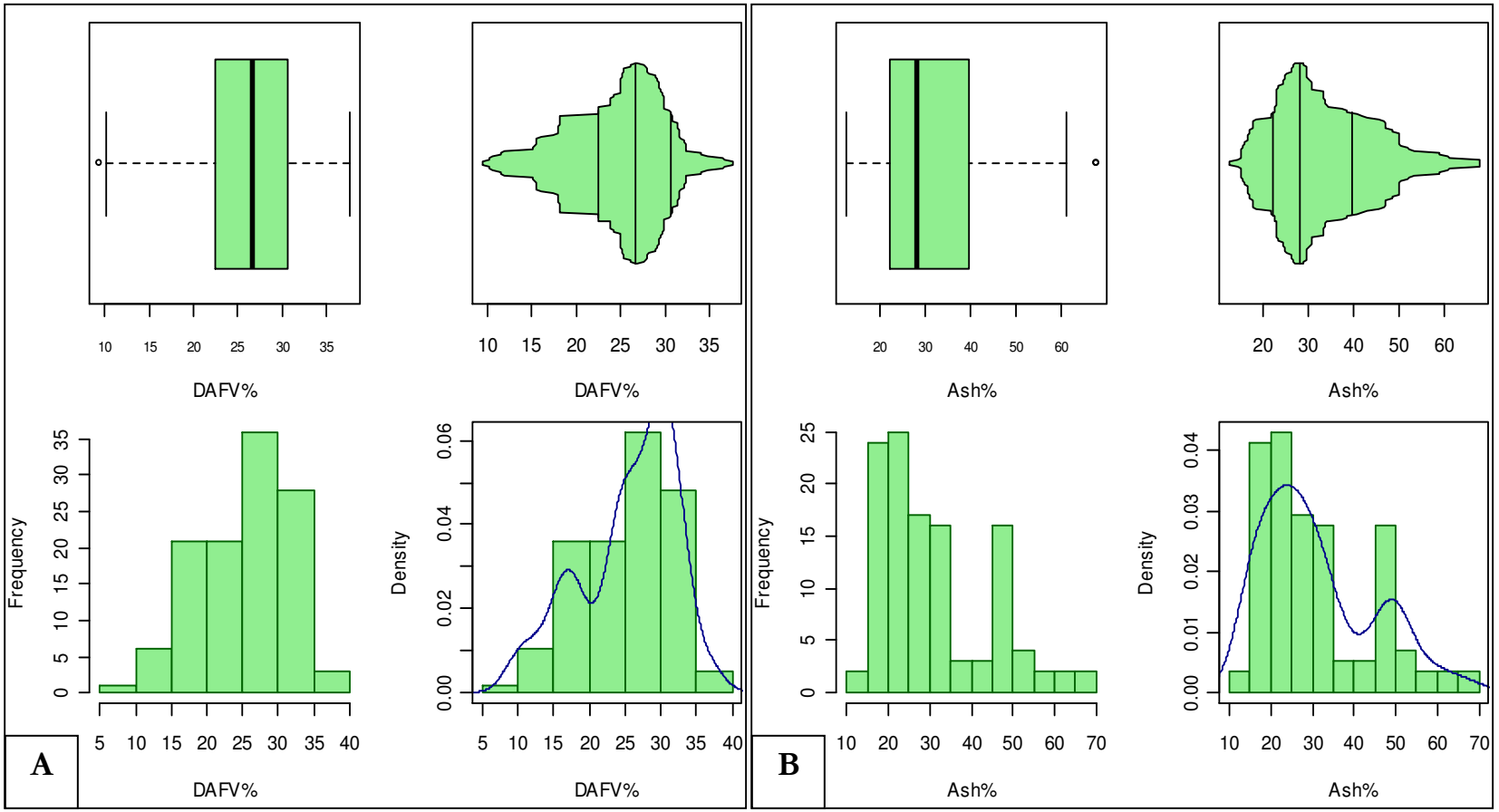

Figure 51: A: Dry ash free volatile percentage % graphical statistics on DO10 dolerite samples. B: Ash % graphical statistics on DO10 dolerite samples.

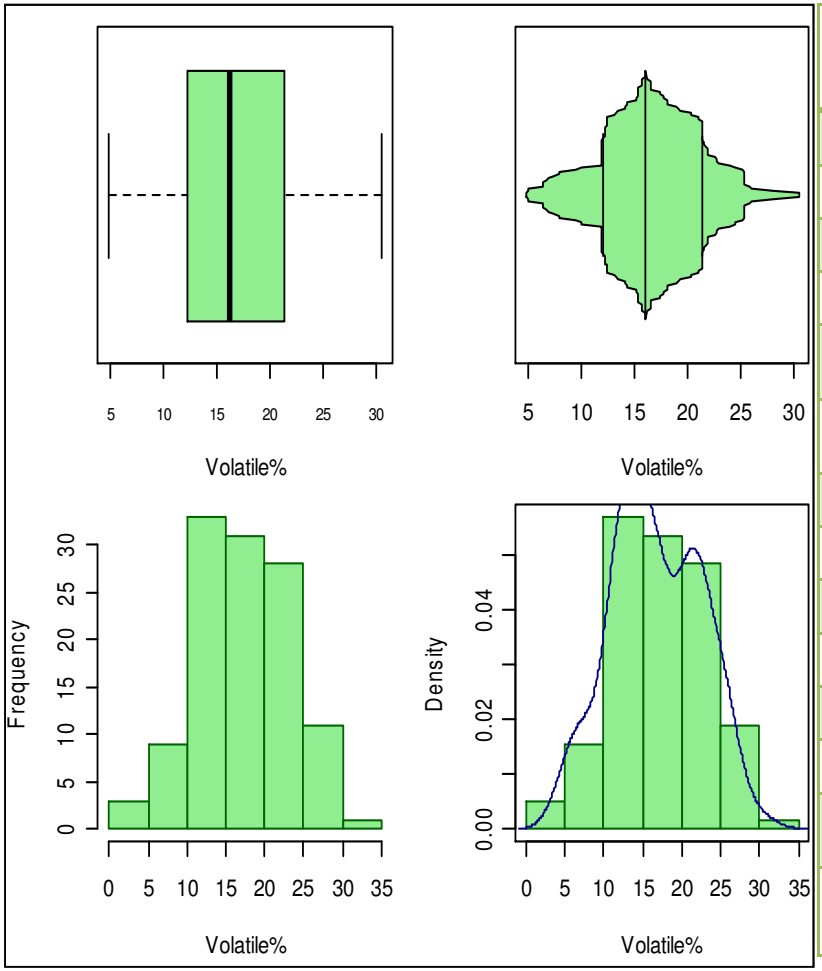

Figure 52: Volatile % graphical statistics on DO10 dolerite samples.

Table 13: Summary statistics of DAFV, Ash and Volatile parameters for the DO10 dolerite

Statistical Measure	DAFV %	Ash %	Volatile %	Devolatilization %
Mean	25.46	31.13	16.64	
Standard Error	0.62	1.25	0.53	
Median	26.70	28.10	16.10	
Mode	25.00	22.90	12.00	
Standard Deviation	6.67	13.44	5.73	
Sample Variance	44.46	180.62	32.78	
Kurtosis	-0.41	-0.22	-0.68	
Skewness	-0.68	0.82	0.02	
Range	28.13	55.00	25.50	
Minimum	9.44	12.70	4.90	
Maximum	37.57	67.70	30.40	
Sample size	116	116	116	
Confidence Level (95.0%)	1.23	2.47	1.05	
Devolatilization %				13.79

4.4. Summary

The investigation of coal quality relative to dolerite proximity begins with analysis of all three dolerite types to establish any dolerite specific trends. Within the geographic relationship of DAFV values seen in Figure 30 no correlation with regards to position of dolerites or type of dolerite can be noted. This lack of correlation continues as the bubble plots in Figures 31-45 show no correlation with regard to dolerite distance from the coal seam and dolerite thickness against DAFV, Ash and Vols with no trends or groupings noted, irrespective of the scale used to show dolerite distance from the coal seam.

The analysis of each specific dolerite type was done in attempt to filter the data and note any trends or groupings over a smaller range of values. Each dolerite produced the same lack of trends or grouping as seen in the initial investigation of all the data points.

The statistical analysis of the complete data set showed that there seem to be multiple peaks in the proximate analysis parameters over all the dolerite types. The peak patterns noted in Figures 46 and 47 were mirrored in the DO4 and DO8 statistics whereas the DO10 statistics showed lesser variation and a smoother pattern in the graphics. The DO4 and DO8 dolerites also showed similar values in the devolatilization percentages in the summary statistics with ~18% and ~20% respectively, whereas the DO10 dolerites maintained a lower ~13%.

The summary statistics in tables 10-13 show that the coal quality data does not have normal distributions (high skewness and kurtosis values as well as the variations in the values for the indicators of location *i.e.* the mode, median and mean which should all be equal in a normal distribution). These values and the graphical statistical representations show that data is not uniform but rather complex.

To summarize, the coal quality relative to the dolerite proximity was shown here to be highly variable with no defining trends noted within the proximate analysis values of the data set. Thus, any effect the dolerites have on the coal is complex and cannot be described by a simplistic normal distribution, as would be expected if thermal contact metamorphism related to volume of intrusion was the main cause of coal quality loss

CHAPTER 5: DISCUSSION

The relationship between the Secunda dolerite sills and the coal in close proximity to the intrusions has been investigated on three grounds:

- The physical and mineralogical properties of the Secunda dolerite sills.
- The geochemical properties of the Karoo, Lebombo and Secunda dolerites.
- The metamorphic effects of the Secunda dolerites.

The implications and interpretation of each factor will be approached individually to allow clarity as to each sections impact on the devolatilization of coal in proximity to dolerites. The final focus will be on the combination of all these factors to evaluate the impact of the Secunda sills on coal quality.

5.1. Physical and mineralogical properties of the Secunda Dolerites

The physical properties of the investigated DO4, DO8 and DO10 Secunda dolerite sills discussed in Chapter 2 showed that minor textural and mineralogical variations can be noted within the dolerites. The textural variations are illustrated within by the orientation and size variations of plagioclase grains. Two distinct size variations in plagioclase, possibly showing two generations (possibly related to quenching effects during intrusion) can be noted within the DO8 and DO10 sills. The DO8 is identifiable by its large needle-like plagioclase phenocrysts, whereas the DO10 contains star-shaped or nodular plagioclase phenocryst arrangements. Both the DO8 and DO10 show weak variolitic texture within the second generation of plagioclase crystal growth. The DO4 dolerite shows only a singular generation of plagioclase growth and also has consistently higher levels of alteration and much lower levels of competency in hand specimen. The subtle textural variations and physical character differences shown in Chapter 2 are markers of unique crystallization processes for each of the three dolerite types. These variations can also be noted in the minor mineralogical differences between the sills. The most identifiable is the occasional presence of olivine within the DO8 dolerites and the subtle distinctions in mineral abundances between the three dolerites. The minor textural and mineralogical distinctions can be postulated as indicators of the unique conditions within the magma conduit both mechanically and geochemically during the intrusion and crystallization of the dolerites.

5.2. Geochemistry of the Secunda dolerites

The geochemical analysis of the Secunda dolerites seen in Chapter 3 was approached through the use of Harker and bivariant plots of major elements, trace elements and elemental ratios, in order to identify variation between the three sills under investigation. The data was then plotted against average geochemical data from Karoo Large Igneous Province to identify how the Secunda dolerites fitted with the known formations within the Karoo.

The major and trace elemental analysis of the Secunda dolerites showed that the DO8 dolerites are readily distinguishable from the DO4 and DO10 dolerites, whereas the DO4 and DO10 dolerites are inseparable on their major element geochemistry. The DO8 dolerite showed enriched TiO_2 and Y concentrations when compared to the other Secunda dolerites, and relatively depleted MgO and Al_2O_3 concentrations, despite being the only Secunda dolerite to contain olivine. The low MgO levels may be due to the olivine hosted in DO8 being Fe-rich fayalite. When elemental ratio plots were applied to the Secunda dolerites the DO8 was once again readily distinguishable from the DO4 and DO10 dolerites, displaying heightened TiO_2/Zr and TiO_2/Y values.

The DO4 and DO10 dolerites showed comparable major element values in the analysis of Figures 14-16 (MgO SiO_2, Al_2O_3 and TiO_2), but some separation can be noted in the trace elements shown in Figures 17-19 (Nb, Y, Zr). Figure 19 (Y vs. Zr) shows clear separation of the three dolerites; also noted here is the two distinct groups within the DO4 dolerite data. This separation can be continually noted throughout the major and trace element analysis but is most clearly visible in Figures 15-17 and 19, where the DO4 data has a grouping of tightly clustered values and a second grouping of values which show a near-linear progression. The separation of the DO4 into two distinct groups is postulated to be caused by varying alteration levels within the specific dolerite samples, which may explain the near-linear progression and tight clustering of values noted in the major and trace element plots. The near-linear progression may depict increasing levels of alteration in the sampled material while the tight clustered values represent samples with low levels of alteration. The DO10 dolerite shows comparable values to the second (unaltered) grouping of the DO4 dolerite but has a much narrower range of values and is most easily distinguishable from the DO4 on the basis of low Nb, Zr, and Yr concentrations in the DO4 dolerites.

When the Secunda dolerites were compared to the formations of the Karoo Large Igneous Province, analysis showed the DO4 and DO10 Secunda dolerites are conformable with the Barkley East, Sabie (LTZ) and Lesotho Formations, whereas the DO8 dolerites plot slightly differently to all known Karoo dolerites. The DO8 show features of both the high Ti zones and low Ti zones of the Karoo as seen in Figure 25 where DO8 show equivalent Y concentrations to that of the Sabie (HTZ) Formation but Nb concentration equal to that of the Lesotho Formation.

To summarize, it can be shown that the three Secunda dolerites have some unique geochemical characteristics when directly compared and show the three dolerites have unique character. The separation of the Secunda dolerites is less pronounced when compared to the average geochemistry of the Karoo Igneous Province which shows that the geochemical character of these dolerites is in line formations of the Karoo Igneous Province.

5.3. Coal quality changes induced by the Secunda dolerites

The investigation of dolerite metamorphic effect used proximate analysis values to quantify the location and extent of coal quality deterioration, or “devolatilization”. This relationship was graphically depicted in three ways: firstly by geographic interpolation to identify areas of devolatilization in comparison to dolerite type and geographic position; secondly, bubble plots were drawn to obtain a three dimensional (distance, thickness and proximate analysis value) analysis of the devolatilization; and finally, statistical analysis was used where the variable degrees of devolatilization were compared to identify any implicit patterns within the proximate analysis data.

The geographic devolatilization relationship made use of the DAFV values as seen in Figure 30. This showed no correlation with regards to position of dolerites or type of dolerite can be noted. This lack of correlation is strange as regions on the map with high densities of dolerites were expected to correspond to an increase in devolatilization, but no such correlation occurs. A secondary note could also be made that there is no dolerite specific metamorphic effect seen on this map, as regions populated with a majority of a singular dolerite group show the same variable devolatilization effects. This irregular relationship was initially inferred as being a result of sill thickness and position in relation to the C4L seam but this hypothesis was disproved by the bubble

plots. An expected linear correlation as seen in Figure 54 was postulated based on the concepts of contact metamorphism.

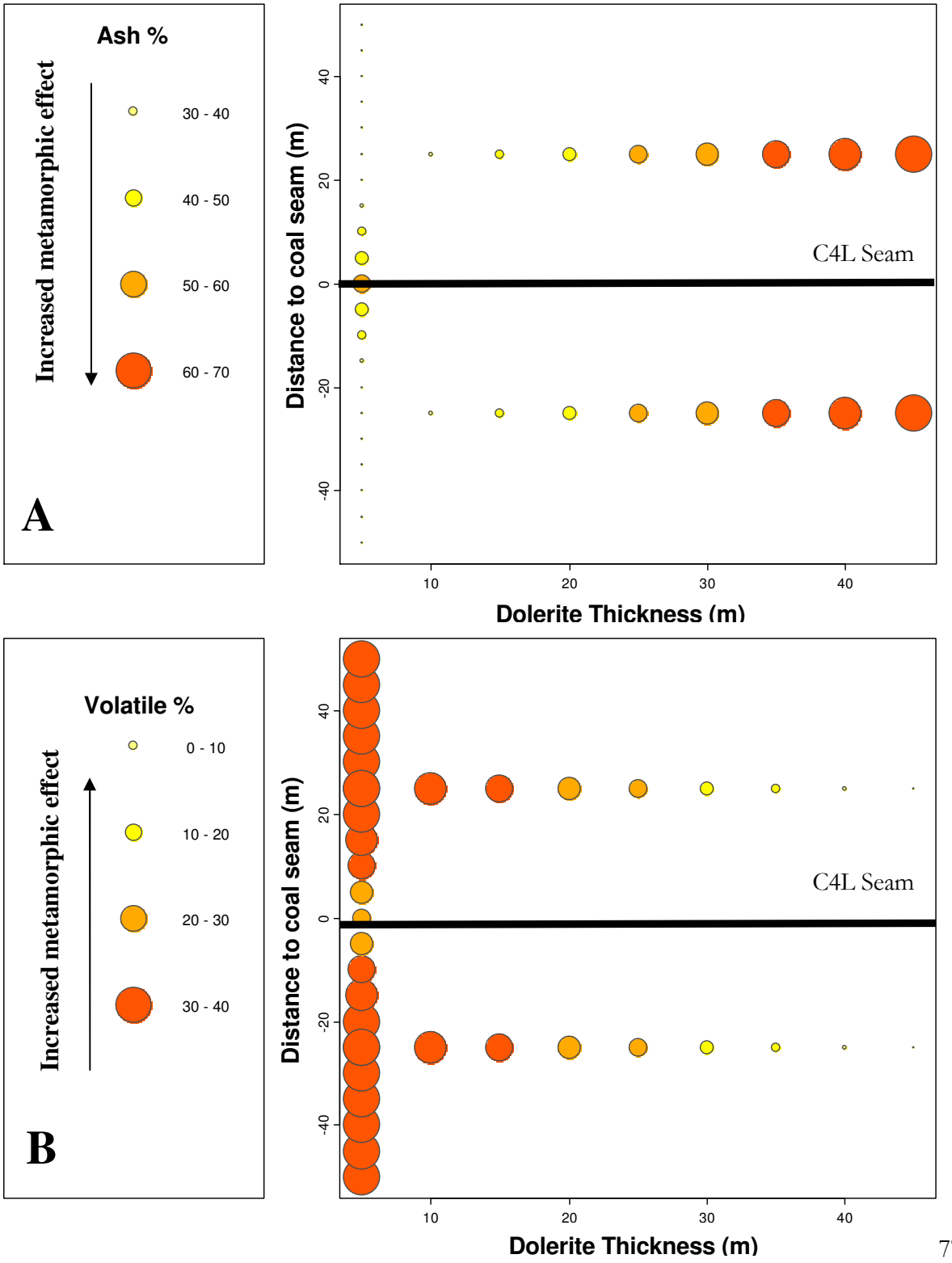

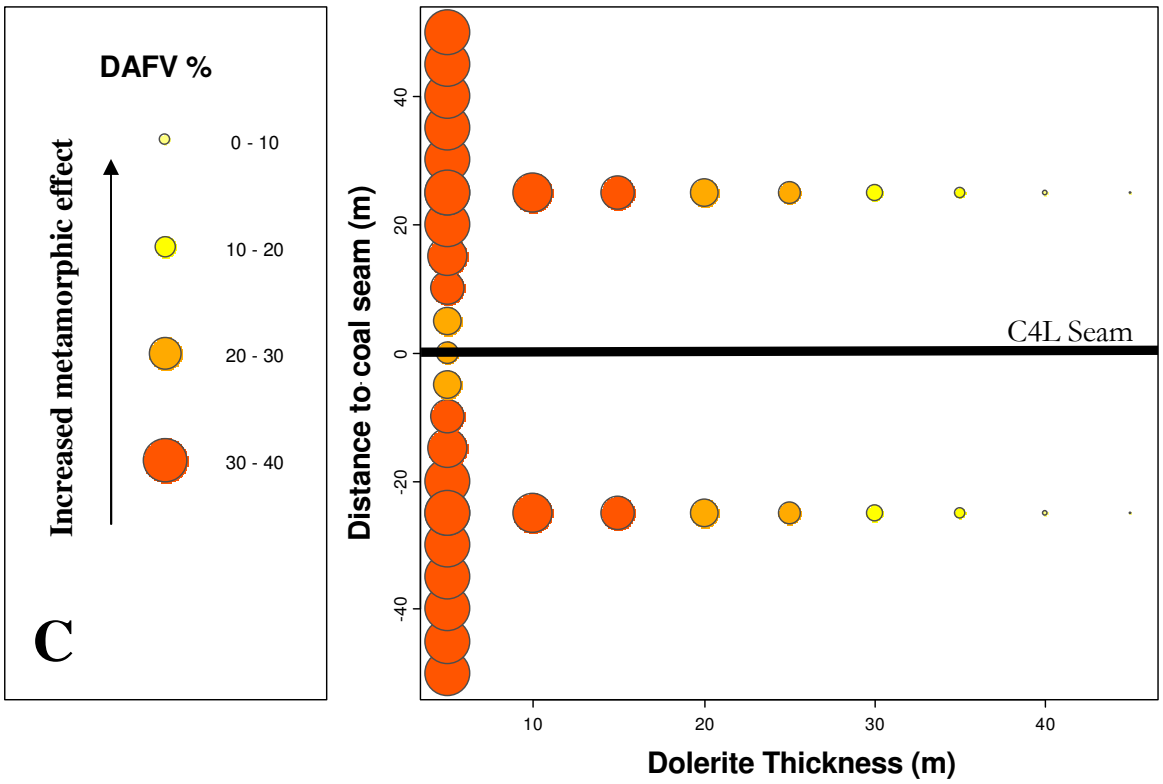

Figure 53: Expected trends of proximate analysis figures when compared to dolerite thickness and distance from coal seam. A: Ash % B: Volatile % C: Dry ash free volatile percentage %

The bubble plots shown in Figures 31-45 show no such correlation with regard to dolerite distance from the coal seam and dolerite thickness against any of the proximate analysis values investigated (i.e. DAFV, Ash and Vols). No trends or groupings can be seen irrespective of the scale used to show dolerite distance from the coal seam. Figures 41-48 displayed individual dolerite types to investigate whether the lack of correlation could be attributed to dolerite specific metamorphic effects, but this once again showed no discernible trends, correlations or groups. This graphic data was further investigated through statistical analysis of the proximate analysis data sets in Chapter 4. This analysis (Figures 46-53) showed data depicting complex histograms with multiple peaks and indicators of location *i.e.* the mode, median and mean values well beyond the limits of normal distributions. The skewness and kurtosis figures show the same deviation from normality. Within the density plots of Figures 46 and 47 there seems to be multiple peaks in the proximate analysis parameters over all the dolerite types. The peak patterns noted in Figures 46 and 47 where mirrored in the DO4 and DO8 statistics while the DO10 showed lesser variation and

a smoother pattern in the graphics. The DO4 and DO8 dolerites also showed similar values in the devolatilization percentages in the summary statistics with ~18% and ~20% respectively while DO10 maintained a lower ~13%. The graphical statistics and the summary statistical tables both indicate complex data which is far from normally distributed. This once again shows that any contact metamorphic effect caused by the dolerite intrusions deviates from an ideal contact metamorphic regime.

The major inferences that can be made about the Secunda sill's effect on the quality of the C4 L seam are that they are complex and that the data compiled herein shows that the effect is not that of simplistic contact metamorphic regimes. The graphical, geographical and statistical measures calculated in this study show comprehensively that the sills have a unique effect on the coal regardless of their type, size or proximity to the C4L coal seam. Thus it is necessary to redefine the method and mechanics with which these sills affect the coal.

5.4. Resultant devolatilization models for the Secunda dolerites

The lack of a linear relationship noted in section 5.3 indicates that the relationship between the dolerite intrusives and coal quality is complex, and does not conform to a simplistic contact metamorphic regime. To explain the lack of relationship between levels of devolatilization and sill distance from the coal seam, several processes are postulated to explain the relationship of the Secunda dolerites and the C 4 lower coal seam:

Process 1: Dolerite emplacement dynamics

The emplacement properties of the dolerites is the regulating factor of its metamorphic effect, thus each dolerite has unique contact metamorphic effect related to its intrusion dynamics. As stated in Chapter 1, the intrusion of dykes and sills is reliant on multiple factors:

- The distance from the source the doleritic magma has travelled
- The density of the magma
- The piezometric pressure on the magma
- The flow rate of the magma
- The magma chamber overpressures
- The flow regime within the magma conduit

- Depth of emplacement
- Temperature of the magma

The factors listed above define the movement of the magmatic material through the country rock. The movement will define how much country rock assimilation occurs as well as if a chilled margin develops.

The flow regime within the magma conduit is vitally important to how much country rock is assimilated. The Reynolds number defines whether a fluid experiences turbulent or laminar flow, as explained by the equation below:

$$Re \equiv \frac{\rho_{liq} \bar{U} w}{\eta}$$

- $\bar{U}$ is the average velocity
- w is the half-thickness of the flow
- ρ_{liq} is the liquid density
- η is its viscosity

A change in Re can be induced if any of the following parameters are altered:

1. *The distance from the source the magma travels:*

   The distance the magma has travelled will influence the temperature of the magma within the conduit and in turn the viscosity.

2. *The density of the magma*

   The density of the magma is directly related to the flow rate and the viscosity; the more dense the magma the higher resistance to flow it will have.

3. *The piezometric pressure on the magma*

   The gravitational force induced from the height differential of the magma conduit and the source of melting is a major source of pressure on the magma. This pressure will define the

rate of flow of the magma. Thus a higher piezometric pressure will produce magma with a higher flow rate.

4. *The flow rate of the magma*

The flow rate of the magma can be directly inserted into the Reynolds number equation, but this figure is also related to the other factors of propagation and emplacement.

5. *The magma chamber overpressures*

As with piezometric pressure the magma chamber overpressures will define the force with which the magma travels through the conduit, which defines the rate of flow of the magma.

6. *Temperature of the magma*

Magma temperature and viscosity are inversely proportional, and thus an increase in magma temperature will decrease the viscosity.

If the Reynolds number is high, turbulent flow will occur, whereas if the Reynolds number is low laminar flow will occur (Kavanagh *et al*., 2006). The transition between laminar and turbulent flow can be anywhere in the range of 10-1000, but within mafic magmas this value is ~28 (Kavanagh *et al*., 2006).

Thus if a dolerite magma was undergoing turbulent flow, which can be likened to white water in a river, a system of eddies would develop as the dolerite propagates, and these eddies would enable greater thermal erosion and assimilation of country rock. During this process the dolerite would release its thermal energy throughout the process of assimilation and thus would not produce a large metamorphic aureole.

If dolerite magma undergoes laminar flow, which can be likened to a slow flowing or meandering stream, the amount of contamination and assimilation would be greatly reduced as the magma's thermal erosive impetus would be lower. This laminar flow regime would also allow the production of amorphous glass chilled margins, which would insulate the dolerite conduit. This insulating effect would allow for longer cooling rates and a greater amount of heat energy would be released by conduction, thus creating a more pronounced contact metamorphic aureole.

To summarize, if a Secunda dolerite maintained a laminar flow it would create a large metamorphic aureole, whereas if it maintained a turbulent flow the contact metamorphic aureole would be much less pronounced. This flow regime-based metamorphism would be a dynamic system which could change along the length of the conduit as the magma physical properties, such as viscosity (which is related to temperature), change along the dolerites course.

Process 2: Hydrothermal metasomatism

Although contact metamorphic effects will surely be apparent when dolerites are in very close proximity to the coal, this type of metamorphism is not the major source of devolatilized coal. The intrusion of the doleritic magmas would also be associated with the production of heated fluids from the magmas and the surrounding sediments as the intrusives cool. These 100-200°C fluids would be mobile and able to percolate through the porous and permeable sedimentary strata surrounding the coal. A metasomatic hydrothermal agent could explain the lack of a linear relationship between dolerite proximity and coal quality, as fluids are more mobile and less homogenous, and so will not produce the same linear relationship as expected from contact metamorphism.

A more plausible scenario for the variation in coal quality relative to the dolerite intrusions is one where both the dynamic emplacement of the dolerite and the effect of hydrothermal fluids are taken into account. When these factors are combined it produces a complex situation where the dimensions of dolerite sill or dykes metamorphic "aureole" or rather the metamorphic range are dictated by the way in which the dolerite was emplaced and what (if any) fluids were released or produced by that dolerite. These two factors would define how dramatic the effect of the dolerites presence would be on the coals chemistry and physical properties.

Essentially there would be four main or end member scenarios when both these factors are taken into account:

1. A fast flowing magma with turbulent flow which incorporates large amounts of country rock and produces a small metamorphic aureole, but creates large amounts of hydrothermal fluids during cooling and interaction with the sedimentary strata.

2. A fast flowing magma with turbulent flow which incorporates large amounts of country rock and produces a small metamorphic aureole, and produces only small amounts of hydrothermal fluids during cooling and interaction with the sedimentary strata.
3. A slow flowing magma with a laminar flow which produces an even chilled margin and a larger metamorphic aureole, and produces large amounts of hydrothermal fluids during cooling and interaction with the sedimentary strata.
4. A slow flowing magma with a laminar flow which produces a even chilled margin and a larger metamorphic aureole, and produces small amounts of hydrothermal fluids during cooling and interaction with the sedimentary strata.

CHAPTER 6: CONCLUSION AND RECOMMENDATIONS

When the Secunda dolerites are compared to the formations of the Karoo Large Igneous Province, analysis showed the DO4 and DO10 Secunda dolerites are conformable with the Barkley East, Sabie (LTZ) and Lesotho Formations, with the DO8 dolerites plotting with concentrations slightly different to the known Karoo dolerites. The DO8 dolerites show features of both the high Ti zones and low Ti zones of the Karoo. With this said, the three Secunda dolerites have shown unique geochemical and mineralogical characteristics, but these characteristics are in line with the average geochemistry and mineralogy of the Karoo Igneous Province.

The minor textural and mineralogical distinctions can be postulated as indicators of the unique conditions within the magma conduit, both mechanically and geochemically, during the intrusion and crystallization of the Secunda dolerites.

The petrogenesis of these dolerites will most definitely have an influence on their specific metamorphic properties due to the variations in the chemistry and physical properties (*i.e.* thermal and viscosity) of the source material. This coupled with the dynamic emplacement of dykes and sills, will produce a very complex relationship between the intrusions and the coal seam. The addition of possible hydrothermal fluids as metamorphic agents further complicates the quantification of devolatilization owing to the proximity of dolerite intrusions. Several models have been proposed to describe the variation in coal quality seen within the C 4 lower coal seam with regard to the proximate analysis values, the dimension of the dolerites and the distance the dolerites are from the coal seam.

Thus the final conclusions of this thesis are:

- Dolerite metamorphic aureoles are dolerite specific, and geographically specific. Each dolerite conduit will maintain its own unique metamorphic signature which will differ at every individual point within the length of its conduit.
- The metamorphic effect of dolerites of the Secunda region cannot be ascribed solely to contact metamorphism, but possibly to a combination of metamorphism by hydrothermal fluids produce by the dolerite, and contact metamorphism.

With the above conclusion taken into account it is the recommendation of this thesis that the exact chemically and physical changes of unaltered to devolatilized coal be more thoroughly investigated to better understand the processes through which metamorphism occurs, to be able to differentiate between contact and hydrothermally altered coal. Continued investigation of the relationship between flow dynamics and metamorphic effect should be encouraged with a focus on the relationship between assimilation and thermal exchange.

APPENDIX

Due to the size of the data tables the appendix is stored on the accompanying CD along with descriptions of the data sets.

BIBLIOGRAPHY

Abu El-Enen M.M., Okrusch M., Will T.M., 2004: Contact metamorphism and metasomatism at a dolerite-limestone contact in the Gebel Yelleq area, Northern Sinai, Egypt, *Mineralogy and Petrology*, 81, 135–164

Betton P.J., Armstrong R.A., Manton W.I., 1984: Variations in the lead istopic composition of Karoo magmas, *Special Publication Geological Society of South Africa,* 13, 331-339

Bristow J.W., Allsopp H.L., Erlank A.J., Marsh J.S., Armstrong R.A., 1984: Strontium isotope characterization of Karoo volcanic rocks, *Special Publication Geological Society of South Africa,* 13, 295-329

Cañón-Tapia E., Merle O., 2006: Dyke nucleation and early growth from pressurized magma chambers: Insights from analogue models, *Journal of Volcanology and Geothermal Research*, 158, 207–220

Compston W., McDougall I., Heier K.S., 1968: Geochemical comparison of the Mesozoic basaltic rocks of Antarctica, South Africa, South America and Tasmania, *Geochim. Cosmochim. Acta,* 32, 129-149

Cox K.G., Bristow J.W., 1984: The Sabine river basalt formation of the Lebombo monocline and South-East Zimbabwe, *Special Publication Geological Society of South Africa,* 13, 125-147

De Olivera D.P.S. and Cawthorn R.G., 1999: Dolerite intrusion morphology at Majuba Colliery, northeast Karoo Basin, Republic of South Africa, *International Journal of Coal Geology,*41, 333-349

Dufek J., and Bachmann O., 2010: Quantum magmatism: Magmatic compositional gaps generated by melt-crystal dynamics, *Geology,* 38, 687-690

A.R. Duncan and J.S. Marsh., 2006: The Karoo Igneous Province. In: Johnson, M.R., Anhaeusser, C.R. and Thomas R.J. (Eds), The Geology of South Africa. Geological Society of South Africa, Johannesburg/Council for Geoscience, Pretoria, 501-519.

Du Toit, A.L., 1954: Geology of South Africa, 3, Oliver and Boyd, London, Editor Haughton S.H.

Elburg M., Goldberg A., 2000: Age and geochemistry of Karoo dolerite dykes from Northeast Botswana, *Joumal of African Earth Sciences,* 31, 314, 539-554

Encarnacion, J., Fleming, T.H., Elliot D.H., Eales, H.V., 1996: Synchronous emplacement of Ferrar and Karoo dolerites and the early break up of Gondwana, *Geology,* 24, 535-538.

Erlank A.J., Marsh J.S., Duncan A.R., Miller R.M., Hawkesworth C.J., Betton P.J., Rex D.C., 1984: Geochemistry and petrogenesis of the Etendeka volcanic rocks from Swa/Namibia, *Special Publication Geological Society of South Africa,* 13, 247-266

Fredericks M.P., Warebrooke P., Wilson M.A., 1985: A study of the effect of igneous intrusions on the structure of an Australian high volatile bituminous coal, *Org. Geochem,* 8, 5, 329-340

Galerne C.Y., Neumann E.R., Planke S., 2008: Emplacement mechanism of sill complexes: Information from the geochemical architecture of the Golden vally sill complex, South Africa, *Geotherm. Res.*, 177, 425-440

Golab A.N., Carr P.F., 2004: Changes in geochemistry and mineralogy of thermally altered coal, Upper Hunter Valley, Australia, *International Journal of Coal Geology*, 57, 197– 210

Hancox, P.J., and Rubidge, B.S., 2001: Breakthrough in the biodiversity, biogeography, biostratigraphy, and basin analysis of the Beaufort group. *Journal of African Earth Sciences*, 33, 563 - 577.

Hawkesworth C.J., Marsh J.S., Duncan A.R., Erlank A.J., Norry M.J., 1984: The role of continental lithosphere in the generation of the Karoo volcanic rocks: Evidence from combined Nd and Sr isotope studies, *Special Publication Geological Society of South Africa,* 13, 341-354

Huppert H.E., Woods A.W., 2002: The role of volatiles in magma chamber dynamics, *Nature,* 420, 493-495

Johnson, M.R., Van Vuuren, C.J., Hegenberger, W.F., Key, R., and Shoko, U., 1996. Stratigraphy of the Karoo Supergroup in southern Africa: an overview. *Journal of African Earth Sciences*, 23, 3-15.

Journdan F., Féraud G., Bertrand H., Kampunzu A.B., Tshoso G., Le Gall B., Tiercelin J.J., Capiez P., 2004: The Karoo Triple Junction questioned: Evidence from Jurassic and Proterozoic $^{40}Ar/^{39}Ar$ ages and geochemistry of the Giant Okavango Dyke Swarm (Botswana), *Earth Planet. Sci. Lett.,* 222, 989-1006

Jourdan F., Féraud G., Bertrand H., Watkeys M.K., 2007: From flood basalts to the inception of oceanization: Example from the $^{40}Ar/^{39}Ar$ high-resolution picture of the Karoo large igneous province, *Geocehmistry Geophysics Geosystems,* 8, 2

Kavanagh J.L., Menand T., Stephen R., Sparks J., 2006: An experimental investigation of sill formation and propagation in layered elastic media, *Earth and Planetary Science Letters,* 245, 799–813

Le Gall B., Tshoso G., Jourdan F., Féraud G., Kenna T.C., Tiercelin J.J., Kampunzu A.B., Mondisi M.P., Dyment J., Maia M., 2002: $^{40}Ar/^{39}Ar$ geoghronology and structural data from the Giant Okavango and related mafic dyke swarms, Karoo Igneous Province, Northern Botswana, *Earth Planet. Sci. Lett.,* 202, 595-606

Le Roex A.P., Reid D.L., 1978: Geochemistry of Karoo dolerite sills in the Calvinia district, Western Cape Province, South Africa, *Contrib. Mineral. Pertrol.,* 66, 351-360

Lombaard B.V., 1952: Karoo dolerites and lavas, *Trans. Geol. Soc. South Africa,* 55, 175-198

MacDonald R., Crossley R., Waterhouse K.S., 1983: Karoo basalts of Southern Malawi and their regional pertrogenetic significance, *Mineral. Mag., 47, 281-289*

Marsh J.S., Eales H.V., 1984: The chemistry and petrogenesis of igneous rocks of the Karoo central area, Sothern Africa, *Special Publication Geological Society of South Africa,* 13, 27-67

McLeod P., Tait S., 1999: The growth of dykes from magma chambers, *Journal of Volcanology and Geothermal Research*, 92, 231–245

Mitha V.R., 2006: An insight into magma supply to the Karoo igneous province: A geochemical investigation of Karoo dykes adjacent to the north-western sector of the Lesotho volcanic remnant, unpublished MSc thesis, Rhodes University

Mussett A.L. and Khan M.A, 2000: Looking into the Earth, Cambridge University Press, New York

Poland M.P., Moats W.P., Fink J.H., 2008: A model for radial dike emplacement in composite cones based on observations from Summer Coon volcano, Colorado, USA, *Bull Volcanol*, 70, 861–875

Prior G.T., 1910: Petrographical notes on the dolerites and rhyolites of the Natal and Zululand, *Ann. Natal Mus.,* 2, 141-157

Reynolds O., 1883: An Experimental Investigation of the Circumstances Which Determine Whether the Motion of Water Shall Be Direct or Sinuous, and of the Law of Resistance in Parallel Channels, *Philosophical Transactions of the Royal Society of London*, 174, 935-982

Riley T.R., Curtis M.L., Leat P.T., Watkeys M.K., Duncan R.A., Millar I.L., Owens W.H., 2006: Overlap of the Karoo and Ferrar magma types in KwaZulu-Natal, South Africa, *Journal of Petrology,* 47, 3, 541-566

Sasol mining, unpublished internal reports.

South African Committee for Stratigraphy (SACS), 1980. Stratigraphy of South Africa. Part 1 (Comp.L.E.Kent). Lithostratigraphy of the Republic of South Africa, South West Africa/Namibia, and the Republic of Bophuthatswana, Transkei and Venda: Handb.geol.Surv.S.Afr., 8

Speight J.G., 2005: Handbook of coal analysis, John Wiley and Sons, New Jersey, Print

Spiegelman M. and McKenzie D., 1987: Simple 2-D models for melt extraction at mid-ocean ridges and island arcs, *Earth and Planetary Science Letters*, 83, 137-152

Van Niekerk J.L., 1995: Geochemistry of the dolerites and the intrusion mechanisms of two major sills in the Secunda coal field, unpublished PhD thesis, University of Stellenbosch

White R. and McKenzie D., 1989: Magmatism at Rift Zones: The Generation of Volcanic Continental Margins and Flood Basalts, *Journal of Geophysical Research,* 94, 86, 7685-7729

White W.M.: 2003, Geochemistry, John-Hopkins University Press, New York, Online

Yi-Gang Xu., Bin He., Sun-Lin Chung., Menzies M.A., 2004: Geologic, geochemical, and geophysical consequences of plume involvement in the Emeishan flood-basalt province, *Geology*, 32, 10, 917–920